論文 / 著書情報
Article / Book Information

題目(和文)	紫外線と原子状酸素の影響を受けたシリコーン汚染物質を起源とする微小スペースデブリに関する研究
Title(English)	Microparticle Space Debris Derived from Silicone Contaminants Affected with Ultraviolet and Atomic Oxygen
著者(和文)	山中理代
Author(English)	Riyo Yamanaka
出典(和文)	学位:博士(工学), 学位授与機関:東京工業大学, 報告番号:甲第10509号, 授与年月日:2017年3月26日, 学位の種別:課程博士, 審査員:小田原 修,山口 孝夫,吉本 護,山口 孝夫,中村 一隆,和田 裕之,矢野 豊彦
Citation(English)	Degree:Doctor (Engineering), Conferring organization: Tokyo Institute of Technology, Report number:甲第10509号, Conferred date:2017/3/26, Degree Type:Course doctor, Examiner:,,,,,,
学位種別(和文)	博士論文
Type(English)	Doctoral Thesis

A Doctoral Dissertation

Microparticle Space Debris Derived from Silicone Contaminants Affected with Ultraviolet and Atomic Oxygen

by

Riyo YAMANAKA

Department of Innovative and Engineered Materials
Interdisciplinary Graduate School of Science and Engineering
Tokyo Institute of Technology

March 2017

≪Table of Contents≫

Chapter 3: Chemical Changes of Silicone Contaminants

Chapter 4: Morphological Changes of Silicone Contaminants

List of Abbreviations

AO	: atomic oxygen
CVCM	: collected volatile condensable materials
EDX	: energy dispersive X-ray
ESD	: Equivalent sun days
ESEM	: Evaluation of Space environment and Effects on Materials
EURECA	: European Retrievable Carrier
ExHAM	: Exposed Experiment Handrail Attachment Mechanism
F-OSR	: flexible optical solar reflector
FT-IR	: Fourier Transform Infrared
GEO	: Geostationary Earth Orbit
GTO	: Geostationary Transfer Orbit
HEO	: High Earth Orbit
HST	: Hubble Space Telescope
IADC	: The Inter-Agency Space Debris Coordination Committee
ISS	: the International Space Station
LDEF	: Long Duration Exposure Facility
LEO	: Low Earth Orbit
MEEP	: MIR Environmental Effects Payloads
MFD	: Manipulator Flight Demonstration
MISSE	: Materials International Space Station Experiment
MPAC	: Micro-Particles Capturer
PECs	: Passive Experiment Containers
POSA 1	: Passive Optical Sample Array 1
PPMD	: Polished Plate Micrometeoroid Detector
SEED	: Space Environment Exposure Device
SEES	: Space Environment & Effects System
SEM	: Scanning Electron Microscopy

SFU	: Space Flyer Unit
SM	: the Russian Service Module
SSA	: Space Situational Awareness
STEM/EDX	: Scanning Transmission Electron Microscope / energy dispersive X-ray
STS	: Space Transform System
TML	: total mass loss
TQCM	: Thermoelectric Quartz Crystal Microbalance
UV	: ultraviolet
XMA	: X-ray microanalysis
XPS	: X-ray Photoelectron Spectroscopy

Chapter 1:

General Introduction

1.1 Introduction

Thousands of spacecraft had been launched into orbit for the scientific, commercial, environmental, and national security purposes over the last 60 years. Consequently, these spacecraft have been creating a large number of objects which do not serve any useful function, so-called space debris, in orbit around the Earth. ESA (**E**uropean **S**pace **A**gency) had presented the concerns that 29,000 space debris objects for sizes larger than 100 mm, 670,000 space debris objects for sizes larger than 10 mm, and more than 170 million space debris objects for sizes larger than 1mm were estimated to exist in Earth orbit in 2013. Much of these space debris will remain in orbit for hundreds of years or more, and pose a long-term hazard to future space exploration.

It is widely known that collision of a spacecraft to space debris objects with size larger than 100 mm can cause catastrophic consequences such as loss of mission, while an impact of millimeter-sized debris can cause severe structural damage to a spacecraft. However, it has become clear that not only large space debris but also space debris smaller than 1 mm in diameter can damage spacecraft recently by analyzing the retrieved exterior materials of the **H**ubble **s**pace **t**elescope (HST)[(1-1), (1-2)], the Russian Space Station "Mir"[(1-3)], and others[(1-4), (1-5)]. Although these analyses clarified the existence of many space debris smaller than 1 mm in diameter on orbit, a sufficient amount of them could not be collected for analyzing and evaluating their components because their shapes were destroyed upon collision with spacecraft[(1-1)]. Thus, the origin of space debris with size less than 1 mm remains mainly unknown. However, it is important to make clear the origin of such space debris for reducing small space debris and protecting spacecraft against them.

The followings should be needed to promote the space exploration in our future.

*International space law have to be prepared. (e.g. space and planet utilization)

*New durable materials are need for space environments for long term space exploration.

*New outgas free materials are need for high accuracy optical sensors and thermal control systems.

*New method for reducing space debris.

The most prior item to be resolved is “new method for reducing space debris” because all spacecraft are still effected by space debris on orbit. Therefore the present work focuses to small space debris.

1.2 Space Debris

1.2.1 The Definition of Space Debris

The **C**ommittee **o**n **P**eaceful **U**ses of Outer **S**pace (COPUOS) was established to govern the exploration and use of space for the benefit of all humanity: for peace, security and development. The Committee was tasked with reviewing international cooperation in peaceful uses of outer space, studying space-related activities that could be undertaken by the UN **(U**nited **N**ations). COPUOS has two subcommittee, the STSC (**S**cientific and **T**echnical **S**ub**c**ommittee) and the Legal Subcommittee. The definition of Space debris is as below in Technical Report on Space Debris, 1999, by UN/COPUOS/STSC.

“Space debris are all man-made objects, including their fragments and parts, whether their owners can be identified or not, in Earth orbit or re-entering the dense layers of the atmosphere that are non-functional with no reasonable expectation of their being able to assume or resume their intended functions or any other functions for which they are or can be authorized”.

The IADC (**I**nter-**A**gency Space **D**ebris **C**oordination Committee), which was established to exchange information on space debris activities between its member

space agencies, also adopted the following definition: “Space debris are all man-made objects including fragments and elements thereof, in Earth orbit or re-entering the atmosphere, that are non-functional” in a document IADC-04-06 [1-6].

Then, it can be understood that definition of space debris include the next characteristics:

1) All man-made object including fragments and parts/elements,

2) In Earth orbit or re-entering the atmosphere, and

3) Non-functional.

1.2.2 Origin of Space Debris

Since the first space lunch of Sputnik-1 on October 1957, space activities which release objects into space bring the generation of the large number of the objects including space debris on orbit. Table 1-1 shows the main categories of space debris, cause of generation, and sources of space debris. The identification is described in guidelines, ‘Support to the IADC Space Debris Mitigation Guidelines’ which was established by the IADC as a document IADC-04-06 [1-6].

Table 1-1. Sources of space debris[1-6].

Main Categories	Causes	Debris Sources
Mission- related objects (Parts Released during Mission Operation)	**objects re-leased by design**	**operational debris** (fasteners, covers, wires, etc.)
		objects released for experiments (needles, balls, etc.)
		tethers designed to be cut after experiments
		others (released before retrieval)
	unintentional-ly released objects	**fragments caused by ageing** (flakes of paints and blankets resulting from degradation)
		tether systems cut by debris or meteoroids
		objects released before retrieval to ensure safety
		liquids (leaked from nuclear power systems, etc.)
		particles ejected from solid motors
On-orbit break-ups	**intentional destruction**	**destruction for scientific or military experiments** (including self-destruction, intentional collision, etc.)
		destruction prior to re-entry in order to minimise ground casualty
		destruction to ensure security of on-board devices and contained data
	accidental break-ups	**explosion caused by failure during mission operation**
		explosion caused by command destruct systems, residual propellants, batteries, etc., after mission termination
	on-orbit collisions	**fragments caused by collision with catalogued objects**
		fragments caused by collision with un-catalogued objects
Mission-terminated space systems		**systems left in near-GEO, GTO, LEO, and HEO**

1.2.3 Present Situation of Space Debris Observation

The document IADC-04-06, 'Support to the IADC Space Debris Mitigation Guidelines' defines two protected regions about the Earth[1-6]. The **l**ow **E**arth **o**rbit (LEO) is the first protected region and the **ge**osynchronous **o**rbit (GEO) is the second protected region. LEO extends from the lowest maintainable orbital altitude up to a height of 2,000 km above the surface of the Earth. GEO includes the volume of space bounded in altitude by -200 km of the geosynchronous altitude (35,786 km) to +200 km of the geosynchronous altitude and in inclination by -15 degrees of latitude to +15 degrees of latitude[1-6], [1-7].

Optical telescopes are mainly suited for the surveillance of GEO because

ground-based optical telescope can detect down to 100mm in size. While radars are suitable to the surveillance of LEO because ground-based radars can detect LEO debris down to a few mm in size.

By using optical telescopes and radars, the objects larger than 100 mm in LEO and larger than 1 m at GEO are cataloged and regularly surveyed by the US Space Surveillance Network and the Russian Space Surveillance System[1-7] - [1-10]. Consequently, the catalog covers objects larger than approximately 100 mm in LEO and 1 m at GEO.

However, there are no sufficient observation facilities at East Asia. Therefore, **J**apan **A**erospace E**x**ploration **A**gency (JAXA) is building **S**pace **S**ituational **A**wareness (SSA) by cooperating with Bisei Space Guard Center and Kamisaibara Space Guard Center. Bisei Space Guard Center has two kinds of optical telescopes for observing the objects in GEO and Kamisaibara Space Guard Center has a radar for observing the objects in LEO in Japan. The SSA will contribute to the building of global SSA.

Objects between 2 mm and 100 mm in LEO and between 100 mm and 1 m in GEO are detected by special ground-based sensors. In GEO some efforts are underway to develop a catalog-like database for these objects.

The presence of objects smaller than 2 mm in LEO is inferred by the examinations of the surface of spacecraft which have been returned to the Earth (e.g. **L**ong **D**uration **E**xposure **F**acility (LDEF), solar arrays of the HST, **Eu**ropean **Re**trievable **Ca**rrier (EURECA) and others). However, they cannot be observed from the Earth.

Fig.1-1 shows the summary of number of objects in Earth orbit officially cataloged by the US Space Surveillance Network[1-11]. Each other types of object in Earth orbit may be classified as belonging to one of four types of debris: non-functional spacecraft, rocket bodies, mission-related debris, and fragmentation debris. “Fragmentation debris” include satellite breakup debris and anomalous event debris, and is assumed to cover a size regime mainly within diameters of 0.1 mm $\leqq$ d $\leqq$ 1 m. “Mission-related debris” include all objects dispensed, separated, or released as part of the planned mission. The significant increase of objects is shown in 2007 and 2009. The former is caused to the

satellite destroy experiment by China, and the latter is caused to the collision accident between American satellite and Russian satellite[1-12]. They mean that international cooperation is important for making a defense from the increase of space debris.

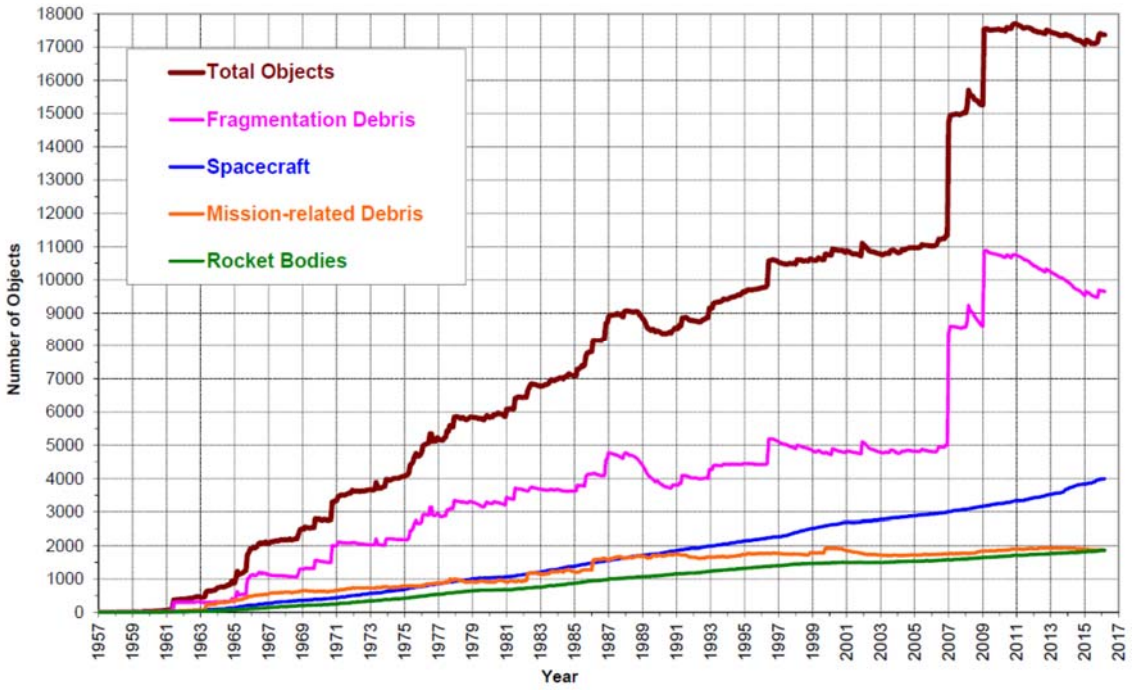

Fig.1-1. Monthly number of objects in Earth orbit by object type[1-11].

1.2.4 Impact Effects of Space Debris

The impact effects of space debris are “electromagnetic emissions (e.g. visible light flash, infra-red radiation, and microwave radiation)”, “acoustic emissions (within the impact structure)”, “secondary debris cloud and ejecta”, “plasma cloud”, “shock-induced accelerations”, “size and shape of crater or hole”, and “chemical properties of crater material residue”. According to the document IADC-08-03 ‘Sensor Systems to Detect Impacts on Spacecraft’, the dependence of damage effects on impactor size is summarized (shown in Table 1-2) [1-13].

Table 1-2. Dependence of hypervelocity impact damage effect on particle size (Note: Larger particles usually have all the effects listed under the smaller sizes as well) [1-13].

Minimum particle size for which effect is noticeable	Effect
< 1 μm	No or little individual effect. Some surface degradation (sandblasting effect) leading to a change of thermal, optical or electrical properties.
1 μm	Temporary saturation and permanent damage of exposed CCD pixels (e.g. for x-ray telescopes). Degradation of mirrors and sensors by direct impacts and by secondary ejecta. Penetration of outer coatings and surface layers allowing subsequent attack of other environment components (plasma, Atomic Oxygen). Triggering of electrostatic discharges of pre-charged surfaces (effect demonstrated but minimum particle size still uncertain). Creation of new small debris by ejecta.
10 μm	Noticeable individual craters, e.g.: • craters visible to naked eye (> 200 μm) on brittle surfaces (glass) • potential sealing problem of exposed hatches Effects of momentum transfer (which can be 5-20 times larger than the incoming momentum because of secondary ejecta) leading to: • disruption of stable attitude • disturbance of formation flying Electromagnetic interference from impact plasma. Optical light flash. Impact generated radio waves.
100 μm	Noticeable damage on sensitive sensors and surfaces (Shuttle windows require replacement). Cutting of thin tethers, springs, wires. Penetration of MLI. Penetration of 300-500 μm wall thickness. Penetration of heat pipes, coolant loops, radiators. Penetration of solar cells (short circuits, arc burning).
1 mm	Craters/holes from 2mm to 1 cm in diameter or larger depending on type and thickness of material impacted. Penetration of 3-5 mm wall thickness with damage on equipment behind wall. Structural damage of exposed equipment. Penetration of tanks, baffles, sun-shields, external cables, etc.
1 cm	Structural damage/ destruction on any spacecraft part hit. Penetration of all shields, including special protection of manned modules. Creation of many new large debris pieces.
10 cm	Complete destruction of satellite or subsystem hit. Interference with astronomical observations.
1 m	Solid spacecraft parts can survive re-entry and hit ground.

Table 1-2 clarified the importance of space debris smaller than 1 mm in diameter on orbit, however, they cannot be observed using ground-based observation systems.

Actually, impact effects of space debris smaller than 1 mm in diameter on orbit are reported. The followings are instances that were effected by impacts smaller than 1mm in diameter.

The first one is an impact damage of space debris detected on windows of post-flight space shuttle[1-14]. Windows of space shuttle were often replaced by the impact damages of space debris. The impact damages had risks to loss of human life. Fig. 1-2 shows an image of an impact crater in window of STS-7 space shuttle[1-15]. It is needed to replace the window by this sized craters.

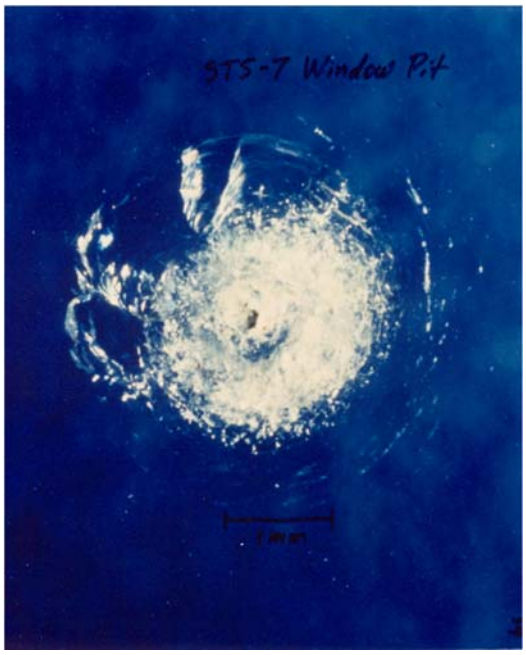

Fig. 1-2. An impact crater in window of STS-7 space shuttle[1-15].

The second shows the degradation of solar array blanket on the **I**nternational **S**pace **S**tation (ISS) [1-16), (1-17)]. Fig. 1-3 are images of the solar array blanket box on the ISS after one year in LEO. Although the solar array blanket was coated with aluminum for

protecting from **a**tomic **o**xygen (AO), the solar array blanket was degraded by AO. One of the cause is thought to be attributed to holes formed by impacts of micrometeoroid and space debris, because synergistic effect was discovered between hypervelocity impacts and AO exposure of polyimide thin film[1-18]. So, it was predicted that AO eroded the solar array blanket from the holes as base points.

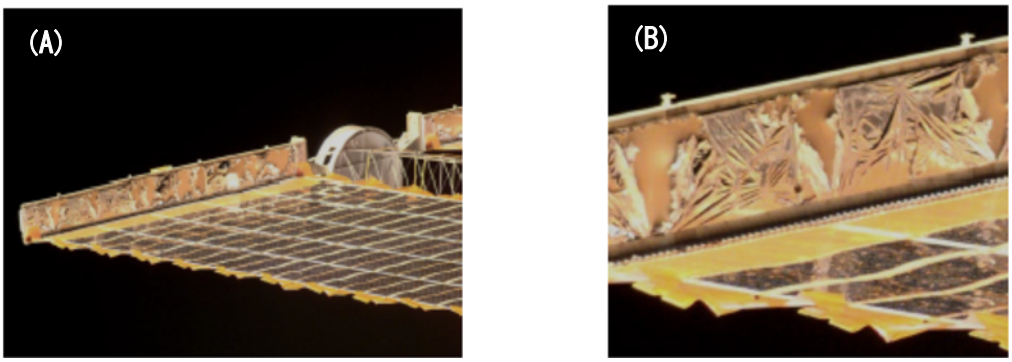

Fig. 1-3. ISS solar array blanket box after one year in LEO[1-16].
(A) ISS solar array blanket box and (B) close-up of damage.

1.3 Microparticle Space Debris Captured in Space

The **M**icro-**Par**ticles **C**apturer (MPAC) experiment units had been developed in order to clarify the abundance and composition of micrometeoroid and space debris and deployed along with the **S**pace **E**nvironment **E**xposure **D**evice (SEED) experiment units on the Russian **s**ervice **m**odule (SM) of the ISS. Summary of the SM/MPAC&SEED experiment is described in Chapter 2 Section 2.3.

Silica aerogel (hereafter “aerogel) is one of the microparticles capturer materials mounted on the MPAC experiment units in order to capture micrometeoroid and space debris and analyze its composition, collision energy and direction of approach[1-19) - (1-21)]. As a result, space debris was captured by the aerogel exposed to space environment for

315 days (Fig. 1-4 (A)), secondary debris was captured by the aerogel exposed to space environment for 865 days (Fig. 1-4 (B)), and micrometeoroid was captured by the aerogel exposed to space environment for 1405 days (Fig. 1-4 (C))[1-21), (1-22)]. And many SiO_2-based microparticles of ac. 10 μm in diameter were also captured by retrieved aerogels (Fig. 1-5)[1-21)]. Fig. 1-5 (A) is an optical image of microparticles captured by the aerogel exposed to space environment for 315 days, Fig. 1-5 (B) is an optical image of microparticles captured by the aerogel exposed to space environment for 865 days, and Fig. 1-5 (C) is an optical image of microparticles captured by the aerogel exposed to space environment for 1405 days[1-21), (1-22)]. The number of them was increased belong to the exposure periods[1-21)]. In order to clarify the origin of the microparticles, they were analyzed by using an **X**-ray **m**icro**a**nalysis (XMA) and a microscope **F**ourier **t**ransform **i**nfra**r**ed (FT-IR) spectroscopy[1-21)]. The results of analyses revealed that silicon dioxide (SiO_2) is the main container of the microparticles and they have Alkanes, CO, Si-CH_3, Si-O-Si bonds, and hydroxyl group. However, their origin was not clarified[1-21)].

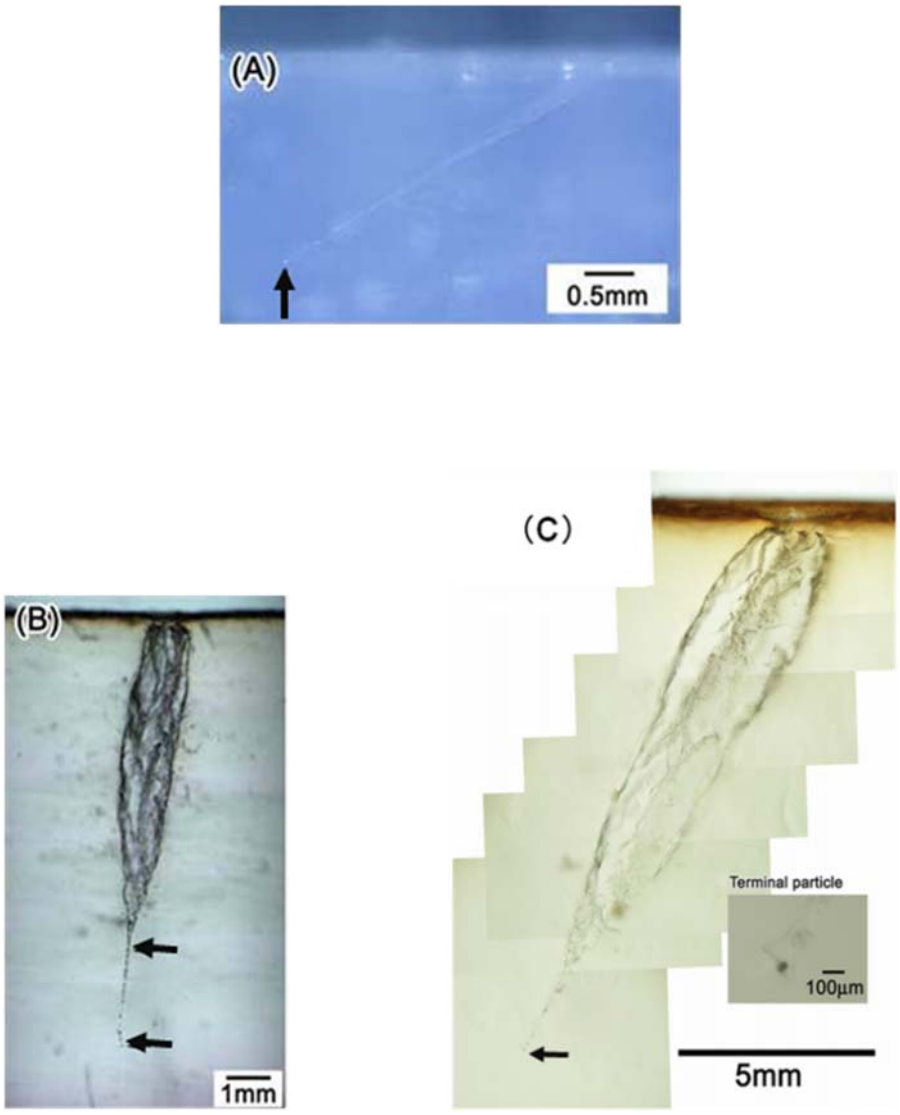

Fig. 1-4. Microparticles captured by the aerogels mounted on the MPAC Experiment units[(1-21), (1-22)].

(A) space debris, (B) secondary debris and (C) micrometeoroid.

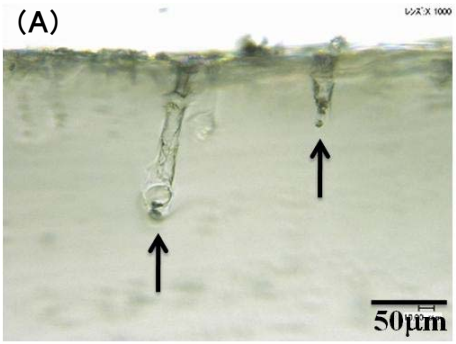

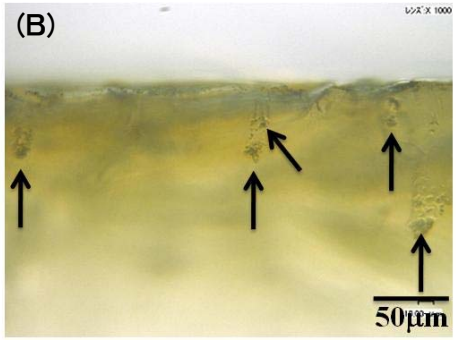

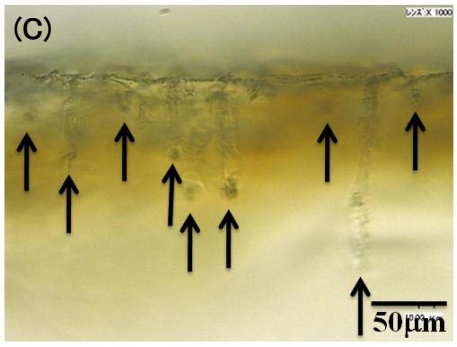

Fig. 1-5. The SiO_2-based microparticles captured by retrieved aerogels mounted on the MPAC Experiment units[1-21].

(A) for 315 days, (B) for 865 days and (C) for 1405 days.

The SiO_2-based microparticles are shown with arrows for being able to be found clearly.

1.4 Contaminants in Space

Contaminants are substances which are generated as a result of human space activities under effects of space environment such as solar irradiation and vacuum. There are two kinds of contaminants known in the field of space activities. One is molecular contaminant and the other is particulate contaminant. Contaminants deposit on the surface of spacecraft or remain near spacecraft. Deposition of contaminants means degradation of transmittance, reflectance, solar absorbance, and thermal emittance of materials used in spacecraft. Consequently, performances of solar arrays, radiators, optical instruments, sensors, and other systems are reduced. Therefore, the control of contaminants is important for space activities[1-23].

Fig. 1-6 is the throughput data observed by the optical telescope assembly which had been on-board of satellite Solar-B (other name is HINODE) [1-24]. Solar-B is a solar observational satellite which was equipped with solar optical telescope, X-ray telescope and extreme **u**ltra**v**iolet (UV) imaging spectrometer, and launched on September 22, 2006. The degradation of throughput can be observed from Fig. 1-6. It was concluded that the degradation depended on the deposition of contaminants[1-24].

Most of spacecraft use silicone materials such as adhesives for solar cells and optical solar reflectors, potting compounds for electronic components and lubricants. The reason to use silicone adhesive for bonding solar cells is that silicone adhesive forms the flexible bond between the support structure and solar cells. However, usage of silicone materials results in production of silicone contaminants. Unfortunately, UV light interacts with silicone contaminants and cause a polymerized contaminant layer to build up[1-23]. While AO oxidizes silicone contaminants and strips hydrocarbons such as CO and CO_2, a silica-based surface layer is formed and it can resist further reactions with AO[1-23].

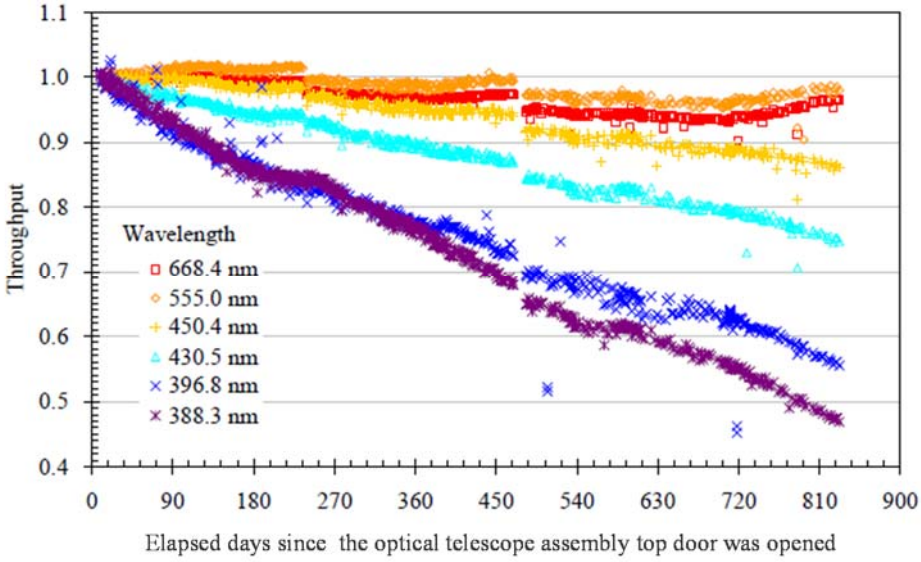

Fig. 1-6. Throughput data observed by the optical telescope assembly of HINODE [1-24].

For reducing contaminants from materials on orbit, materials are screened before being used to spacecraft. NASA (**N**ational **A**eronautics and **S**pace **A**dministration) applies ASTM E-595[1-25] which is the standard of American Society for Testing Materials about outgassing measurement. JAXA also refer to ASTM E-595 for screening materials.

The outgassing test measure the **t**otal **m**ass **l**oss (TML) of materials which are heated to 125°C for 24 hours, the mass of **c**ollected **v**olatile **c**ondensable **m**aterials (CVCM) which are collected by collector plate made of aluminum maintained at 25°C, and the mass of water vapor regain. Materials whose TML $<$ 1% and CVCM $<$ 0.1 % are acceptable[1-25]. Fig. 1-7 is an image of Outgas Measuring System at Tsukuba Space Center. There is outgassing test which measures characteristics of outgas and time-dependent change of discharge on a widespread temperature[1-26].

Fig. 1-7. Outgas Measuring System.

1.5 Space Environments

There are some of different environmental elements in orbit compared with on the Earth. Then, this section describes about other space environments mainly related to the present work except space debris and contaminants.

ⅰ) Meteoroids

Table 1-3 shows comparison between meteoroids and space debris. Meteoroids have extraterrestrial natural origin, and their average velocity is 20 km/s [1-27].

Table 1-3. Comparison between meteoroids and space debris[1-27].

Particles	Natural--------"Meteoroids"	Artificial-------"Space Debris"
Origins	• Asteroids / Comets • ß-meteoroids • Ejecta from planets and satellites • Inter-Stellar Particles (ISP)	• Non-operational space instruments • Break-ups, Collisions, Fragmentation • By-products of spacecraft operations • Surface degradation
Dynamics	Unbound to Earth (Omni-Direction)	Bound to Parent Body Orbits
Velocity w.r.t. Earth	• Streams: Up to 70 km/s • Sporadic: Average 20 km/s • ISP: Can be > 100 km/s	• Circular in LEO: ~8 km/s • GTO: Varies with perigee altitude • Circular in GEO: ~3 km/s

ii) Ultraviolet Light

The solar spectrum outside atmosphere of the Earth is the air mass zero solar spectrum[1-23), (1-28), (1-29]. The spectral irradiance data from satellites, space shuttle missions, high-altitude aircraft, rocket soundings, ground-based solar telescopes, and modeled spectral irradiance are the basic data of the air mass zero solar spectral irradiance[1-28]. The air mass zero solar spectrum is shown in Fig. 1-8 [1-23]. It can be seen from the air mass zero solar spectrum that irradiance begins to increase from approximately 200 nm, and its peak is at approximately 500 nm (Fig. 1-8). Generally, the UV range is defined as light having the wavelength between 4-400 nm. However, the wavelength shorter than approximately 120 nm is negligible in the air mass zero solar spectrum. The UV range of wavelengths can be classified in two bands; vacuum UV as the 100-200 nm range and near UV as the 200-400 nm range[1-23].

UV degrade polymers, because common chemical bonds in polymers can absorb UV. Consequently, photochemical reactions are led, and polymers are degraded causing such effects as discoloration or loss of mechanical properties by chemical changes[1-23]. Table 1-4 shows dissociation energies of common polymeric bonds[1-30].

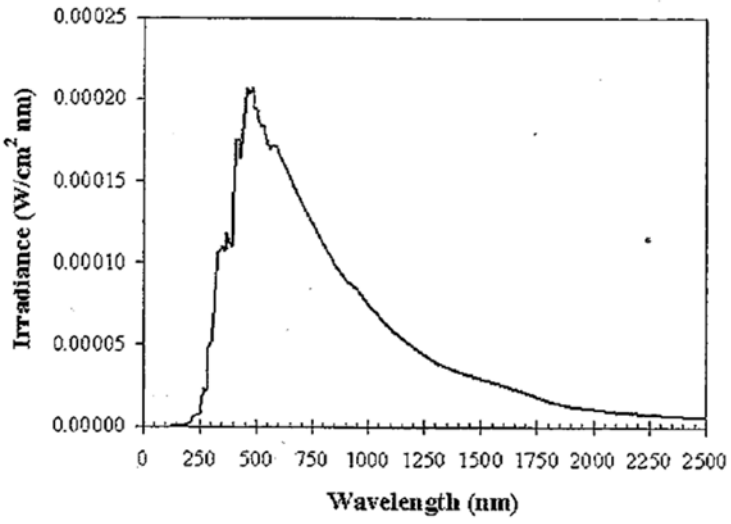

Fig. 1-8. The air mass zero solar spectrum[1-23].

Table 1-4. Dissociation energies of common polymeric bonds[1-30].

Chemical Bond	Dissociation Energy	(μm) Wavelength of Energy	Typical Material
C-H	3.5-4.4	0.36-0.28	Aliphatic polymers
C_6H_5-H	4.8	0.26	Aromatic polymers
-C_6H_4-C(=O)-	3.9	0.32	Kapton, Mylar
-C_6H_3-H	4.8	0.26	Aromatic compounds
C=C	6.3	0.20	Aliphatic compounds
C≡C	8.7	0.14	Aliphatic compounds
O=CO	5.5	0.23	Carboxylic acid
C=O	7.7-7.8	0.16	Aldehydes, ketones
-CH_2-CH_2-	3.9	0.32	Mylar, polyethylene and aliphatic compounds
CF_3-CF_3	4.3	0.29	FEP Teflon
-CF_2-F	5.5	0.23	FEP Teflon
CH_3CF_3	4.4	0.28	-$(CH_2$-$CF_2)_n$-
C-N	3.2	0.39	Kapton
C-S	2.8	0.44	Vulcanized rubber
-Si-O-	8.3	0.15	Silicones and SiO_2
-Si-CH_3	3.1	0.40	Silicones
-Zr-O-	8.1	0.15	Protective ctg.
-Al-O-	5.3	0.23	Protective ctg.

iii) Atomic Oxygen

AO is formed by molecular bond breakage of O_2 by solar photons (the equation (1-1) [1-31]). Since h is Planck's constant (6.626E-34 Js) and v is frequency of photons, hv means energy of photons. Short wavelength ($<$ 243 nm) of UV has sufficient energy to break the 5.12 eV O_2 diatomic bond. Therefore, UV (the wavelength range; $<$ 243 nm) form AO from O_2 [1-30), (1-31].

$$O_2 + hv \rightarrow O + O \qquad (1\text{-}1)$$

Fig. 1-9 shows number density of individual species and total number density as a function of altitude[1-32]. It is clarified that AO is the most abundant species at approximately 200-600 km of the LEO.

In the LEO, the surface materials of spacecraft are collided with AO, and attacked chemically which is subject to oxidation[1-33]. AO react with polymers and many metals. As a result of the reaction, the surface of polymers and metals is oxidized. The oxidation produces volatile oxidation products like CO and CO_2, and results in erosion and mass loss in the case of polymers[1-23), (1-30]. Summary of the possible reactions mechanisms between AO and polymers are described in Fig. 1-10 [1-30), (1-34]. In the case of metals, nonvolatile metal oxides are formed, and the nonvolatile metal oxides tend to work as a shield from further oxidation by AO[1-23]. Silicone contaminants are also existing in space because silicone materials (methyl silicones and methyl phenyl silicones) are used frequently on spacecraft. It is reported that AO reacts with silicones and generates silicon oxide (SiOx). As a result, silicone contaminants are fixed and degrade the optics and thermal control systems[1-35].

The sensitivity of hydrocarbon materials to reaction with AO can be quantified by the AO erosion yields. Erosion yield of polyimide Kapton H, namely 3.0 X 10^{-24} cm^3/atom for 4.5 eV AO (collision energy of AO at LEO) is well known[1-23), (1-36]. Thus, Kapton H is often used as an AO monitor material.

The number density of individual species and total number density as a function of

altitude at approximately 80-400 km of Venus is shown in Fig. 1-11, and the number density of individual species and total number density as a function of altitude at approximately 80-300 km of Mars is shown in Fig. 1-12[1-37]. It is confirmed that AO also exists at low altitude of Venus and Mars by Fig. 1-11 and Fig. 1-12.

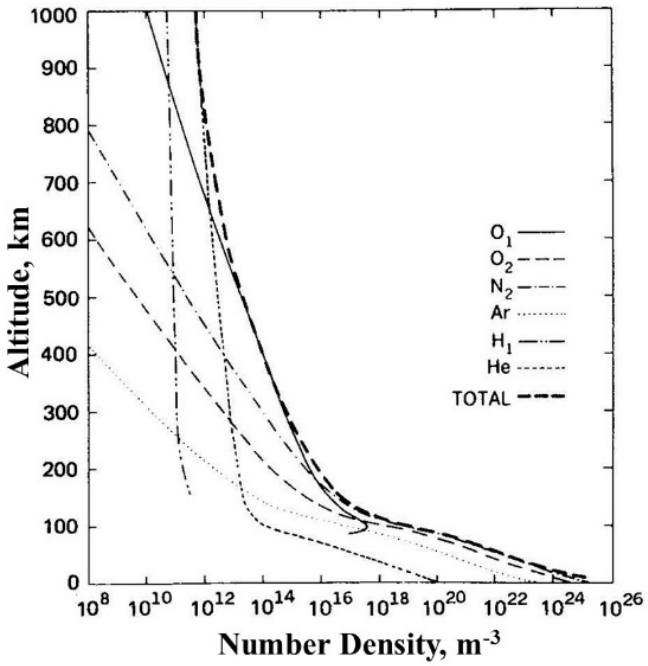

Fig. 1-9. Number density of individual species and total number density as a function of altitude[1-32].

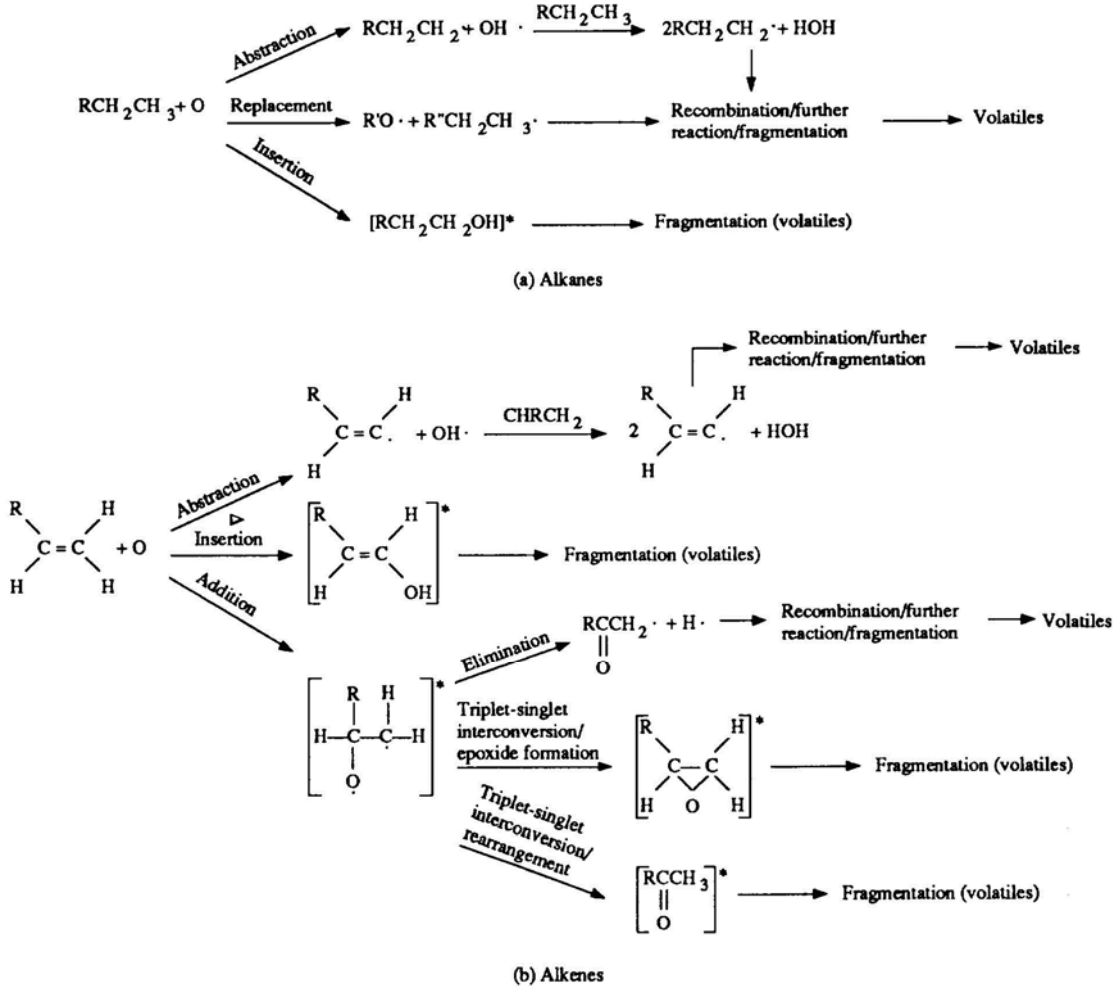

Fig. 1-10. AO reaction mechanisms[1-30].

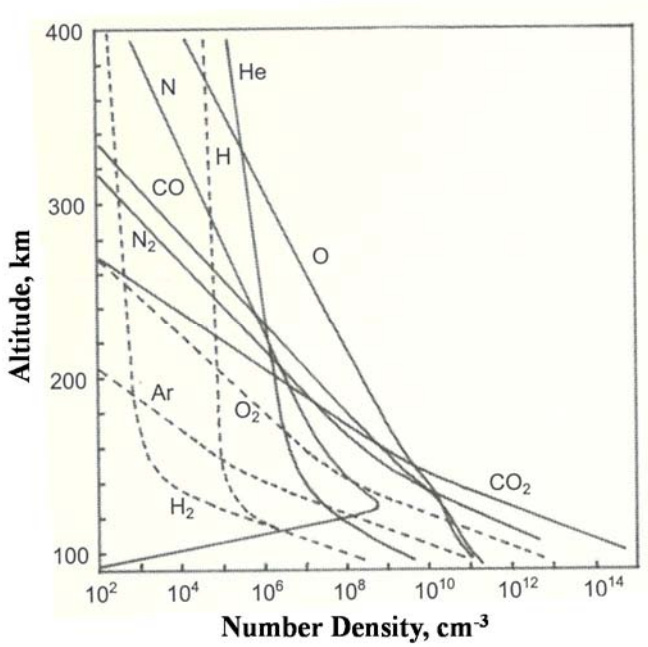

Fig. 1-11. Number density of individual species and total number density as a function of altitude at approximately 80-400 km of Venus[1-37].

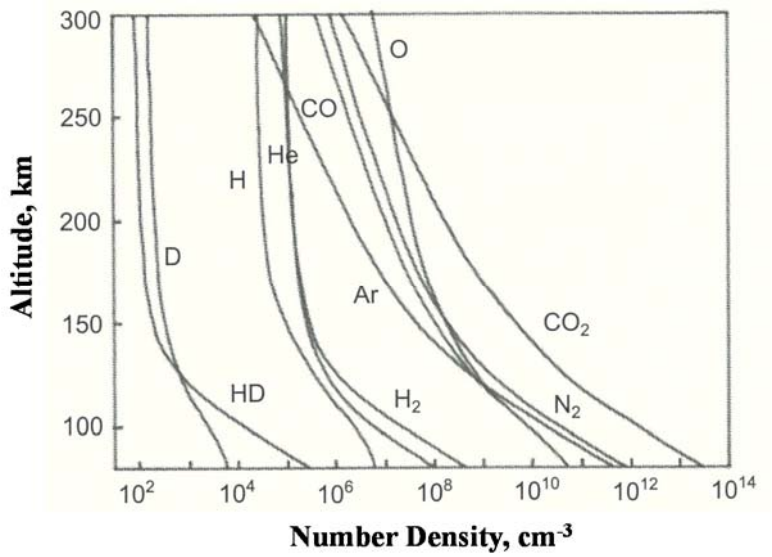

Fig. 1-12. Number density of individual species and total number density as a function of altitude at approximately 80-300 km of Mars[1-37].

ⅳ) Vacuum

Fig. 1-13 shows total pressure and mass density as a function of altitude[1-38]. The vacuum environment of the ISS (altitude; approximately 400 km) is 10^{-5} Pa.

Typically, polymers include low weight fragments, additives and absorbed gases. High vacuum environment accelerate the outgassing of low weight fragments, additives and absorbed gases from polymer materials[1-39]. Consequently, outgassing leads to generation of contaminants on the surface of spacecraft on orbit.

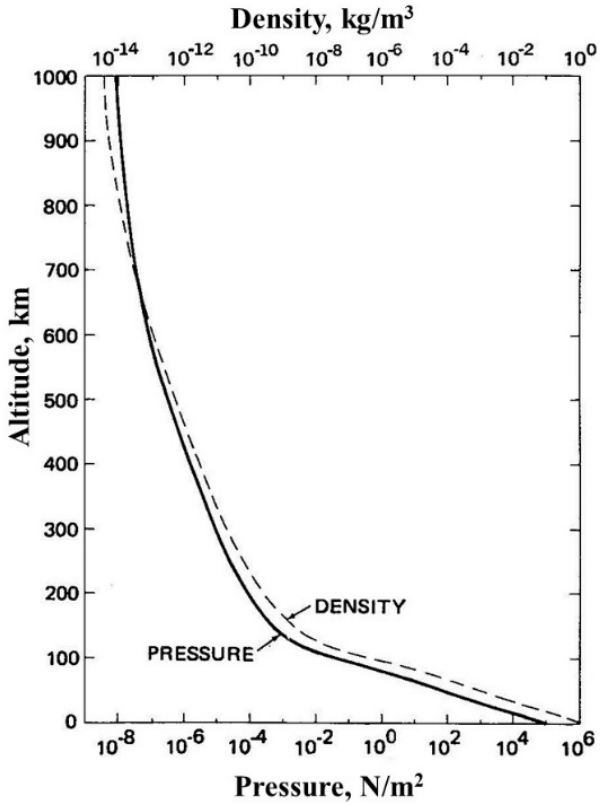

Fig. 1-13.Total pressure and mass density as a function of altitude[1-38].

1.6 Purpose of the Present Work

1.6.1 Space Debris Problems Solved in the Present Work

Although it has been clarified that small space debris (< 1 mm) can result in much severe damages on spacecraft, the self-guarding would be quite complex against such small space debris because it is difficult to identify them from the Earth and it has been still under discussion about origins of them. Therefore, it is important to identify the origin of small space debris, especially of size-level less than 1 mm, for developing a new method which can play an effective role in reducing problems damaged from space debris on orbit.

As a result of the previous space experiments, many SiO_2-based microparticles have been confirmed, for example, from the aerogel mounted on the MPAC experiment units. In order to make clear the reason why SiO_2-based microparticles be and how they exist observably in space, the present work has been carried out under main concerns with silicone adhesive of RTV-S691(room-temperature-vulcanizing adhesive) commonly used in space activities. In the present work, main focus is on possible connection between SiO_2-based microparticles captured on orbit and silicone contaminants derived from silicone materials which are widely used in spacecraft. Therefore, the scope of the research covers formation process of microparticles with size between 0.1 and 100 μm consisting mainly of SiO_2. The origin of such particles in space is proposed to be from silicone contaminants, which transform under effects of space environment into particles.

The purpose of the present work is classified in the following two items;

1. to find out the formation process of the SiO_2-based microparticles derived from silicone contaminants, which compare with the results of the MPAC experiment, and
2. to make a model and demonstrate small space debris formation process with the results of SiO_2-based microparticles formation from silicone contaminants under irradiations of UV and/or AO through simulating the conditions in space.

1.6.2 Outlines of the Thesis Content

Chapter 1 “General Introduction” presents summary about space debris, space environment, space debris’ origin and possible damages to spacecraft. And, it is also explained that small-sized space debris can cause serious damages to spacecraft and thus are required mitigation. For the reduction of small space debris with size less than 1 mm, it is indispensable to understand their origin, which is mainly unclear at present as shown in this chapter. The author’s past work on capturing SiO_2-based microparticles of unknown origin is introduced in this chapter, and the purpose of clarifying the origin of these microparticles is established.

Chapter 2 “Space Exposure Experiments” introduces the instance of space exposure experiments which were operated to study a variety space environmental effects, micrometeoroid, space debris and contaminants detected on the retrieved materials.

Chapter 3 “Chemical Changes of Silicone Contaminants” focuses on the chemical changes of silicone contaminants affected with UV and/or AO for clarifying the formation process of microparticle space debris. The details of experimental procedures and conditions are described in this chapter. In addition, the facilities and equipment which were used in the experiments for obtain clues for clarifying the formation process of microparticle space debris are also explained in this chapter.

Chapter 4 “Morphological Changes of Silicone Contaminants” focuses on the morphological changes of silicone contaminants affected with UV and/or AO for clarifying the formation process of microparticle space debris. The results of the experimental investigation on the effects of UV and/or AO to silicone contaminants deposited on polyimide films from the viewpoint of morphological changes are indicated in this chapter.

Chapter 5 “Modeling of the Formation Process of Microparticle Space Debris from Silicone Contaminants” shows the formation process modeling of microparticle space debris which was based on the results of chemical and morphological changes of silicone contaminants affected with UV and/or AO investigated in Chapter 3 and Chapter 4.

Chapter 6 “Comparison of the Microparticles Obtained in the Present Work with the Ones Captured on Orbit” compares the microparticles captured on orbit with the microparticles produced experimentally in the present work. The purpose of the comparison is to study the microparticles produced experimentally are actually produced on orbit or not.

Chapter 7 “General Conclusion” concludes the research results on the microparticles space debris derived from silicone contaminants affected with UV and/or AO.

References

(1-1) G.A. Graham, N. Mcbride, A.T. Kearsley, G. Drolshagen, S.F. Green, J.A.M. Mcdonnell, M.M. Grady, and I.P. Wright, "The Chemistry of Micrometeoroid and Space Debris Remnants Captured on HUBBLE Space Telescope Solar Cells," *Int. J. Impact Engng*, **26** (2001) pp.263-274.

(1-2) G. Drolshagen, T. McDnnell, Jean-Claude Mandeville,and A. Moussei, "Impact Studies of the HST Solar Arrays Retrieved in March 2002," *Acta Astrinautica*, **58** (2006) pp.471-477.

(1-3) V.E. Skurat, I.O. Leipunsky, I.O. Volkov, P.A. Pshechenkov, and N.G. Beriozkina, "Changes of Solar Array Surfaces on Orbital Station Mir," *J. Spacecraft and Rockets*, **48** (1) (2011) pp. 53-58.

(1-4) S.G. Love, D.E. Brownlee, N.L. King, and F. Horz, "Morphology of Meteoroid and Debris Impact Craters Formed in Soft Metal Targets on the LDRF Satellite," *Int. J. Impact Engng*, **16** (3) (1995) pp.405-418.

(1-5) G.Drolshagen, J.A.M. McDonnell, T.J.Stevenson, S. Deshpande, L. Kay, W.G. Tanner, J.C. Mandevulle, W.C. Carey, C.R. Maag, A.D. Griffiths, N.G. Shrine, and R. Aceti, "Optical survey of micrometeoroid and space debris impact features on EURECA," *Planetary and Space Science*, **44** (4) (1996) pp.317-340.

(1-6) Inter-Agency Space Debris Coordination Committee (IADC), "Support to the IADC Space Debris Mitigation Guidelines," IADC-04-06, (2014).

(1-7) H. Klinkrad, "SPACE DEBRIS -Models and Risk Analysis-," Praxis Publishing, (2006) pp.5, 22, 27-47.

(1-8) National Research Council, "ORBITAL DEBRIS -A Technical Assessment-," National Academy Press, (1995) pp.1-9.

(1-9) National Research Council, "ORBITAL DEBRIS -A Technical Assessment-," National Academy Press, (1995) pp.17-30.

(1-10) Inter-Agency Space Debris Coordination Committee (IADC), "Space Debris - IADC Assessment Report for 2010," IADC-11-04, (2010).

(1-11) Orbital Debris Quarterly News, **20** (1 & 2) (2016).

(1-12) M.L.R. Walker, R.P. Russell, and L.A. Singh, “Utilization of Residual Helium to Extend Satellite Lifetimes and Mitigate Space Debris,” *J. Propulsion and Power*, **28** (6) (2012) pp.1406-1412.

(1-13) Inter-Agency Space Debris Coordination Committee (IADC), “Sensor Systems to Detect Impacts on Spacecraft,” IADC-08-03, (2013).

(1-14) E.L. Christiansen, J.L. Hyde, and R.P. Bernhard, “Space Shuttle Debris and Meteoroid Impacts,” *Advances in Space Research*, **34** (2004) pp.1097-1103.

(1-15) G. Drolshagen, “Impact Effects of Small Size Meteoroids and Space Debris,” *Advances in Space Research*, **41** (2008) pp.1123-1131.

(1-16) B.A. Banks, A. Snyder, S.K. Miller, and K.K. de Groh, “Atomic-Oxygen Undercutting of Protected Polymers in Low Earth Orbit,” *J. Spacecraft and Rockets*, **41** (3) (2004) pp. 335-339.

(1-17) B.A. Banks, K.K. de Groh, and S.K. Miller, “Low Earth Orbital Atomic Oxygen Interactions with Spacecraft Materials,” NASA/TM-2004-213400, (2004).

(1-18) E. Grossman, I. Gouzman, and R. Verker, “Debris/Micrometeoroid Impacts and Synergistic Effects on Spacecraft Materials,” *MRS bulletin,* **35** (01) (2010) pp.41-47.

(1-19) Y. Kimoto, J. Ishizawa, E. Miyazaki, and M. Suzuki, “SM/MPAC&SEED Experiment Overview,” *Proc. International Symposium on “SM/MPAC & SEED Experiment,* JAXASP-08-015E, (2008) pp.5-9.

(1-20) M.J. Neish, K. Imagawa, T. Inoue, J. Ishizawa, Y. Kitazawa, Y. Yamaura, A. Murakami, and Y. Och, “Microparticle Capture on the International Space Station Using Aerogel and Polyimide Form,” *Proc. the International Symposium on Materials in a Space Environment*, ESA SP-540, (2003) pp.431-435.

(1-21) R. Yamanaka, T. Noguchi, and Y. Kimoto, “Analysis Results of SM/MPAC Experiment Samples,” *J. Spacecraft and Rockets*, **48** (5) (2011) pp.867-873.

(1-22) T. Noguchi, T. Nakamura, T. Ushikubo, N.T. Kita, J.W. Valley, R. Yamanaka, Y. Kimoto, and Y. Kitazawa, “A Chondrule-like Object Captured by Space-exposed Aerogel on the International Space Station,” *Earth and Planetary Science Letters*,

309 (2011) pp.198-206.

(1-23) J. Dever, B. Banks, K.de Groh, and S. Miller, "Degradation of Spacecraft Materials. Handbook of Environmental Degradation of Materials," *William Andrew Publishing*, (2005) pp.465-501.

(1-24) F. Urayama, K. Yano, R. Yamanaka, E. Miyazaki, and Y. Kimoto, "Molecular Contamination Assessment on Hinode Solar Optical Telescope," *J. The Japan Society for Aeronautical and Space Sciences*, **56** (658) (2008) pp.543-550.

(1-25) ASTM Standard, "Standard Test Method for Total Mass Loss and Collected Volatile Condensable Materials from Outgassing in a Vacuum Environment," E-595, (1996).

(1-26) ASTM Standard, "Standard Test Method for Contamination Outgassing Characteristics of Spacecraft Materials," E-1559, (2014).

(1-27) K. Kuriki, M. Takei, N. Wakasugi, and T. Yasaka, "Meteoroid and Space Debris Impact Investigation in SFU Post Flight Analysis Activities: Preliminary Results and Further Directions," *The Institute of Space and Astronautical Science Report No.666,* (1997) pp.5.

(1-28) ASTM Standard, "Standard Solar Constant and Zero Air Mass Solar Spectral Irradiance Tables," E-490-00a, (2014).

(1-29) K. Mori, and E. Miyazaki, "Evaluations of Polymeric Materials in Space Environment for Space Use," *Nippon Gomu Kyokaishi*, **86** (12) (2013) pp.367-372. (in Japanese)

(1-30) J.A. Dever, "Low Earth Orbital Atomic Oxygen and Ultraviolet Radiation Effects on Polymers," NASA Technical Memorandum 103711, (1991).

(1-31) H. Inokuchi, "Science for Space Utilization Research," Syokabo, (2000). (in Japanese)

(1-32) NASA, "U.S. Standard Atmosphere, 1976," NASA-TM-X-74335, (1976) pp.13.

(1-33) B.A. Banks, S.K. Rutledge, B.M. Auer, and F. DiFilippo, "Atomic oxygen undercutting of defects on SiO_2 protected polyimide solar array blankets," NASA CP-19910065180, (1990) pp.15-33.

(1-34) T.K. Minton, and D.J. Garton, “Dynamics of Atomic-oxygen-induced Polymer Degradation in Low Earth Orbit” in “Chemical Dynamics in Extreme Environments,” World Scientific, (2001) pp.420-489.

(1-35) P.T. Chen, “Contamination Effects due to Space Environmental Interactions,” *39th Aerospace Science Meeting & Exhibit, AIAA*, (2001) pp.1-11.

(1-36) ASTM Standard, “Standard Practices for Ground Laboratory Atomic Oxygen Interaction Evaluation of Materials for Space Application,” E-2089-00, (2014).

(1-37) M. Onishi, J. Abe, J. Ishizawa, M. Iwata, A. Okamoto, S. Okamoto, H. Kawasaki, A. Kobayashi, Y. Shinozaki, H. Sugita, M. Tagawa, S. Tachikawa, Y. Tanaka, K. Toyota, H. Nagano, T. Harada, I. Mase, S. Miyazaki, K. Mori, T. Yamada, and R. Yamanaka, “Thermal Design of Spacecraft,” The University of Nagoya Press, (2014). (in Japanese)

(1-38) NASA, “U.S. Standard Atmosphere, 1976,” NASA-TM-X-74335, (1976) pp.15.

(1-39) E. Grossman, and I. Gouzman, “Space Environment Effects on Polymers in Low Earth Orbit,” *Nucl. Instr. and Meth. in Phys. Res,* B 2008 (2003) pp.48-57.

Chapter 2:

Space Exposure Experiments

2.1 Introduction

All spacecraft are not only effected by space environment but also collide with meteoroid and space debris. Consequently, surfaces of spacecraft returned to the Earth are found to have many small craters resulting from impacts of meteoroid and space debris. Most of craters are too small to have any effects on the operation of spacecraft. However, important clues can be obtained about the origin and abundance of microparticles by examining them.

Therefore, various space exposure experiments have been operated to study a variety space environmental effects including impacts of meteoroid and space debris, deposition of contaminants, UV light exposure, AO exposure and so on. Space exposure experiments can also evaluate combined environmental effects of them.

2.2 World Wide Space Exposure Experiments

2.2.1 Long Duration Exposure Facility

The space shuttle Challenger placed the LDEF in LEO in April, 1984, and the space shuttle Columbia retrieved it in January, 1990 [(2-1), (2-2)]. Consequently, LDEF was placed in LEO for 5.7 years[(2-1), (2-2)]. LDEF was a 14-faced (i.e., a 12-sided cylinder and two ends), gravity-stabilized spacecraft that was host to 57 individual scientific experiments[(2-1), (2-2)]. Several of these experiments were designed to characterize various aspects of micrometeoroid and space debris environment during the nominal nine month mission[(2-2) - (2-5)]. However, as a result of LDEF's unexpectedly long exposure time (5.7

years) and the heightened awareness of the man-made debris collisional threat, it was decided to utilize the entire spacecraft as a micrometeoroid and space debris detector.

As a result of the gravity-gradient stabilized orbital nature of LDEF (i.e., the same general surface pointed into the velocity vector during the entire mission), the large exposed surface area (about 150 m^2) of LDEF provided a unique source of information concerning the LEO particulate environment and associated directionality effects for both natural and man-made particles[2-6]. Over 20,000 impacts have been documented on LDEF, approximately 1,000 of which have been chemically analyzed in an attempt to determine the origin of the projectile. The largest impact crater on the LDEF was 5.7 mm in diameter. And, silica and/or methyl silicone were detected on most external surfaces of the retrieved LDEF[2-7]. Fig. 2-1 shows the image of LDEF referred from NASA's web site.

Fig. 2-1. LDEF.

2.2.2 Solar Array of Hubble Space Telescope

One of the first solar array wing "-V2" of HST was retrieved in 1993 from the LEO after being exposed to hypervelocity impacts (micrometer to millimeter scale) from both micrometeoroids and space debris[2-8]. The first survey of creators between 100-1000 μm showed micrometeoroid remnants are dominant, while the second survey of creators between 10-100 μm identified almost space debris which contain aluminum and aluminum oxide residues[2-8), (2-9]. The image of HST is shown in Fig. 2-2 referred from NASA's web site.

Both second solar array wings of HST have a total exposed area of 40 m^2 covered by solar cells[2-10]. After they had been operated in orbit at an attitude 600 km for 3,011 days (8.24 years), they were retrieved by the space shuttle Columbia in March 2002 and the most outer surface of them were surveyed[2-10]. Fig. 2-3 shows front-top impacts smaller than 1 mm in diameter on HST solar cells[2-10].

Fig. 2-2. HST.

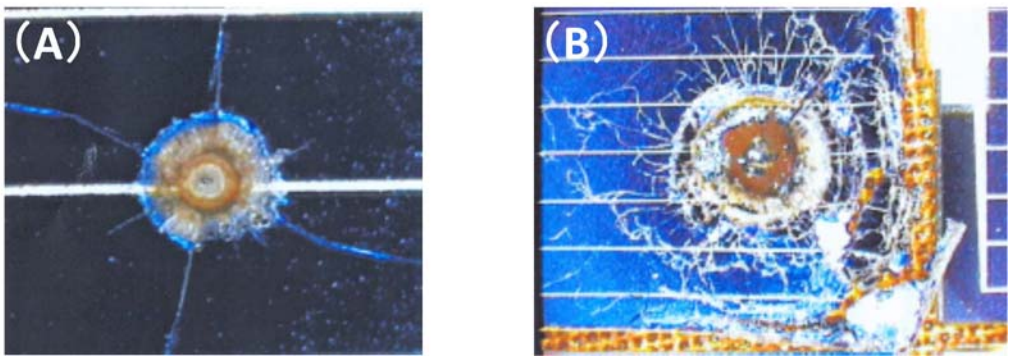

Fig. 2-3. Front-top impacts[2-10].

(A) Front-top impact on HST solar cell. Size 0.8mm, and (B) one of the biggest perforations caused by an impact on the front side (clear hole diameter ≒ 1 mm).

2.2.3 European Retrievable Carrier

EURECA had been released from the space shuttle Atlantis on August 1992 at an initial altitude of 426 km, was boosted to 502 km, and was returned from space in June 1993 by the space shuttle Endeavor after almost 11 months in the LEO[2-6), (2-11) - (2-13)]. The image of EURECA is shown in Fig. 2-4 referred from ESA's web site. The total exposed surface of EURECA was about 140 m^2 [2-6]. All outer surfaces (mainly Multi Layer Insulation blankets and front and rear sides of solar arrays) were surveyed, the impact features on them were measured, and the impacts whose diameter ranges from about 30 μm to 6.5 mm were recorded[2-6]. Since the impacts on the cover glass of the solar cell are detected easily, the 225 out of 703 impacts showed signs of directionality on these glass surfaces[2-6]. Consequently, a large number of impact features have been documented[2-6), (2-12)]. Contaminants were analyzed by using **i**nfra**r**ed (IR) spectroscopy, **e**nergy **d**ispersive **X**-ray (EDX) spectroscopy and electron spectroscopy for chemical analysis[2-13]. Most contaminants underwent a high degree of carbonization which was induced by chemical processes (dehydrogenation), which resulted browning on all over the spacecraft. And, the surface of the spacecraft was deposited with silica formed by AO degradation of outgassed siloxane[2-13]. The IR spectra show always the presence of siloxane, and often C=O (1700 cm-1), CH_2 and CH_3 (2930 cm^{-1}, 2960 cm^{-1}) [2-13]. The

surfaces which were not exposed to UV were not detected a measurable contamination level[2-13].

Fig. 2-4. EURECA captured by the space shuttle Endeaver.

2.2.4 MIR Environmental Effects Payloads

MIR **E**nvironmental **E**ffects **P**ayloads (MEEP) was installed on the MIR docking module on March 1996 during STS-76 and retrieved on October 1997 by STS-86 after 18 months exposure to Mir space environment in a 390km orbit[2-14) - (2-16]. MEEP consist of four **P**assive **E**xperiment **C**ontainer**s** (PECs) which housed the experiment trays. Four PECs consists of **P**olished **P**late **M**icrometeoroid **D**etector (PPMD), the **P**assive **O**ptical **S**ample **A**rray **1** (POSA 1), POSA 2, and the **O**rbital **D**ebris **C**ollector [2-15].

Both of the Mir-facing side of POSA 1 and the space-facing side of POSA 1 were visibly contaminated. Electron spectroscopy for chemical analysis with depth profiling clarified the presence of 250 – 315 Å silicate on the Mir-facing side with few

impurities. And it was confirmed the presence of 5000 - 10000 Å silicate whose density is 1.0 g/cm^3 on the space-facing side of POSA 1 by electron spectroscopy for chemical analysis with depth profiling[2-16].

2.2.5 Materials International Space Station Experiment and Others

Thousands of materials have been tested by **M**aterials **I**nternational **S**pace **S**tation **E**xperiment (MISSE) series. They are in order to test how spacecraft materials withstand the harsh space environment including solar radiation, AO erosion, thermal cycling, micrometeoroid and space debris impacts, and contamination from spacecraft[2-17) - (2-19].

MISSE-1 and -2 are testbeds for more than 400 materials and coatings samples. Both MISSE-1 and -2 were deployed in August 2001 during the STS-105 mission and were retrieved to the Earth in August 2005 after approximately four years exposure to space environment on the ISS[2-17), (2-18]. Coated polyimide film sample was mounted on MISSE-2 for measuring its erosion on orbit[2-19]. Two gold mirror samples mounted MISSE-2 were analyzed with **X**-ray **P**hotoelectron **S**pectroscopy (XPS) to evaluate the composition and thickness of contaminants' layer after four years[2-20]. A contaminants deposited layer of approximately 50 Å was determined by the evaluation of the Ram-facing gold mirror, and the contaminants layer consisted of the elemental composition including carbon, oxygen, silicon, and traces of selenium and magnesium[2-20]. The evaluation of the Wake-facing gold mirror clarified the contaminants deposited layer of approximately 500 Å was formed on the Wake-facing gold mirror, and the elemental composition of the contaminants layer contained carbon, oxygen and silicon[2-20].

MISSE-3 and 4 were deployed in August 2006 and retrieved in August 2007, and the durability of eight materials (73 samples) were examined on MISSE-3 and 4 [2-17].

MISSE-5 was deployed on the ISS from August 2005 until September 2009, and MISSE-5 consisted of the Prototype Communications Satellite 2, Forward Technology Solar Cell Experiment and the Thin Film Material Experiment[2-17]. The Prototype

Communications Satellite 2 was a communication system, the Forward Technology Solar Cell Experiment characterized the durability and the electrical output of 39 advanced solar cell samples, and the Thin Film Material Experiment consists of 254 thin film samples that were attached to the thermal blanket protecting the Prototype Communications Satellite 2 hardware.

MISSE-6 consists of MISSE-6A and 6B. MISSE-6A and 6B were deployed on the ISS during the STS-123 shuttle mission in March 2008, and MISSE-6 was returned to the Earth during the STS-128 shuttle mission in September 2009 after approximately 1.45 years[2-17].

MISSE-7 consists of two PECs, 7A and 7B, and its samples are over 700 new and affordable materials. MISSE-7 were brought to the ISS in November 2009 aboard mission STS-129 and mounted on the outside of the ISS[2-17]. Orientation of PEC 7A will be zenith/nadir (space facing/Earth facing) and orientation of PEC 7B will face Ram/Wake (front/rear) relative to the ISS orbit. MISSE-7 were return to the Earth during the STS-134 mission in June 2011[2-17].

Details of MISSE series are described by Groh et al. (2009)[2-17], Finckenor (2006)[2-18], Miller et al. (2010)[2-19], and Soares et al. (2012)[2-20].

According to NASA's web site, MISSE-8 was launched in May 2011 by the STS-134, and was returned by SpaceX Dragon capsule as part of the SpaceX cargo resupply mission 3 in May 2014.

Images of MISSE-1 and MISSE-2 are shown in Fig. 2-5.

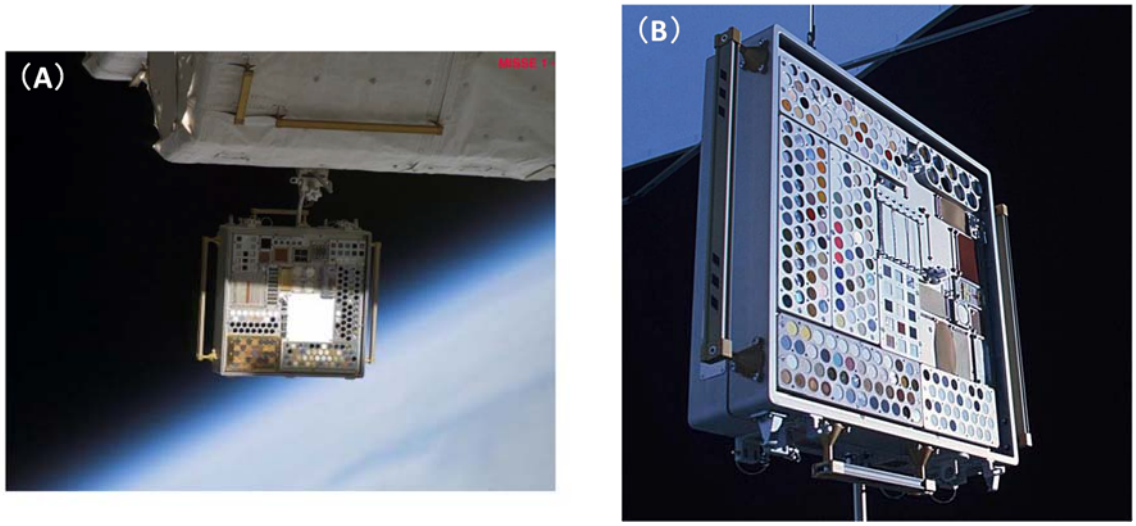

Fig. 2-5. MISSE-1 and MISSE-2 [2-18].

(A) MISSE-1, and (B) MISSE-2.

Japan had planned and operated other materials space exposure experiments[2-21] - [2-23]. They and new Japanese space exposure experiment feature are introduced in below.

Evaluation of **O**xygen **I**nteraction with **M**aterials-3 (EOIM-3) is the first Japanese materials exposure experiment. EOIM-3 was launched on STS-46 (the space shuttle Atlantis) on July 1992, and returned to the Earth on August 1992 [2-21], [2-22]. The experiment was participated in NASA's materials space exposure project, and 26 kinds of 46 Japan's material samples were mounted[2-21]. The purpose of EOIM-3 were to confirm effect of space environment on the surface of materials and to find out the degradation mechanism of space environment especially AO[2-21], [2-22].

Space **F**lyer **U**nit (SFU) was launched by the H-2 rocket on March 1995 and retrieved by STS-72 (the space shuttle Endeavour) on January 1996 after 301 days exposure to space environment[2-21], [2-23]. The altitude of the satellite was approximately 480 km, and 170 hypervelocity impacts from micrometeoroid and space debris were detected and documented[2-23]. Fig. 2-6 is the image of SFU spacecraft captured by the robot arm of the space shuttle referred from JAXA's web site.

The **M**anipulator **F**light **D**emonstration (MFD) was planned to demonstrate the functions and performance of a robot arm using the space shuttle prior to a JEM launch.

The **E**valuation of **S**pace environment and **E**ffects on **M**aterials (ESEM) is one of piggyback experiments, and its purposes are “to confirm materials durability against LEO environment” and “to capture cosmic dusts with a dust collectors”. MFD-ESEM was launched on 7 August 1997 and retrieved on 19 August 1997 by STS-85 (the space shuttle Discovery) after 12 days exposure at the altitude of 316 km [2-21]. As a result, two space debris were captured by MFD-ESEM[2-23]. The image of Fig. 2-7 is MFD on the space shuttle referred from JAXA’s web site.

Exposed Experiment **H**andrail **A**ttachment **M**echanism (ExHAM) is a new Japanese space exposure experiment feature. According to JAXA’s web site, the size of ExHAM is W100 mm X H100 mm X D20mm, and enables space exposure experiments in space environment by attaching it on to the Japanese experiment module Kibo’s exposed facility. After space experiment is over, ExHAM can be retrieved by using the Kibo’s robotic arm and returned to the Earth. First 6 space exposure experiments using ExHAM had finished, and they were returned to the Earth. Evaluation of the retrieved samples are now ongoing. Fig. 2-8 is the image of ExHAM on orbit referred from JAXA’s web site.

Fig. 2-6. SFU spacecraft captured by the robot arm of the space shuttle.

Fig. 2-7. MFD on the space shuttle.

Fig. 2-8. ExHAM on orbit.

2.3 The Russian Service Module / Micro-Particles Capturer & Space Environment Exposure Device Experiment

The **M**icro-**PA**rticles **C**apturer & **S**pace **E**nvironment **E**xposure **D**evice (MPAC&SEED) experiment units were deployed on SM of the ISS on October 2001[2-24), (2-25)]. The units consisted of three identical units, and they were retrieved after 315 days, 865 days, and 1403 days, respectively[(2-25)]. The first, second and third retrieved units are described as #1, #2 and #3 in this thesis. Fig. 2-9 shows the images of SM/MPAC&SEED units on orbit, and Fig. 2-10 shows the image of an SM/MPAC&SEED unit with both Ram side (front of the ISS) and Wake side (rear of the ISS). The size of an SM/MPAC&SEED unit is W570 mm x H900 mm x D158 mm [(2-25)]. All samples of the MPAC experiment and the SEED experiment were installed on the SM/MPAC&SEED units.

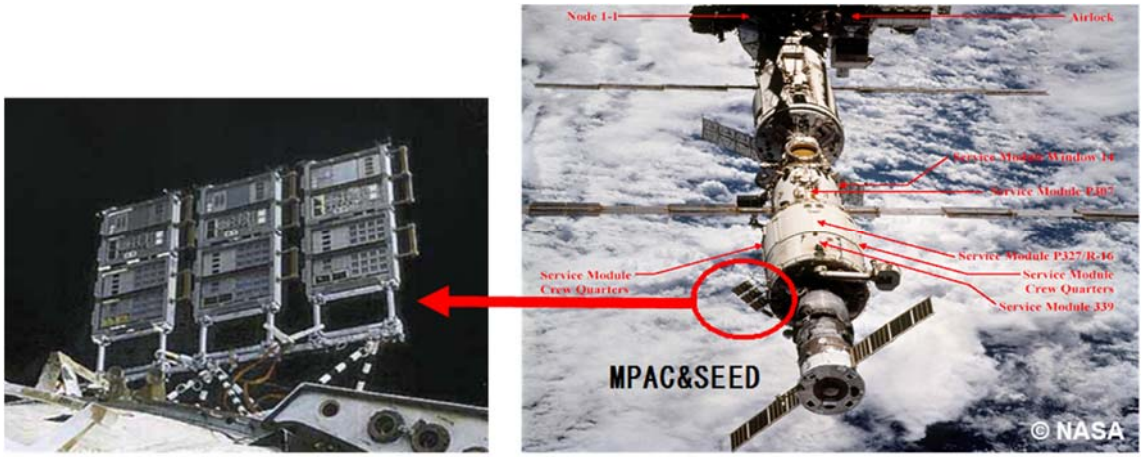

Fig. 2-9. SM/MPAC&SEED units on orbit.

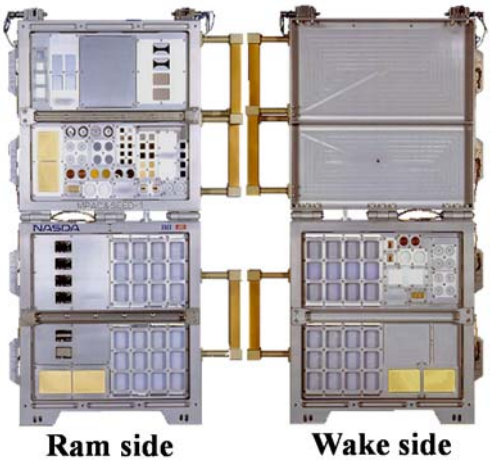

Fig. 2-10. An SM/MPAC&SEED unit with both Ram side (front of the ISS) and Wake side (rear of the ISS).

2.3.1 Space Environment

The SM/MPAC&SEED experiment units were deployed on SM of the ISS, which mean that the units were exposed to space environment attitude approximately 400 km. For monitoring space environments, three kinds of space environment monitoring samples (Vespel for AO fluence monitoring, polyurethane for UV fluence monitoring, and alanine dosimeter for total ionizing dose monitoring) and thermal tapes were mounted on the SM/MPAC&SEED experiment units[2-26]. Table 2-1 is a summary of environmental conditions for the flight samples by the evaluation results of retrieved space environment monitoring samples, and **S**pace **E**nvironment & **E**ffects **S**ystem (SEES) simulations[2-26), (2-27].

Table 2-1. Environmental conditions for the flight samples.

		Ram side			Wake side		
		Flight #1	Flight #2	Flight #3	Flight #1	Flight #2	Flight #3
Exposure duration, days		315	865	1403	315	865	1403
AO fluence, atoms/cm^2	Vespel	2.04 X 10^{20}	2.57 X 10^{20}	2.70 X 10^{20}	1.61 X 10^{20}	2.05 X 10^{20}	3.09 X 10^{20}
	SEES	2.85 X 10^{21}	5.70 X 10^{21}	8.41 X 10^{21}	-	-	-
UV fluence, ESD	Polyurethane	18.1	15.8	13.4	122	201	205
	SEES	73.8	167	271	-	-	-
Total ionizing dose※, Gy	Alanine dosimeter	1.95	15.3	32.0	3.5	21.9	58.3
	SEES	67.6	181	234	-	-	-
Maximum temperature※※, ℃		60	90	90	-	-	-

※ Shield thickness; 0.04 g/cm^2

※※ Temperature at approximately 1 mm depth

2.3.2 MPAC Experiment

The MPAC units had been developed to examine the abundance and composition of micrometeoroid and space debris, and then deployed on the ISS along with SEED units[(2-25), (2-28) , (2-29)]. Silica aerogel (hereafter "aerogel"), polyimide form with polyimide film and aluminum plate were mounted as materials for the SM/MPAC experiment[(2-28), (2-29)]. Aerogel was mounted in order to capture micrometeoroid and space debris and analyze its composition, collision energy and direction of approach[(2-29)]. By examining the 144 pieces of retrieved aerogel, it was found that those pieces had captured micro-debris, secondary debris, a micrometeoroid, and many microparticles of ac. 10 μm in diameter of unknown origin (shown in Chapter 1 Section 1.3) [(2-29), (2-30)]. The microparticles were consequently analyzed to determine their origin by using an XMA and a microscope FT-IR spectroscopy[(2-29)]. Fig. 2-11 shows the XMA spectra of microparticles (Fig. 2-11 (A) and (B)) and the adhesive (Fig. 2-11 (C)) which was used for bonding the micro-particles, and the Microscopic FT-IR spectra of microparticles are shown in Fig. 2-12 (A) and (B) [(2-29)]. The results of analysis revealed that carbon (C), oxygen (O), and silicon (Si) were detected, all of the analyzed microparticles had Alkanes, CO, Si-CH_3, Si-O-Si bonds and hydroxyl group. And, silicon dioxide (SiO_2) was the main container of the microparticles. However, the origin of the microparticles had not been led to elucidation.

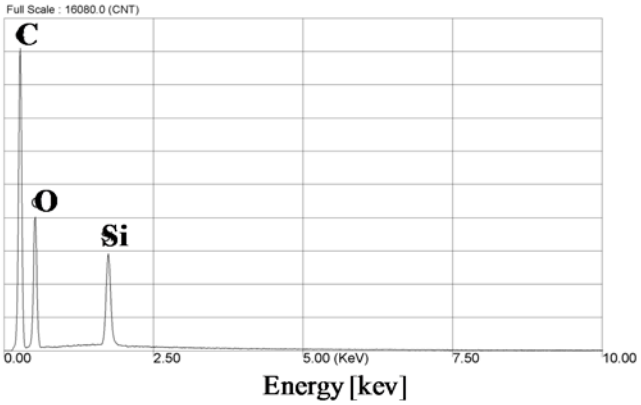

(A)

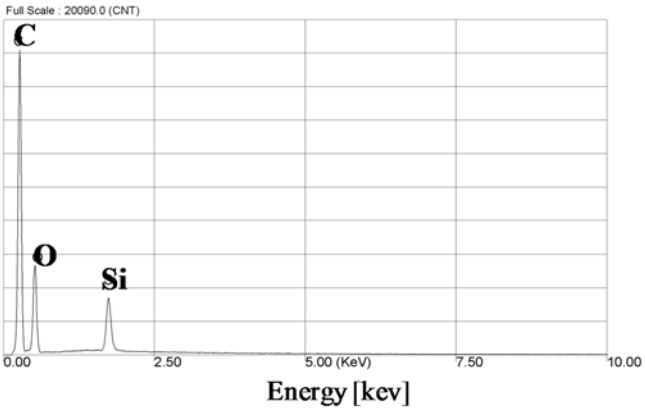

(B)

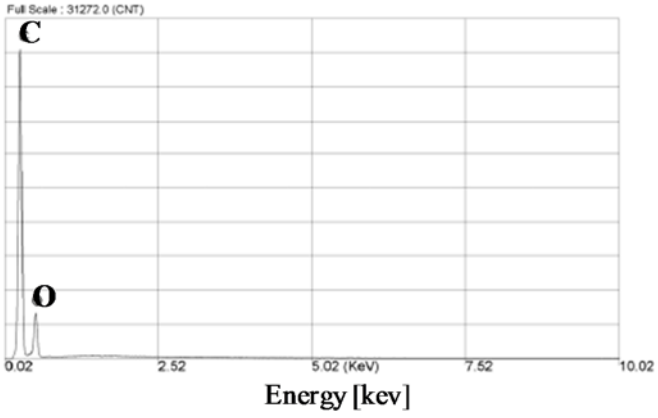

(C)

Fig. 2-11. XMA spectra of the microparticles captured by the SM/MPAC experiment[2-29].

(A) XMA spectrum of the microparticle on Ram side, (B) XMA spectrum of the microparticle on Wake side, and (C) XMA spectrum of the adhesive.

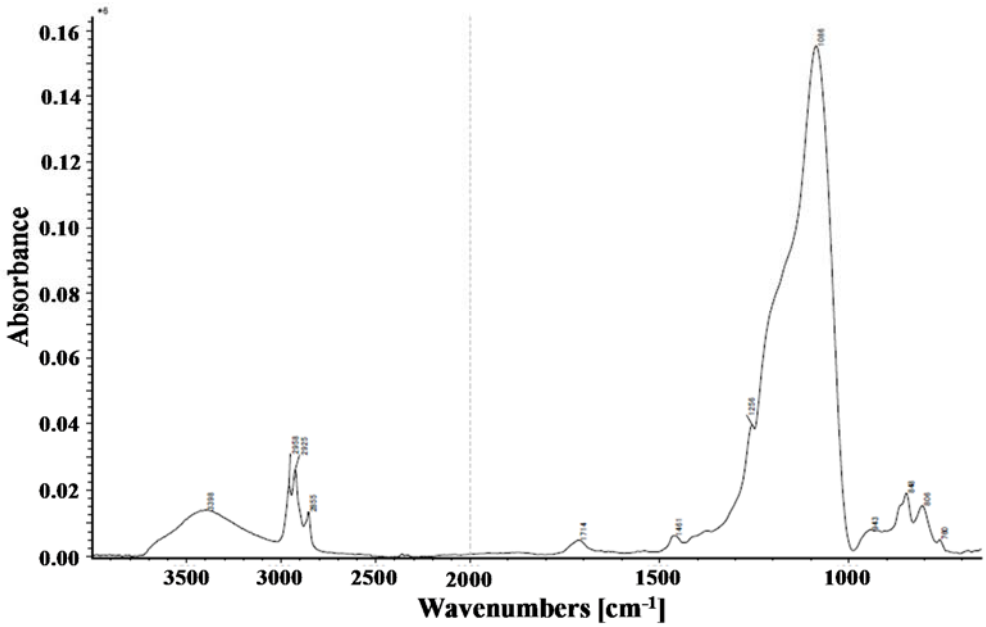

(A)

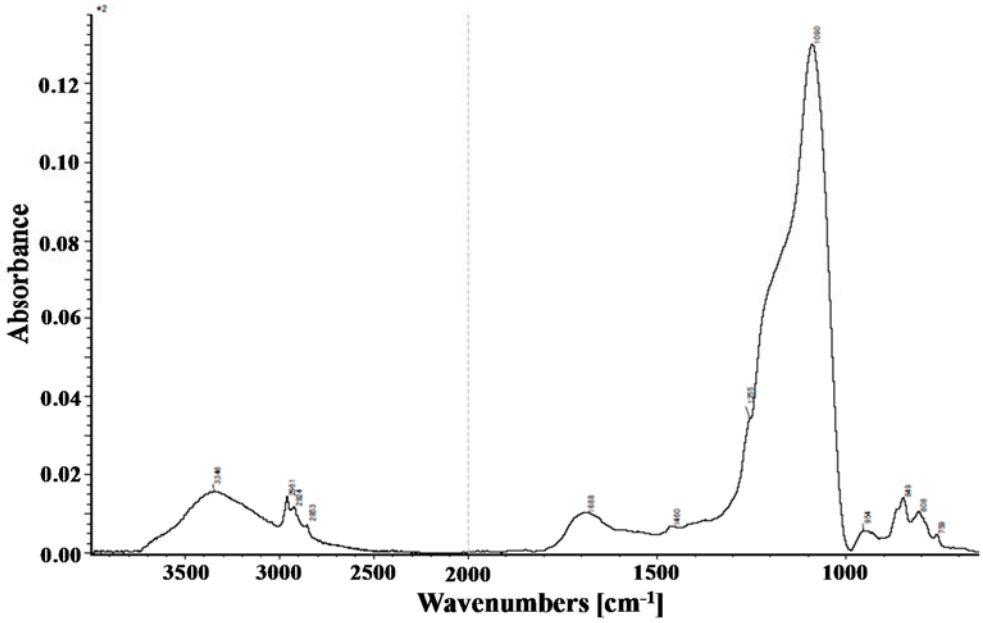

(B)

Fig. 2-12. Microscopic FT-IR spectra of the microparticles captured by the SM/MPAC experiment[2-29].

(A) FT-IR spectrum of the microparticle on Ram side and (B) FT-IR spectrum of the microparticle on Wake side.

2.3.3 SEED Experiment

The SEED experiment unit had been developed to examine the effects of space environment to materials[2-25]. 28 samples were mounted as materials for the SM/SEED experiment (shown in Table 2-2) [2-25].

One of the SEED samples **f**lexible **o**ptical **s**olar **r**eflector (F-OSR), which has characteristics of low solar absorptance αs and high infrared emittance ε with flexibility, is a thermal control film for spacecraft[2-31]. The F-OSR for SEED sample consists of five layers and its size was ϕ 25 mm in diameter with 100 μm thick[2-31]. Two pieces of the F-OSR were mounted on SM/MPAC&SEED units, respectively[2-31]. The investigation of retrieved F-OSRs resulted that thermo-optical properties show no significant changes and the new layer was formed, and the new layer's main components were carbon, silicon and oxygen by **S**canning **T**ransmission **E**lectron **M**icroscope / **E**nergy **D**ispersive **X**-ray (STEM-EDX) analysis[2-31]. The transmission **e**lectron microscopy images of the cross section of the F-OSRs shown in Fig. 2-13 clarified the formation of the new layer on the surface of F-OSR, and the thicknesses of the new layer of #1, #2 and #3 sample were approximately 20nm, 80nm and 12nm, respectively[2-31]. EDX spectrum of the new layer are shown in Fig. 2-14[2-31].

Table 2-2. Samples of the SM/SEED experiment.

Sample name	Organization	Main Use
CF/polycyanate, PIXA	Fuji Heavy Industries Ltd.	Structural materials
CF/PIXA		
PEEK (loaded & unloaded)	Hokkaido University	Deployable structures
AlN	Tokyo Institute of Technology	Structural and functional materials
SiC (reaction sintering)		
SiC (Hot pressed)		
TiN coated Al		
TiN-coated Al_2O_3		
Ball-bearing (3 types)	Tohoku University	Mechanism application
SUS304	National Institute for Lubrication Materials Science	Lubrication
Cu-coated SUS304		
CuBN-coated SUS304		
TiN-coated SUS304		
MoS_2-coated SUS304		
MoS_2-coated Ti alloy	IHI Aerospace	Lubrication
Polyimide film (UPILEX-S) (loaded & unloaded)	Japan Aerospace Exploration Agency	Deployable structures
Modified polyimide film		Thermal control
F-OSR		Thermal control
White paint		Thermal control
Adhesive		Adhesion
Potting compound		Potting

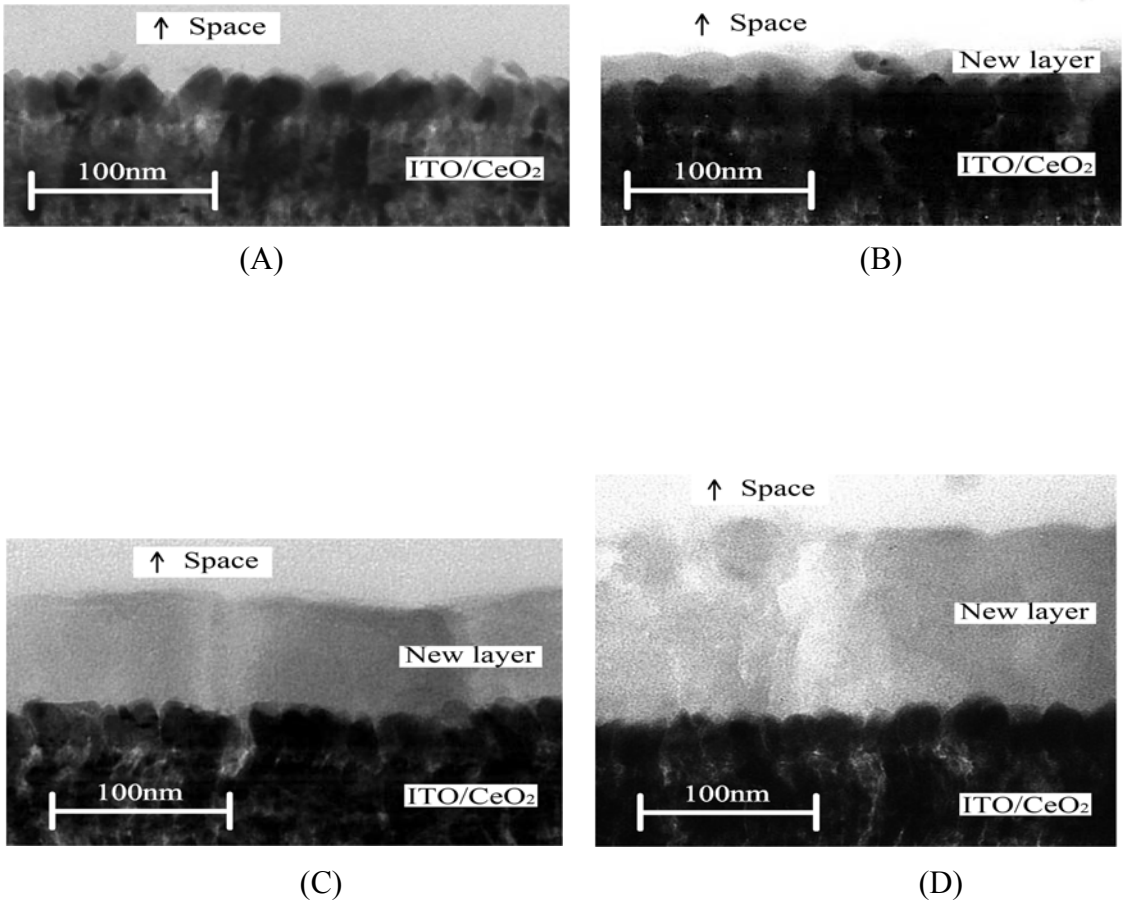

Fig. 2-13. Transmission electron microscope images of the cross section of the F-OSRs[2-31].

(A) Blank sample, (B) #1 sample, (C) #2 sample, and (D) #3 sample.

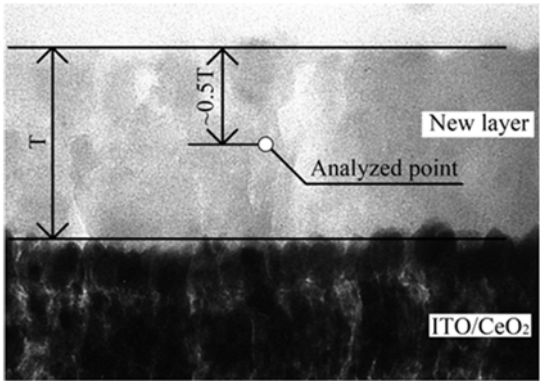

(A)

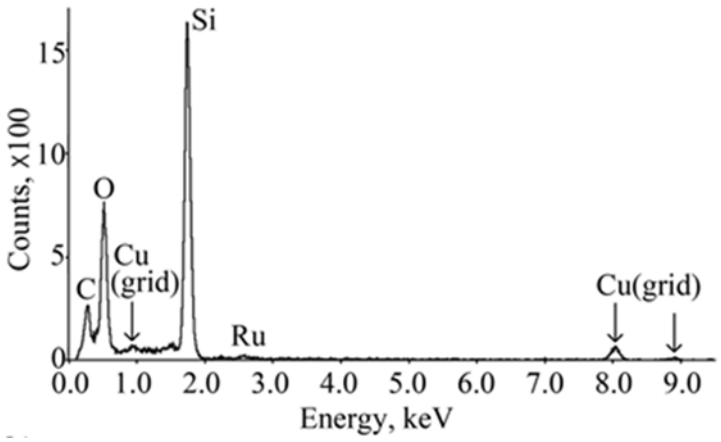

(B)

Fig. 2-14. EDX spectrum of the new layer on the surface of F-OSR[2-31].

(A) Analyzed point and (B) EDX spectrum.

2.4 Conclusion

Japanese space exposure experiment named the SM/MPAC&SEED experiment and other principal space exposure experiments are summarized in this chapter.

Follows are common characteristics between space exposure experiments.

1) A new layer, which was formed on the surface of materials by the deposition of silicone contaminants containing the elements of C, O, and Si in common.
2) A number of impacts, whose sizes are submillimeter in diameter, were detected on the surface of materials.

Additionally, the microparticles which were captured unexpectedly by the aerogel mounted on the MPAC experiment units also contained the elements of C, O, and Si, and the microparticles were based on SiO_2. Moreover, the number of them were increased accompanying with the duration of exposure to space environment.

Characteristics described above mean that there is a possibility that the origin of the microparticles which were captured by the aerogel mounted on the MPAC experiment units is silicone contaminants. Therefore the present work demonstrate that SiO_2-based microparticles can be formed from silicone contaminants in space environment by performing experiments on the ground under the conditions simulating the conditions in space. And, to make clear the connection between the SiO_2-based microparticles captured by the aerogel mounted on the MPAC experiment units and silicone contaminants because it is important to make clear the origin for reducing small space debris and protecting spacecraft against them.

Main points investigation in this chapter and Chapter 1 are open in a paper (2-29) entitled as “Analysis Results of Microparticles Capture Experiment Samples on Service Module.”

References

(2-1) R.L. O'Neal, and E.B. Lightner, "Long Duration Exposure Facility--A General Over View," *Proc. the LDEF-69 Months in Space First Post-Retrieval Symposium*, NASA CP-3134 Part1, (1991) pp.3-48.

(2-2) D.H. Hume, "Large Craters on The Meteoroid and Space Debris Impact Experiment," *Proc. the LDEF-69 Months in Space First Post-Retrieval Symposium*, NASA CP-3134 Part 1, (1991) pp.399–418.

(2-3) C.G. Simon, J.L. Hunter, J.J. Wortman, and D.P. Griffis, "Ion Microprobe Elemental Analyses of Impact Features on Interplanetary Dust Experiment Sensor Surfaces," *Proc. the LDEF-69 Months in Space First Post-Retrieval Symposium*, NASA CP-3134 Part1, (1991) pp.529-548.

(2-4) T.E. Bunch, F.R. diBrozolo, R.H. Fleming, D.W. Harris, D. Brownlee, and T.W. Reilly, "LDEF Impact Creators Formed by Carbon Rich Impactors: A Preliminary Report," *Proc. the LDEF-69 Months in Space First Post-Retrieval Symposium*, NASA CP-3134 Part1, (1991) pp.549-564.

(2-5) M.E. Zolensly, H.A. Zook, F. Hörz, D.R. Atkinson, .R. Coombs, A.J. Watts, C.B. Dardano, T.H. See, C.G. Simon, and W.H. Kinard, "Interim Report of the Meteoroid and Debris Special Investigation Group," *Proc. the LDEF-69 months in Space Second Post-Retrieval Symposium*, NASA CP-3194 Part 2, (1992) pp.277-302.

(2-6) G. Drolshagen, J. A. M. McDonnell, T.J. Stevenson, S. Deshpande, L. Kay, W.G. Tanner, J.C. Mandeville, W.C. Carey, C.R. Maag, A.D. Griffiths, N.G. Shrine, and R. Aceti, "Optical Survey of Micrometeoroid and Space Debris Impact Features on EURECA," *Planetary and Space Science*, **44** (4) (1996) pp.317-340.

(2-7) G.A. Harvey, "Silazane to Silica," *Proc. the LDEF-69 months in Space Second Post-Retrieval Symposium*, NASA CP-3194 Part 3, (1992) pp.797-810.

(2-8) G.A. Graham, N. McBride, A.T. Kearsley, G. Drolshagen, S.F. Green, J.A.M. Mcdonnell, M.M. Grady, and I.P. Wright, "The Chemistry of Micrometeoroid and Space Debris Remnants Captured on Hubble Space Telescope Solar Cells," *Int. J.*

Impact Engng, **26** (1) (2001) pp.263-274.

(2-9) G.A. Graham, A.T. Kearsley, I.P. Wright, M.M. Grady, G. Drolshagen, N. McBride, S.F. Green, M.J. Burchell, H. Yano, and R. Elliot, "Analysis of Impact Residues on Spacecraft: Possibilities and Problems," *Proc. Third European Conference on Space Debris*, ESA SP-437, (2001) pp.197-202.

(2-10) G. Drolshagen, T. McDnnell, Jean-Claude Mandeville, and A. Moussei, "Impact Studies of the HST Solar Arrays Retrieved in March 2002," *Acta Astrinautica*, **58** (2006) pp.471-477.

(2-11) W. Nellessen, "The EURECA Programme Objectives," *EURECA Technical Report*, ESA WPP-069, (1994) pp.13-21.

(2-12) J. A. M. McDnnell, G. Drolshagen, and D.J. Gardner, "EURECA's Exposure in the Near Earth Space Environment. Hypervelocity Impact Creating Distributions at a Time of Space Debris Growth," *Adv.Space Res*, **16** (11) (1995) pp.(11)73-(11)83.

(2-13) M.V. Eesbeek, M.Froggatt, and G. Gourmelon, U. Rieck, H. Kersting, B. Schwarz, and H.J. Rosik, "Post Flight Material Investigation of EURECA Preliminary Findings and Recommendations," *EURECA Technical Report*, ESA WPP-069, (1994) pp.513-527.

(2-14) M.M. Finckenor, R.R. Kamenetzky, and J.A. Vaughn, "Further Investigations of the Passive Optical Sample Assembly (POSA)–I Flight Experiment," *AIAA,* **98** (2001) pp.1-11.

(2-15) G.A. Harvey, D.H. Humes, and W.H.Kinard, "Mir Environmental Effects Payload and Returned Mir Solar Panel Cleanliness," *Proc. SAMPE 44*, (1999) pp.1038-1050.

(2-16) J. M. Zwiener, R. R. Kamenetzky, J. A. Vaughn, and M. M. Finckenor, "Contamination Observed on the Passive Optical Sample Assembly-I (POSA-I) Experiment," *SPIE's International Symposium on Optical Science, Engineering, and Instrumentation. International Society for Optics and Photonics*, (1998) pp.186-195.

(2-17) K.K. de Groh, B.A. Banks, J.A. Dever, D.A. Jaworske, S.K. Miller, E.A. Sechkar,

and S.R. Panko, “NASA Glenn Research Center’s Materials International Space Station Experiments (MISSE 1-7),” NASA/TM-2008-215482, (2009).

(2-18) M.M. Finckenor, “The Materials on International Space Station Experiment (MISSE): First Results from MSFC Investigation,” *44th AIAA Aerospace Sciences Meeting and Exhibit*, (2006) pp.1-9.

(2-19) S.K.R. Miller, and B. Banks, “Degradation of Spacecraft Materials in the Space Environment,” *MRS bulletin*, **35** (2010) pp.1-5.

(2-20) C.E Soares, R. Mikatarian, R. Olsen, A. Huang, C. Steagall, W. Schmidl, B. Wright, and S. Koontz., “External Contamination Control of Attached Payloads on the International Space Station,” *12th International Symposium on Materials in the Space Environment*, (2012).

(2-21) M. Suzuki, H. Shimamura, and K. Imagawa, “Japan’s Material Space Exposure Experiments before SM/MPAC&SEED. *Proc. International Symposium on “SM/MPAC & SEED Experiment”*, JAXASP-08-015E, (2008) pp.1-4.

(2-22) D.E. Brinza, S.Y. Chung, T.K. Minton, and R.H. Liang, “Final Report on the NASA/JPL Evaluation of Oxygen Interactions with Materials-3 (EOIM-3),” NASA CR-198865, (1994) pp.1-26.

(2-23) H. Yano, “Japanese contribution to in-situ meteoroid and space debris measurement in the near Earth space,” *Earth Planets Space*, **51** (1999) pp.1233-1246.

(2-24) F. Imai, and K. Imagawa, “NASDA’s Space Environment Exposure Experiment on ISS –First Retrieval of SM/MPAC&SEED,” *Materials in a Space Environment*, **540** (2003) pp.589-594.

(2-25) Y. Kimoto, J. Ishizawa, E. Miyazaki, and M. Suzuki, “SM/MPAC&SEED Experiment Overview,” *Proc. International Symposium on “SM/MPAC & SEED Experiment”*, JAXASP-08-015E, (2008) pp.5-10.

(2-26) Y. Kimoto, K. Yano, J. Ishizawa, and E.Miyazaki, “Post Retrieval Analysis of Space Environment Monitoring Samples: Radiation Effects, UV, and Atomic Oxygen Fluence,” *Proc. International Symposium on “SM/MPAC & SEED Experiment”*, JAXASP-08-015E, (2008) pp.11-17.

(2-27) H. Shimamura, “Effects of LEO Environment on Mechanical Properties of Polyimide Films Under Tensile Stress,” *Proc. International Symposium on “SM/MPAC & SEED Experiment”*, JAXASP-08-015E, (2008) pp.81-87.

(2-28) M.J. Neish, K. Imagawa, T. Inoue, J. Ishizawa, Y. Kitazawa,Y. Yamaura, A. Murakami, and Y. Och, “Microparticle Capture on the International Space Station Using Aerogel and Polyimide Form,” *Proc. the 9 th International Symposium on Materials in a Space Environment*, ESA SP-540, (2003) pp.431-435.

(2-29) R. Yamanaka, T. Noguchi, and Y. Kimoto, “Analysis Results of Microparticles Capture Experiment Samples on Service Module,” *J. Spacecraft and Rockets*, **48** (5) (2011) pp.867-873.

(2-30) T. Noguchi, T. Nakamura, T. Ushikubo, N.T. Kita, J.W. Valley, R. Yamanaka, Y. Kimoto, and Y. Kitazawa, “A Chondrule-like Object Captured by Space-exposed Aerogel on the International Space Station,” *Earth and Planetary Science Letters*, **309** (2011) pp.198-206.

(2-31) E. Miyazaki, and I. Yamagata, “Results of Space-Environment Exposure of the Flexible Optical Solar Reflector,” *J. Spacecraft and Rockets*, **46** (1) (2009) pp.28-32.

Chapter3:

Chemical Changes of Silicone Contaminants

3.1 Introduction

To obtain clues for clarifying the formation process of microparticle space debris, it is necessary to investigate the effects of UV and/or AO to silicone contaminants on the viewpoint of chemical changes and morphological changes. The followings are procedures to investigate the effects of UV and/or AO to silicone contaminants in the present work and the conceptual diagrams of the experimental procedures are shown in Fig. 3-1.

1) Preparation of materials.
2) Deposition of contaminants on substrate materials.
3) UV and/or AO irradiation to contaminants.
4) Chemical and morphological analysis of samples.

Restriction of these experimental procedures is that samples have to be exposed to the air before the beginning of next procedure. Therefore, it was confirmed that there are no effects of the air to silicone contaminants by using the function of *In-situ* Contamination Spectroscopic Analysis chamber which can in-situ analysis in the air and under vacuum before beginning of the present work.

This chapter deals with the details of experimental conditions and describes about the investigations of chemical changes of silicone contaminants affected with UV and/or AO for clarifying the formation process of microparticle space debris. For the sake of comparison the effects of UV and/or AO to silicone contaminants and confirming that SiO_2 is formed from silicone contaminants with UV and/or AO or not, the irradiation of UV and/or AO to silicone contaminants and detailed investigation were performed. Concretely speaking, FT-IR spectroscopy and **X**-ray **P**hotoemission **S**pectroscopy (XPS) were used for evaluation of chemical changes of silicone contaminants with UV

and/or AO irradiation. As a result, clues for clarifying the formation process of microparticle space debris could be obtained.

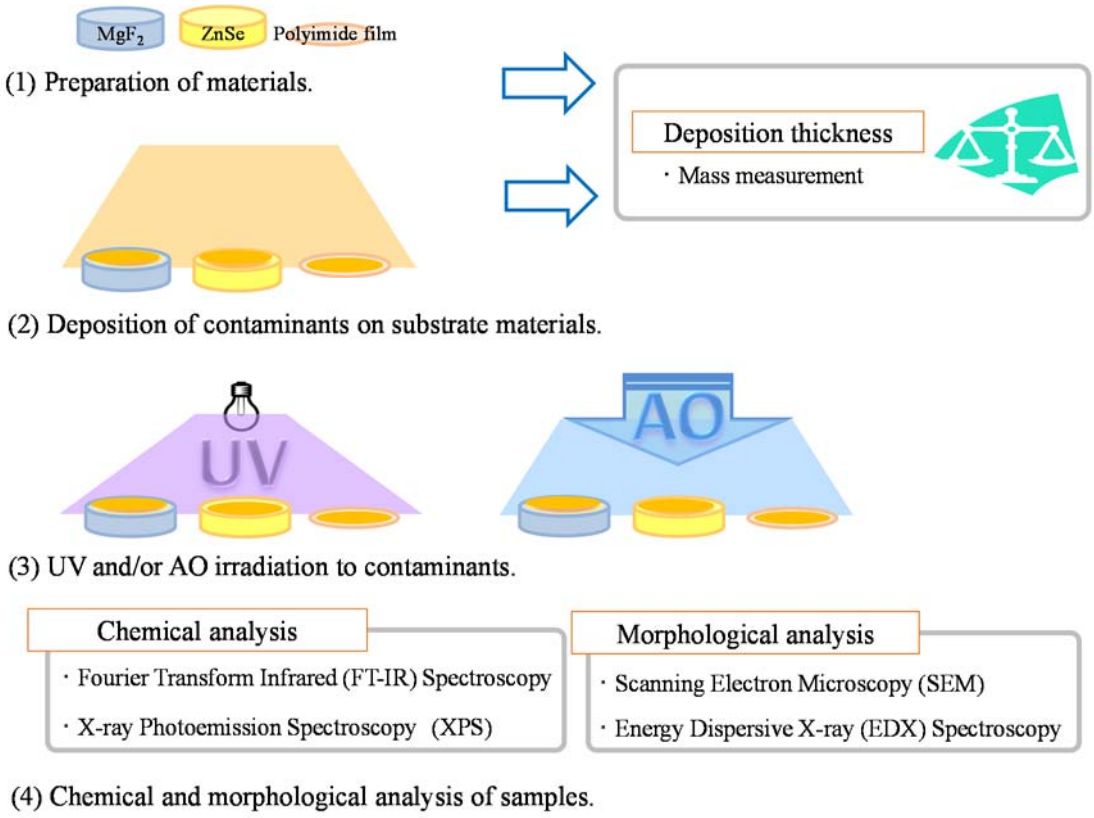

Fig. 3-1. Conceptual diagrams of the experimental procedures.

3.2 Experimental Conditions

Room-temperature-vulcanizing silicon adhesive No. 691 (RTV-S691) from Wacker Asahikasei Silicone Co., Ltd. was selected as a silicone outgassing source because the adhesive is actually designed for a wide range of adhering, sealing, and protection of spacecraft. Two common optical materials of zinc selenide (ZnSe) and magnesium fluoride (MgF_2) were selected as substrate materials deposited by silicone contaminants from RTV-S691. The silicone contaminants deposited on ZnSe and MgF_2 were used for

investigating the chemical change of silicone contaminants. ZeSe is an optical material with high transmittance against visible ranges to far-infrared region, so ZnSe was used for obtaining FT-IR spectra of silicone contaminants. MgF_2 was selected to obtain the depth profiles of Si, O, C including silicone contaminants and peak identification of Si for confirm the chemical bonds.

3.3 Experimental Procedures

3.3.1 Preparation of Materials

Silicone adhesive RTV-S691, whose size was 40 mm X 40 mm X 6 mm, was cured at room temperature. And the optical materials (ZnSe and MgF_2) whose size was ϕ 25 mm and t 1 mm, were dried in vacuum less than 10^{-1} Pa at 150 degree C (°C) for six hours after ultrasonic cleaning with ethyl alcohol, acetone and chloroform.

Measuring masses of materials used as substrate materials is necessary before and after the depositing contaminants for recording the correct mass of deposited contaminants and calculating the deposition thickness of contaminants.

The microbalance (MX6; Mettler Toledo International, Inc.) was used for measuring mass of materials. The microbalance can read 1μg to maximum 6,100 μg. And the deposition thickness of silicone contaminants was calculated under the assumption that contaminants deposited homogeneously on the surface of materials by using the specified values (deposition area: 314 mm^2, density of contaminants[3-1]: 1 mg/mm^3).

3.3.2 Depositing Contaminants on Substrate Materials

For depositing silicone contaminants from RTV-S691 on the optical materials, *In-situ* Contamination Spectroscopic Analysis Chamber (hereafter “contamination chamber”) was used in the present work.

Usually, the contamination chamber is used to investigate about the relations between heating temperature of heated materials, cooling temperature of cooled materials which

are deposited with contaminants from heated materials as outgassing source, amounts of deposited contaminants on cooled materials (usually use gold coated mirror), and FT-IR spectra of contaminants in vacuum less than 10^{-3} Pa by using the equipment, a heater (maximum temperature; 140 ℃), cooling part (minimum temperature; -10 ℃), **T**hermoelectric **Q**uartz **C**rystal **M**icrobalance (TQCM), FT-IR spectroscopy and vacuum pump[3-2].

TQCM (MK-20; QCM Research, sensitivity 15 MHz crystal: 5.10 X 10^8 Hz/g/cm^2) is equipped in the contamination chamber. Mass of contaminants (Δm) deposited on TQCM can calculate by using the equation (3-1), the fixed value of crystal electrode area (A) and value of frequency shift (Δf) obtained by TQCM.

$$\Delta f = \frac{-5.10 \times 10^8 \times \Delta m}{A} \qquad (3\text{-}1)$$

And, the deposition thickness of contaminants can calculate with its density. Fig. 3-2 shows an image of *In-situ* Contamination Spectroscopic Analysis Chamber.

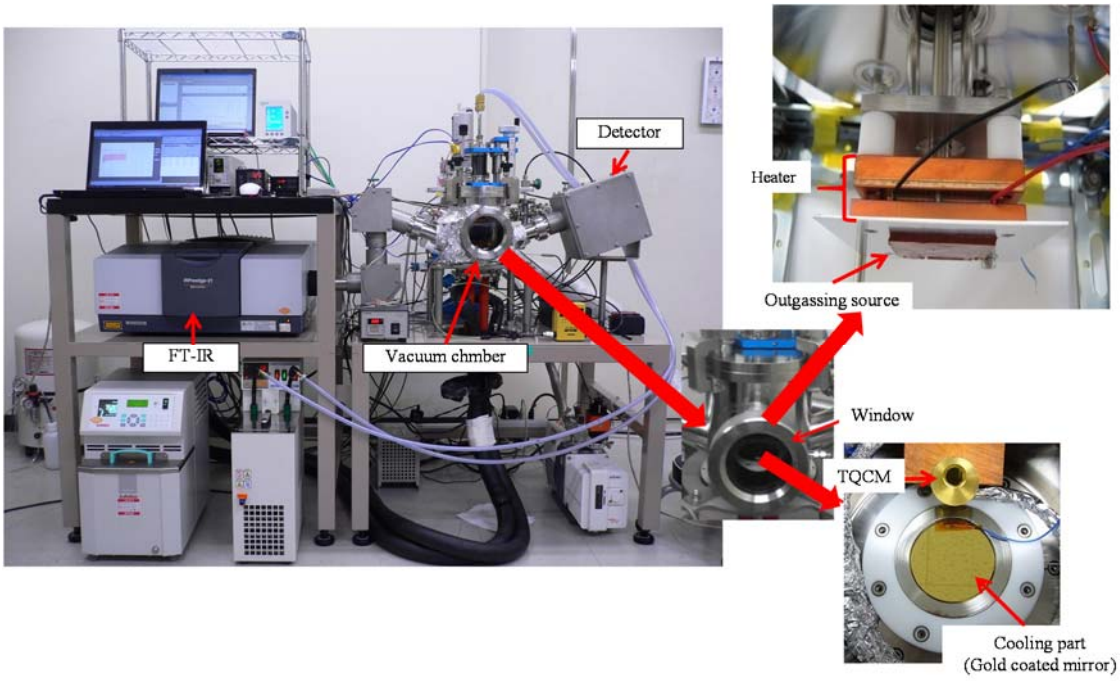

Fig. 3-2. *In-situ* Contamination Spectroscopic Analysis Chamber.

The contamination chamber has the functions which are 1) the function of heating materials with controlled temperature, 2) the function of cooling materials which are deposited with contaminants from heated materials with controlled temperature, and 3) the function of measuring the amounts of deposited contaminants on cooled materials. Therefore, in the present work, the contamination chamber was used for depositing silicone contaminants on substrate materials.

Silicone adhesive RTV-S691 as a silicone outgassing source was heated to 125 ℃ in the contamination chamber under pressure of 10^{-3} Pa, while the optical materials for collecting silicone contaminants were maintained at 25 ℃. The thermal condition was in reference to ASTM E-595. All of the optical materials were deposited with silicone contaminants on one side equally in terms of area (314 mm^2).

3.3.3 UV and/or AO Irradiation to Contaminants.

After being contaminated with silicone contaminants from the RTV-S691, the deposited side of the optical materials was irradiated with UV and/or AO in series. To investigate the effects of UV and/or AO to silicone contaminants, a high-vacuum chamber equipped with a Xe lamp was used for UV irradiation and Combined Space Effects Test Facility was used for AO irradiation in the present work. The irradiation conditions were emulated with the results of passive environment measurement[3-3), (3-4)]. Irradiation of UV-1st, AO-1st, UV-2nd, and AO-2nd was conducted in series. Table 3-1 gives an overview of UV and AO irradiation conditions in the present work. The UV and AO irradiation condition of Expt.-No. 4 was not used in the investigation about chemical changes of silicone contaminants but used in the investigation about morphological changes of silicone contaminants affected with UV and AO shown in Chapter 4.

Table 3-1. UV and AO irradiation conditions.

Experiment No.	Irradiation in series				Irradiation angle
	UV-1st irradiation (J/cm^2)	UV-2nd irradiation (J/cm^2)	AO-1st irradiation ($atoms/cm^2$)	AO-2nd irradiation ($atoms/cm^2$)	
Expt.-No.1	0.9×10^5	0.6×10^5	none	none	90°
Expt.-No.2	none	none	1.5×10^{21}	1.0×10^{21}	90°
Expt.-No.3	0.9×10^5	0.6×10^5	1.5×10^{21}	1.0×10^{21}	Both UV and AO: 90°
Expt.-No.4	0.9×10^5	0.6×10^5	1.5×10^{21}	1.0×10^{21}	UV: 90°, AO: 90° for the 1st irradiation,45° and 135° for 2nd irradiation

ｉ)　Irradiation of Ultraviolet Light

UV light can be irradiated to materials in vacuum less than 10^{-4} Pa by using a high-vacuum chamber equipped with a Xe lamp (Type UXL-2501YA2.5kW Xe short-arc lamp) at Tsukuba Space Center[3-5]. Spectral intensity of 200-400 nm on orbit is 11.8 mW/cm^2 (=1 UV-sun), and UV fluence of 200-400 nm on orbit per day is 1.02 X 10^3 J/cm^2 (=1 ESD (**E**quivalent **s**un **d**ays)). UV flux and fluence levels between the wavelengths of 200-400 nm can be measured by a multispectral radiometer. The light of **i**nfra**r**ed (IR) wavelength region is contained in the light of Xe lamp, and heat materials during UV irradiation. So, a dichroic mirror which reflects the wavelength of UV region and reduces the wavelength of the IR region was used in the facility[3-5]. For preventing heating materials, backsides of materials are cooled with water flow. Additionally, the light with wavelength less than 250 nm is reduced to avoid the creation of ozone by using a lamp coating[3-5]. Fig. 3-3 shows an image of the facility.

Fig. 3-3. High-vacuum chamber.

ii) Irradiation of Atomic Oxygen

AO can be irradiated to materials under a high vacuum by using the Combined Space Effects Test Facility under a high vacuum (10^{-3}-10^{-2} Pa) at Tsukuba Space Center. The AO average flux is 5.5 X 10^{15} atoms/cm^2・s and the AO beam average speed is 8.1 km/s. Their values are controlled referring from the values of space environment measurement. The facility can also irradiate vacuum UV light and Electron Beam[(3-6) - (3-9)]. Fig. 3-4 shows the schematic illustration of the Combined Space Effects Test Facility, and an image of the facility is shown in Fig. 3-5.

The facility generates AO based on laser detonation phenomenon invented by Physical Science, Inc. The energy of the AO generated by the facility is controlled at approximately 5 eV to replicate the LEO environment.

AO fluence is monitored by using mass loss of a polyimide film, Kapton H mounted on the sample holder. Since the erosion yield (E_K) of the Kapton H is known as 3.0 × 10^{-24} cm^3/atom [(3-10)], the total AO fluence (F) can be calculated by measuring the mass loss (Δm_K) of Kapton H after AO irradiation tests using the equation (3-2)[(3-10), (3-11)]. Where A_K and ρ_K are the exposure area and the density of Kapton H, respectively.

$$F = \frac{\Delta m_K}{A_K \rho_K E_K} \qquad (3\text{-}2)$$

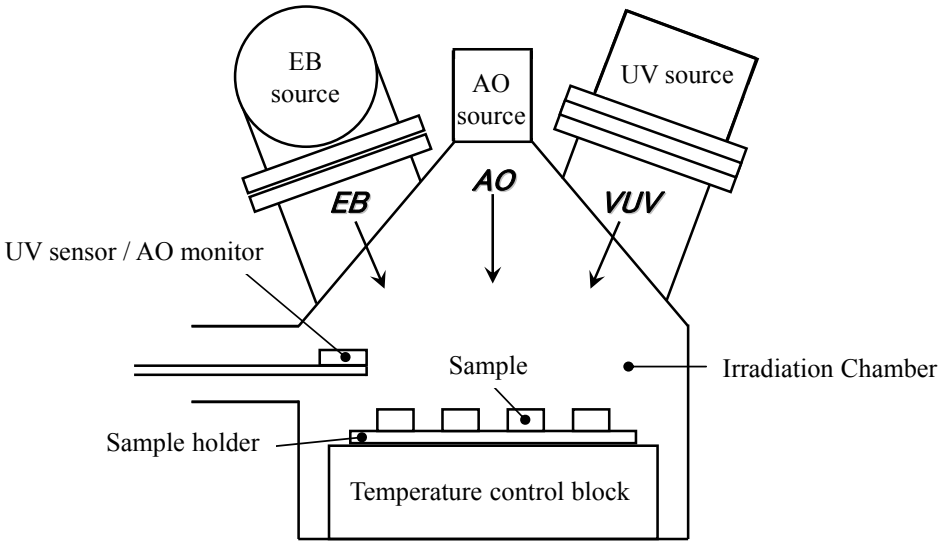

Fig. 3-4. The schematic illustration of the Combined Space Effects Test Facility.

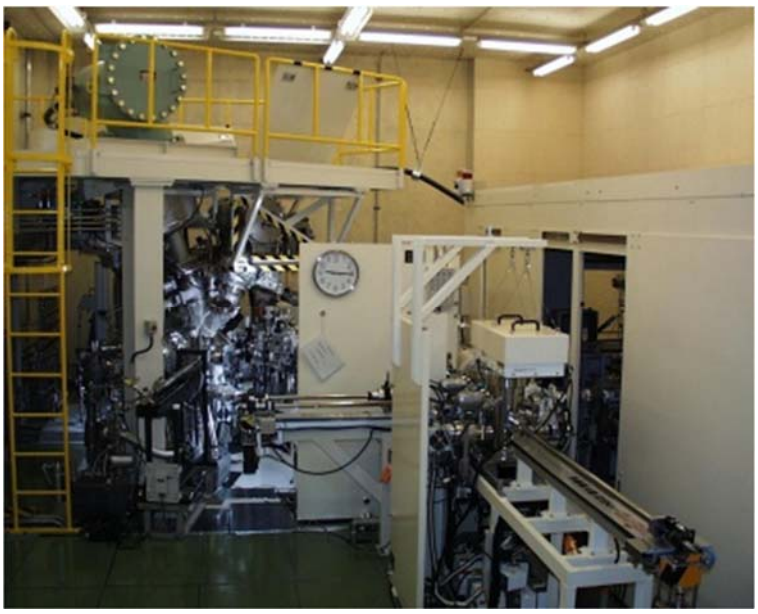

Fig. 3-5. Combined Space Effects Test Facility.

3.3.4 Sample Analysis

To evaluate the chemical changes of silicone contaminants with UV and/or AO irradiation, the FT-IR spectroscopy and XPS were used for obtaining chemical characteristics of silicone contaminants[(3-12) - (3-15)].

The chemical states of silicone contaminants were studied by FT-IR spectroscopy. FT-IR spectral measurements were performed using Perkin Elmer Spectrum One. The samples which were measured by FT-IR spectroscopy are silicone contaminants deposit on one side of ZnSe (ϕ25 mm, t 1 mm). The transmittance data of silicone contaminants affected with UV and/or AO were measured at the region of 4200-650 cm^{-1} with resolving power 4 cm^{-1} and cumulated number 32.

XPS can analyze the constituent elements and their chemical-bonding states. The chemical bond of Si, and depth profile of contaminants were performed by XPS. Thermo SCIENTIFIC K-Alpha was used for the investigation of silicone contaminants irradiated with UV and/or AO. The analyzed samples are silicone contaminants deposit on one side of MgF_2 (ϕ25 mm, t 1 mm) and irradiated with UV and/or AO. The size of analysis area is ϕ 400 μm, analysis source is Al Kα (1486.6 eV), and the depth profile using Ar-ion etching was performed with 3 keV (calculated with SiO_2 standard, ca. 0.25 nm/sec).

3.4 Mass Measurement

Table 3-2 shows the masses of the optical materials before and after the deposition of silicone contaminants and the deposition thicknesses calculated from the weight of deposited silicone contaminants measured by using the microbalance (MX6; Mettler Toledo International, Inc.).

Actually, contaminants are deposited as droplets on the surface of materials, which means the deposition thickness is thicker than the calculated values. As a result, the mass measurement results show that the optical materials are sufficiently deposited with silicone contaminants for investigating the effects of UV and/or AO irradiation to silicone contaminants in terms of optical properties.

Table 3-2. The masses of ZnSe and MgF_2 before and after the deposition of silicone contaminants and the deposition thicknesses.

Material	Sample No.	Deposited contaminants, mg			Deposition thickness, nm
		Before	After	Δ (After-Before)	
ZnSe	None irradiated	2674.117	2674.277	0.160	509.6
	Z-Expt. No.1	2708.672	2708.943	0.271	863.1
	Z-Expt. No.2	2722.342	2722.578	0.236	751.6
	Z-Expt. No.3	2732.448	2732.750	0.302	961.8
MgF_2	None irradiated	1584.047	1584.197	0.150	477.7
	M-Expt. No.1	1580.471	1580.647	0.176	560.5
	M-Expt. No.2	1593.006	1593.162	0.156	496.8
	M-Expt. No.3	1590.109	1590.289	0.180	573.2

3.5 Chemical Changes of Silicone Contaminants with UV and/or AO Irradiation

The effects of UV and/or AO irradiation to the compositions in silicone contaminants were investigated by FT-IR spectroscopy (Perkin Elmer Spectrum One).

3.5.1 Identification of Chemical Bonds in None Irradiated Silicone Contaminants

Fig. 3-6 shows FT-IR transmittance spectra of none irradiated silicone contaminants. Base-line of the FT-IR transmittance spectra was compensated.

In identification of FT-IR peaks measured for none irradiated contaminants, it was supposed that contaminants outgassed from silicone adhesive RTV-S691 would consist of low-weight silicone-related substances. As a reference data on IR spectra and structure correlations for silicones works ECSS (2009)[3-16] and P.J. Launer (1987)[3-17] were used. Table 3-3 shows the IR characteristic wavenumber of contaminants[3-16]. Some hints for the identification were found in the results of previous outgassing measurement clarified that polymethylcyclosiloxanes and phenylsilicones are contained as outgassed species of RTV-S691 heated at 60 ℃[3-18].

Indeed, in the FT-IR spectrum of none irradiated silicone adhesive (Fig. 3-6 (B)) a characteristic group of peaks at 699, 715, and 739 cm^{-1} with intensities increasing with decreasing frequency closely matches that of phenyl silicones having two phenyl groups attached to silicon. A narrow peak at 1429 cm^{-1} and shoulder peak at 1120 cm^{-1} also belong to phenyl silicone. Splitting of shoulder peak at 1120 cm^{-1} is a sign of two phenyls attached to silicon.

Peaks at 1025 and 1080 cm^{-1} match to Si-O-Si vibrations in disiloxanes (1080 cm^{-1}) and cyclic trimers (1025 cm^{-1}). Appearance of strong peaks at 1000 and 1025 cm^{-1} may show presence of cyclotrisiloxanes. In general cyclosiloxanes have characteristic absorption at 1075-1090 cm^{-1} (tetramers and pentamers), which is also observed. Presence of polydimethylsiloxane can be indicated because it shows absorption at 1020 and 1090 cm^{-1}, which is close to observed values of 1025 and 1080 cm^{-1}.

Peaks at 800, 845 and 1262 cm^{-1} indicate presence of Si-CH_3 bond of

polydimethylsiloxane. Shift of the 860 cm^{-1} from 845 cm^{-1} shows that dimethyl units form copolymers (copolymers or alternating), in the case it can be supposed that dimethyl units are combined with diphenyl units.

It is confirmed that none irradiated silicone contaminants have bonds of Alkanes at 3000-2850 cm^{-1}, and Alkenes at 3100-3020 cm^{-1}(Fig. 3-6 (C)). The IR spectrum of none irradiated silicone contaminants shows similar IR spectrum of polydimethylsiloxane (3-17), (3-19).

In conclusion, the main peaks appeared in the FT-IR spectrum of none irradiated silicone contaminants have been identified and presence of the next components was confirmed: polydimethylsiloxane, phenyl silicones having two phenyl groups attached to silicon, disiloxanes, cyclosiloxanes (tri, tetra and pentacyclosiloxanes), alkanes and alkenes. Their structural formulas are shown in Fig. 3-7. Only cyclotrisiloxane is shown in Fig. 3-7 as cyclosiloxanes, but there are cyclotrisiloxane (boiling point: 134℃, melting point: 64-66℃), cyclotetrasiloxane (boiling point: 175℃, melting point: 17.5℃), and cyclopentasiloxane (boiling point: 210℃, melting point: -38℃). It is conceivable that cyclotetrasiloxane is main cyclosiloxane in the present work with the object of thermal conditions.

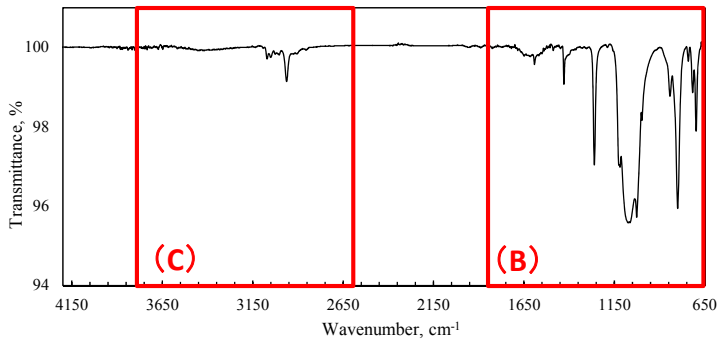

(A)

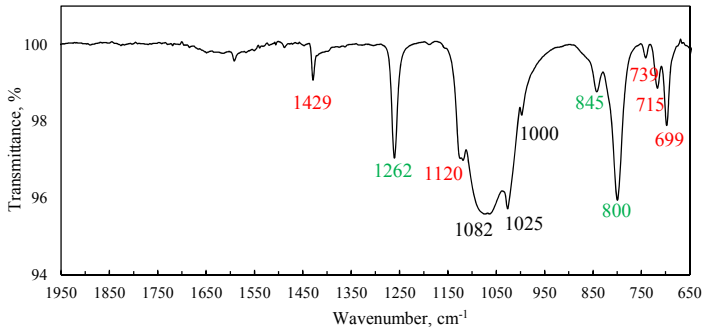

(B)

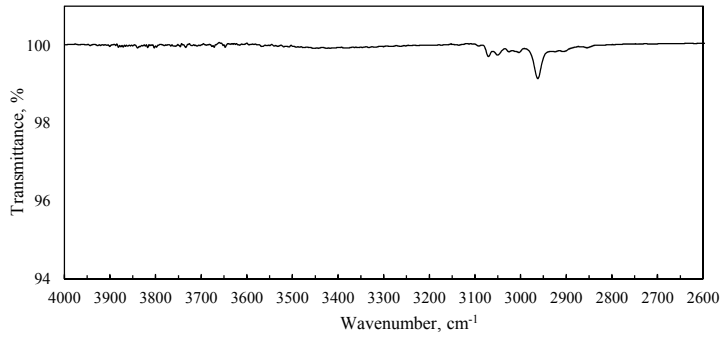

(C)

Fig. 3-6. The FT-IR transmittance spectra of none irradiated silicone contaminants. (A)Spectrum between 4200-650 cm^{-1}, (B) Spectrum between 1950-650 cm^{-1} (red numbers are frequencies belonging to phenyl silicones, black -Si-O-Si- in siloxanes, green -Si-CH_3 groups in polydimethylsiloxane), (C) Spectrum between 4000-2600 cm^{-1}.

Table 3-3. IR characteristic wavenumber[3-16].

Characteristic wavenumber, cm^{-1}	Chemical bond	Signal strength※	Vibration type
860-760	Si-CH_3	vs	Si-C stretching or CH_3 rocking ※※
1125-1100	Si-Aryl	vs	
1130-1000	Si-O-Si	s	Asymmetric stretching
1280-1255	Si-CH3	vs	Symmetric deformation
1300-1050	C-O	s	Stretching
1390-1370	-CH3	m	Symmetric deformation
1470-1440	-CH3	ms	Asymmetric deformation
1750-1735	C=O	s	Stretching (saturated ester)
3000-2850	Alkanes (CH, CH_2, CH_3)	s	2 or 3 bands, Stretching
3100-3020	Alkenes	m	Stretching

※ Strength of signal: vs=very strong, s=strong, ms=medium to strong, m=medium.

※※ One methyl: 765 cm^{-1}, two methyls: 855 and 800 cm^{-1}, three methyls: 845 and 845 cm^{-1}.

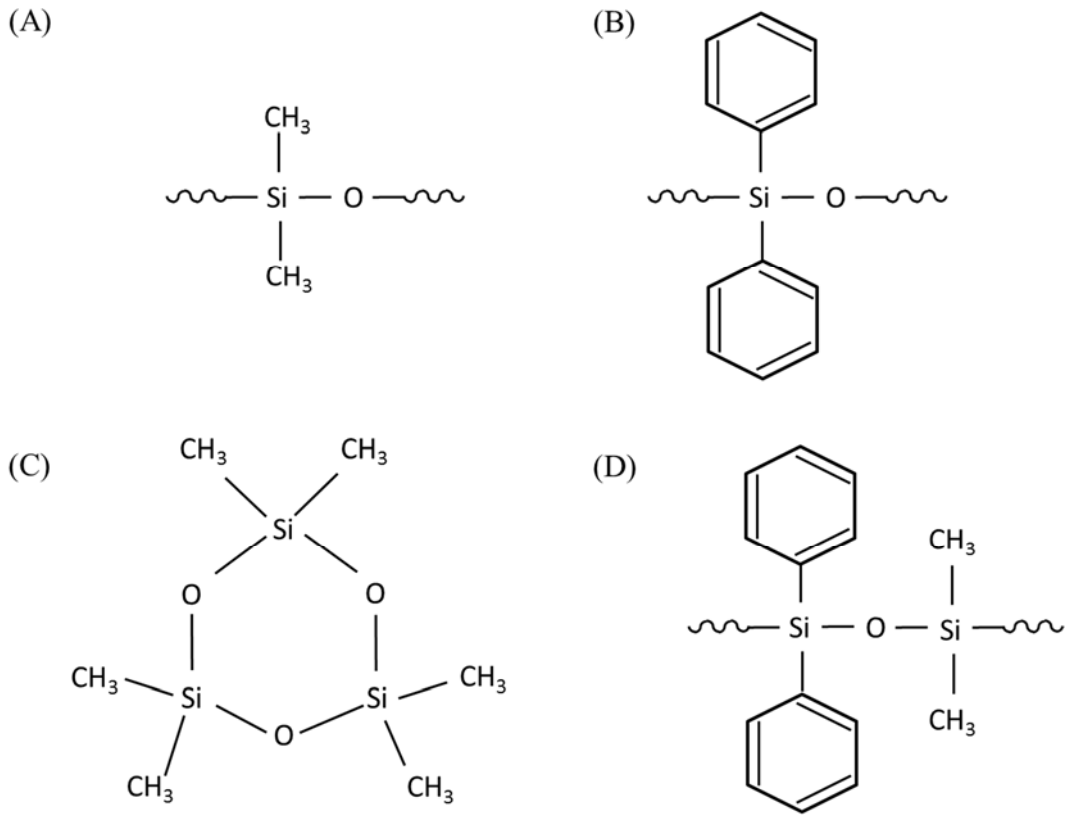

Fig. 3-7. Structural formulas of (A) Polydimethylsiloxane, (B) Polydiphenylsiloxane, (C) Cyclotrisiloxane, (D) Silicone consisting of diphenyl and dimethyl siloxane units.

3.5.2 Irradiation Effects on Chemical Bonds with UV

Fig. 3-8 shows FT-IR transmittance spectra of silicone contaminants after UV irradiation. Base-line of the FT-IR transmittance spectra was compensated. Fig. 3-8 (A) shows wide spectrum, and Fig. 3-8 (B) and (C) show selected areas where absorption was measured. As was described in Section 3.5.1, silicone contaminants contain polydimethylsiloxane, phenyl silicones, cyclosiloxanes, disiloxanes, alkanes and alkenes. At first, effect of UV irradiation on these groups will be discussed. Existence of peaks at 800, 850, and 1260 cm^{-1} shows that polydimethylsiloxane is still present in the sample as shown in Fig. 3-8 (B). Group of peaks at 702 and 720 cm^{-1} and a shoulder at 742 cm^{-1} shows presence of diphenyl silicones, however the shape of peaks is not as sharp as for none irradiated silicone contaminants, which suggests that some chemical changes took place for phenyl groups attached to silicon. Peak at 1120 cm^{-1} is considered to be covered by Si-O-Si absorption that is why it was not observed in the spectrum of UV-irradiated sample. Peak at 1429 cm^{-1} is still can be distinguished. Strong peaks at 800, 850 and 1260 cm^{-1} belong to dimethyl siloxane. Comparing to phenyl silicones their intensity is much higher, that suggest that the bond of Si-Ph in phenyl silicones is cut easier than the bond of $Si\text{-}CH_3$ under UV irradiation. The strongest absorption was measured at 1022 and 1089 cm^{-1}. These peaks correspond to Si-O-Si bond vibration in silicones, especially in polydimethylsiloxane. These peaks are very wide, which suggests that they may include vibrations of Si-O-Si bond in disiloxanes and cyclosiloxanes. In the spectrum of none irradiated silicone contaminants, the intensity ratio between peaks belonging to Si-O-Si vibration and $Si\text{-}CH_3$ are very close, but for UV-irradiated sample the intensity of Si-O-Si vibration is much higher, which means that chemical changes occurred under effect of UV irradiation. Moreover, the intensity ratio between peaks belong to alkanes and alkenes also changed as shown in Fig. 3-8 (C). It can be concluded, that it is confirmed that the bonds of Si-Ph, Si-O-Si, Alkanes, and Alkenes are affected with UV by comparing with IR spectrum of none irradiated silicone contaminants.

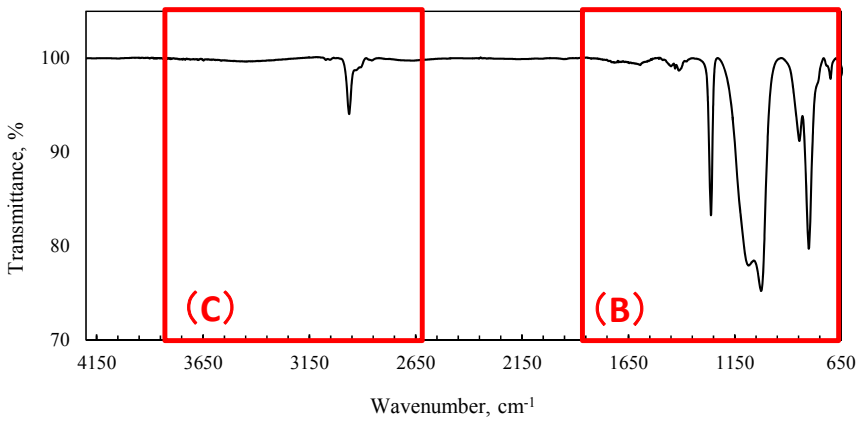

(A)

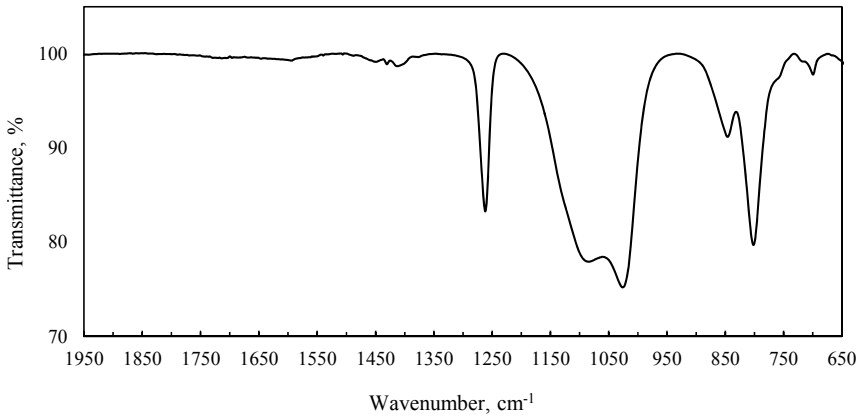

(B)

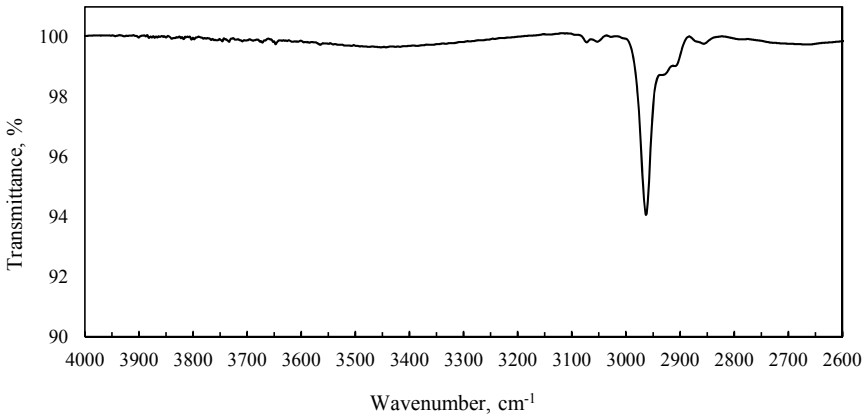

(C)

Fig. 3-8. The FT-IR transmittance spectra of Z-Expt. No.1.

(A)Spectrum between 4200-650 cm^{-1}, (B) Spectrum between 1950-650 cm^{-1}, (C) Spectrum between 4000-2600 cm^{-1}.

3.5.3 Irradiation Effects on Chemical Bonds with AO

Fig. 3-9 shows FT-IR transmittance spectra of silicone contaminants under AO irradiation. Base-line of the FT-IR transmittance spectra was compensated. Fig. 3-9 (A) shows wide spectrum, and Fig. 3-9 (B) and (C) show selected areas where absorption was measured. From Fig. 3-9 (B) it can be seen that characteristic for phenyl silicones peaks appear at 695, 707, 748 cm^{-1}, shoulder at 1120 cm^{-1}, and peak at 1435 cm^{-1}. Peaks characteristic for Si-CH_3 bond in polydimethylsiloxane are observed at 800, 850 and 1262 cm^{-1}. The structure of wide peak responsible for Si-O-Si vibrations is similar to that of none irradiated silicone contaminants, but smoother. The intensity of the peak of Si-O-Si vibrations is higher than that for Si-CH_3. These two facts suggest starting of development of silicon oxide network, while organic component is still present in the sample.

The broad spectral peak in vicinity of wavenumber 3400 cm^{-1}, which is derived by hydroxyl group, could be observed (see Fig. 3-9 (C)). The fact suggests that silicone contaminants are oxidized by AO, and hydroxyl group was produced in the silicone contaminants tested Expt.-No.2. The bonds of Si-O-Si, Si-CH_3, Alkanes, and Alkenes are also affected with AO by comparing with IR spectrum of none irradiated silicone contaminants.

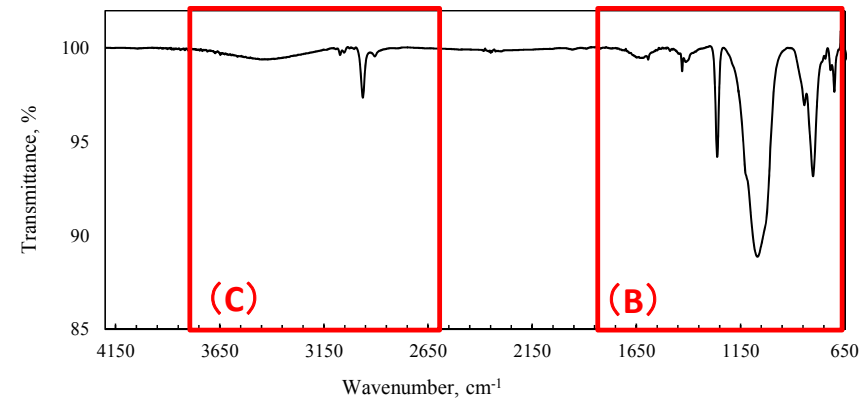

(A)

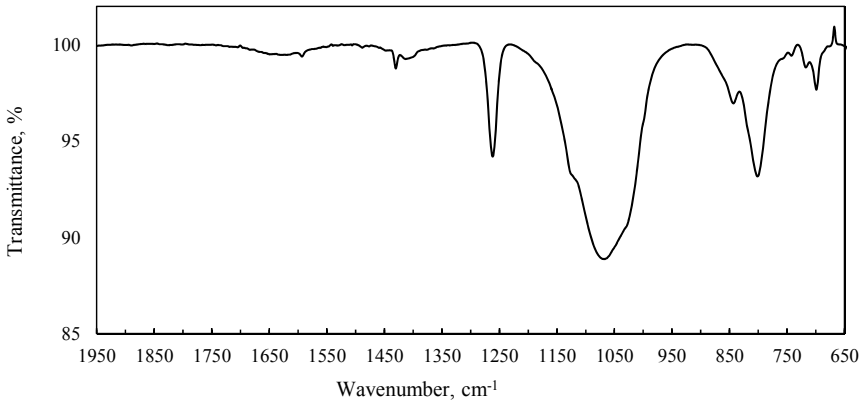

(B)

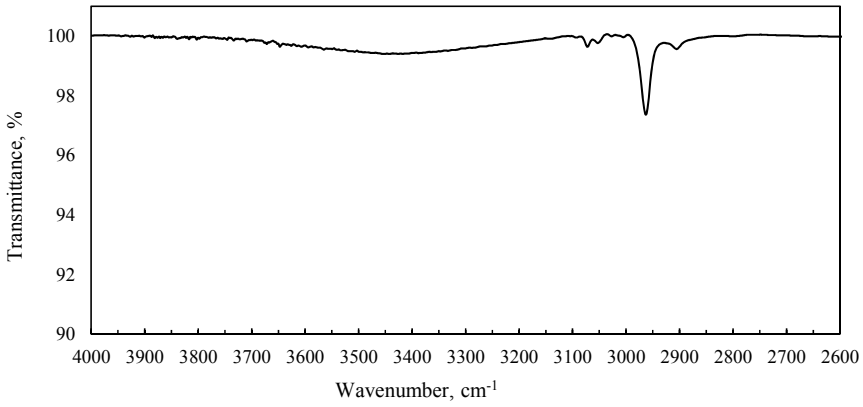

(C)

Fig. 3-9. The FT-IR transmittance spectra of Z-Expt. No.2.

(A)Spectrum between 4200-650 cm^{-1}, (B) Spectrum between 1950-650 cm^{-1}, (C) Spectrum between 4000-2600 cm^{-1}.

3.5.4 Irradiation Effects on Chemical Bonds with UV and AO

Fig. 3-10 shows FT-IR transmittance spectra of silicone contaminants under UV and AO irradiation. Base-line of the FT-IR transmittance spectra was compensated. Fig. 3-10 (A) shows wide spectrum, and Fig. 3-10 (B) and (C) show selected areas where absorption was measured.

From the Fig. 3-10 (B) it can be seen, that characteristic for phenyl silicones peaks at 703, 726, 747, 1418 cm^{-1} are measured. Peak at 1120 cm^{-1} is not observed, because it is covered by wide peak belonging to Si-O-Si vibrations. Peaks of $Si-CH_3$ bond of polydimethylsiloxane are observed at 799, 851 and 1260 cm^{-1}.The strongest absorption was observed between 950 and 1200 cm^{-1}. This area is responsible for Si-O-Si vibrations. Comparing the same peak measured for none irradiated silicone contaminants, it can be seen, that after UV and AO irradiation, the peak became much wider, and its structure is not clear. Such structure is characteristic for amorphous silicon dioxide (silica, SiO_2), as can be seen from the IR spectrum of vitreous SiO_2 shown in Fig. 3-11 [3-20]. It is reported that all forms of SiO_2 show a strong band at 1110-1080 cm^{-1} [3-21]. Differing from sharp peak structure of siloxanes, for amorphous silica a broad peak with a shoulder at 1200 cm^{-1} is characteristic. Development of this shoulder can be confirmed in the FT-IR spectrum of UV and AO irradiated silicone contaminants (Fig. 3-10 (B)). The IR spectra of silicone contaminants under AO irradiation (Fig. 3-9) and especially silicone contaminants under UV and AO irradiation (Fig. 3-10) are similar to the IR spectrum of vitreous SiO_2. It would be suggested that silicone contaminants under AO irradiation and silicone contaminants under UV and AO irradiation contain SiO_2.

The broad spectral peak in vicinity of wavenumber 3400 cm^{-1} derived from hydroxyl group could be observed (see Fig. 3-10 (C)). The fact suggests that silicone contaminants are oxidized by AO, and hydroxyl group was produced in the silicone contaminants tested Expt.-No.3.

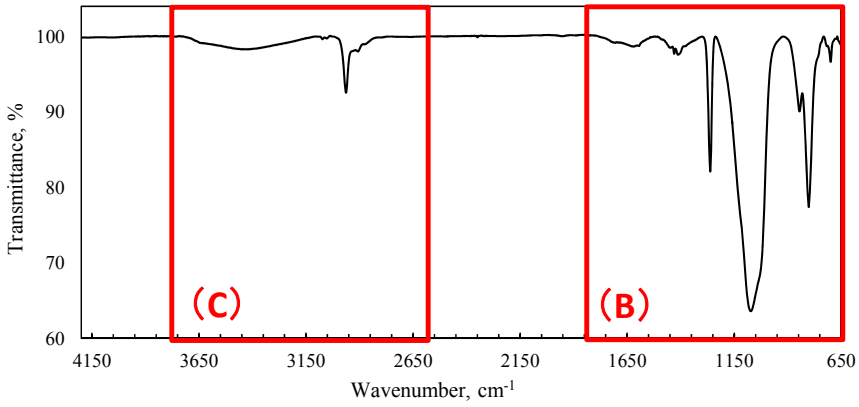

(A)

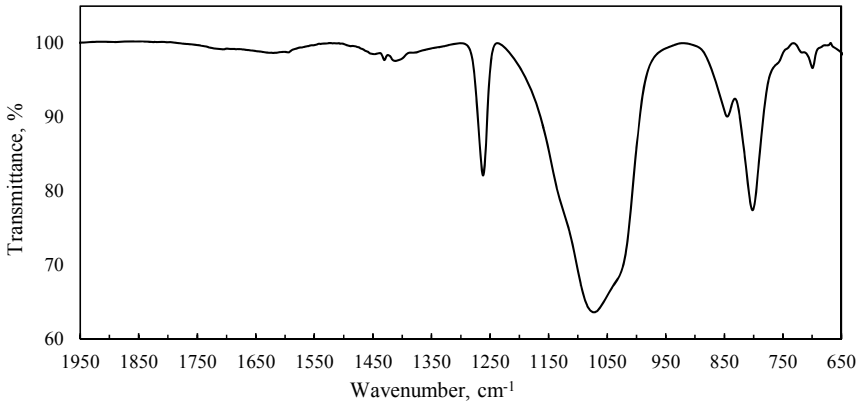

(B)

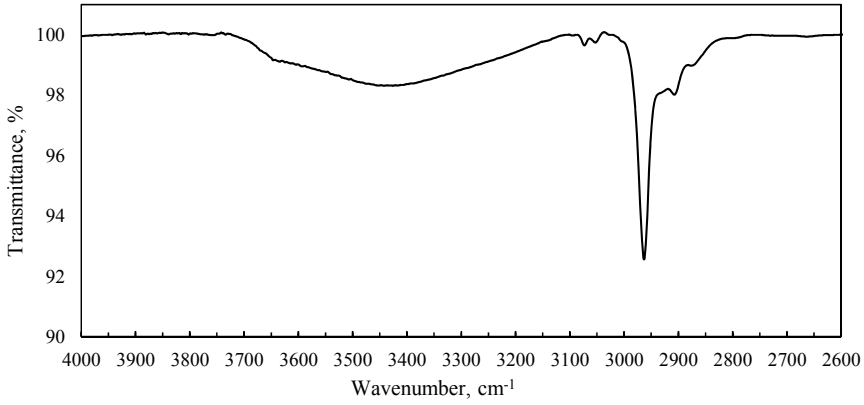

(C)

Fig. 3-10. The FT-IR transmittance spectra of Z-Expt. No.3.

(A) Spectrum between 4200-650 cm^{-1}, (B) Spectrum between 1950-650 cm^{-1}, (C) Spectrum between 4000-2600 cm^{-1}.

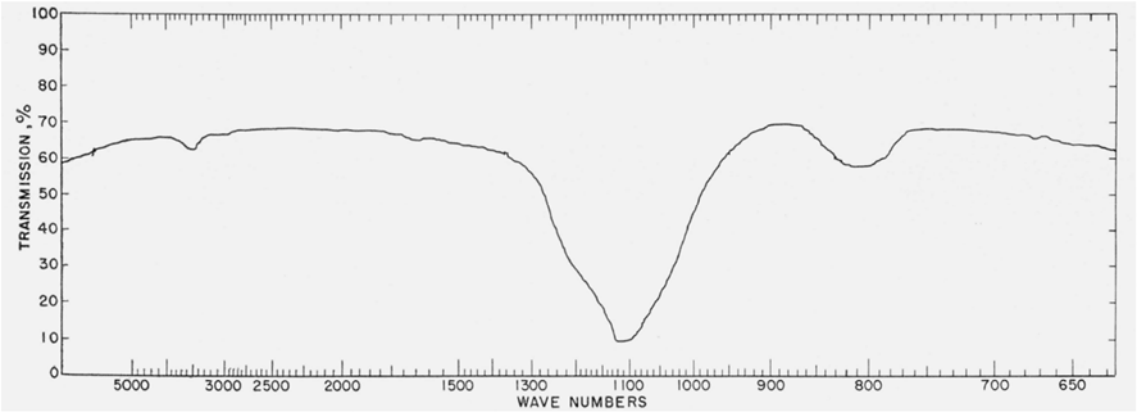

Fig. 3-11. IR spectrum of vitreous SiO_2 [3-20].

3.6 Depth Elemental Distribution Irradiated with UV and/or AO

The elemental depth profiles and chemical bonds of silicon (Si) were obtained by **X**-ray **P**hotoemission **S**pectroscopy (XPS, K-Alpha; Thermo SCIENTIFIC).

The elemental depth profiles of silicone contaminants were obtained using Ar-ion etching. The depth was calibrated with SiO_2 standard (etching rate: ca. 0.25 nm/s). Peak identification of Si was conducted at the three points. The first point is 1 nm from the surface of the samples, the second point is 10 nm from the surface of the samples, and the third point is precipitous change point of atomic % value was observed by the depth profiles.

3.6.1 None Irradiated Silicone Contaminants

Fig. 3-12 shows the survey scan at the third point which is 15 nm from the surface of the sample. The expected peaks of silicon, oxygen and carbon were detected with fluorine and magnesium are contained in the substrate material of the sample. The average depth profiles of none irradiated silicone contaminants are shown in Fig. 3-13. From the Fig. 3-13 it can be seen that main component of the silicone contaminants is carbon, second is silicon, and then oxygen.

The peak spectra of Si 2p between 107 and 97 eV of bonding energy are shown in Fig. 3-14, and the measurement was conducted at the three points. The first point is 1 nm from the surface of the sample, the second point is 10 nm from the surface of the sample, and the third point is 15 nm from the surface of the sample. All spectra have the peak at ca. 102 eV, which is characteristic for silicones that means that silicones are contained in none irradiated silicone contaminants. Atomic concentrations are shown in Table 3-4. It is confirmed that silicone contaminants from RTV-S691 represent silicones because the content ratio of Si : O : C shows ac. 1 : 1 : 2 which is same as for polydimethylsiloxane.

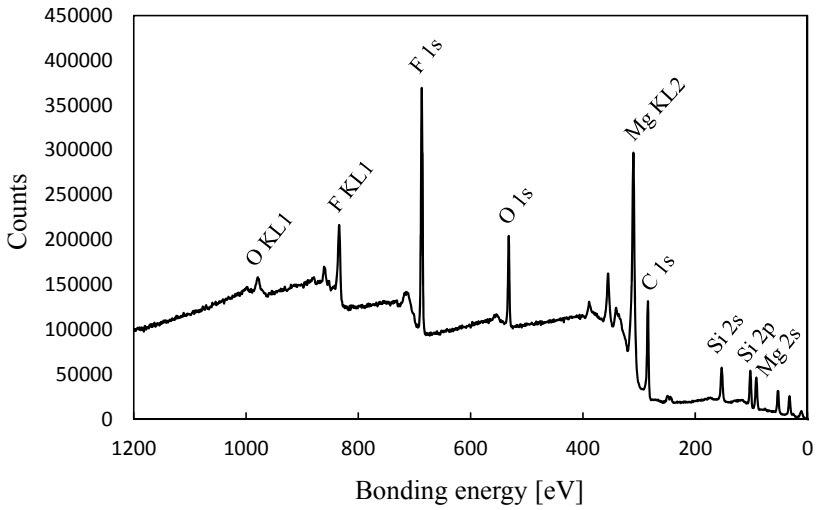

Fig. 3-12. The XPS survey scan of none irradiated silicone contaminants at 15 nm from the surface.

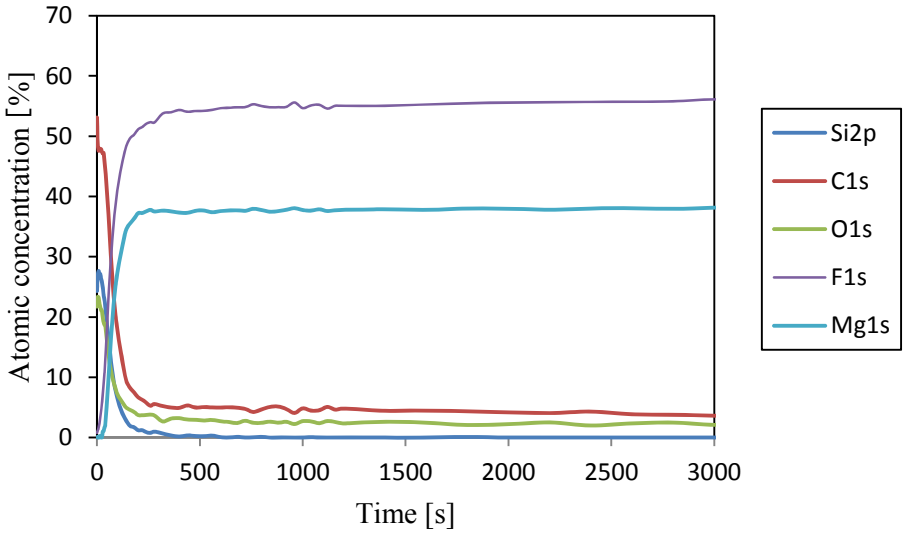

Fig. 3-13. The XPS depth profiles of none irradiated silicone contaminants.

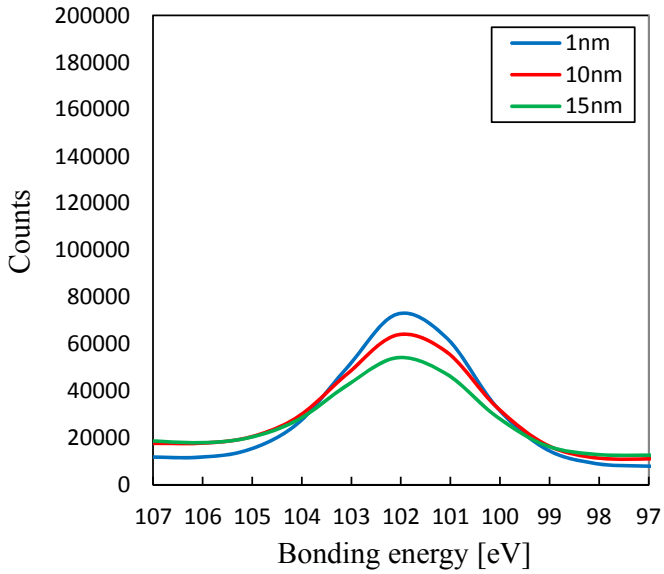

Fig. 3-14. The XPS peak spectra of Si 2p of none irradiated silicone contaminants.

Table 3-4. Atomic concentration of Si, O and C of none irradiated silicone contaminants by XPS.

Depth from the surface	Atomic concentration (%)		
	Si	O	C
1 nm	27.16	23.33	48.30
10 nm	21.79	18.73	44.85
15 nm	15.13	12.61	34.60

3.6.2 Silicone Contaminants Irradiated with UV

The survey scan at the third point which is 95 nm from the surface of the sample is shown in Fig. 3-15. The expected peaks of silicon, oxygen and carbon were detected with fluorine and magnesium which are contained in the substrate material of the sample. Fig. 3-16 shows the average depth profiles of silicone contaminants with UV irradiation. It can be seen from the figure that at the surface contents' order of carbon, oxygen and silicon are almost the same. In the middle of the silicone contaminants layer, the contents order is like in none irradiated silicone contaminants, namely carbon, silicon, oxygen.

The peak spectra of Si 2p between 107 and 97 eV of bonding energy are shown in Fig. 3-17, and the measurement was conducted at the three points. The first point is 1 nm from the surface of the samples, the second point is 10 nm from the surface of the samples, and the third point is 95 nm from the surface of the samples. All spectra have the peak at ca. 102.5 eV. Fig. 3-18 is the peak identification of Si at the second point (10 nm from the surface of the sample). It is confirmed that UV irradiation to silicone contaminants from RTV-S691 formed SiO_2. The phenomena was reported by G.A. Harvey (1992)[3-22].

Table 3-5 indicates atomic concentrations of silicone contaminants irradiated with UV.

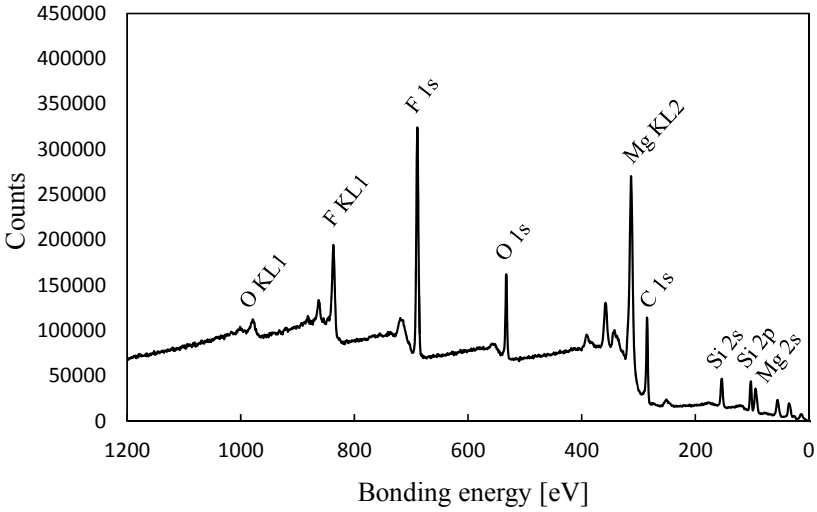

Fig. 3-15. The XPS survey scan of silicone contaminants irradiated with UV at 95 nm from the surface.

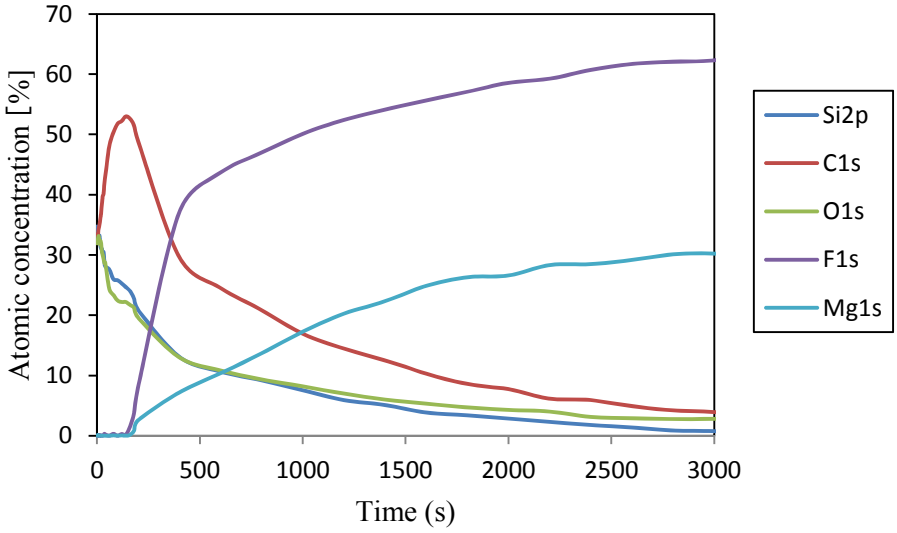

Fig. 3-16. The XPS depth profiles of silicone contaminants Expt.-No.1.

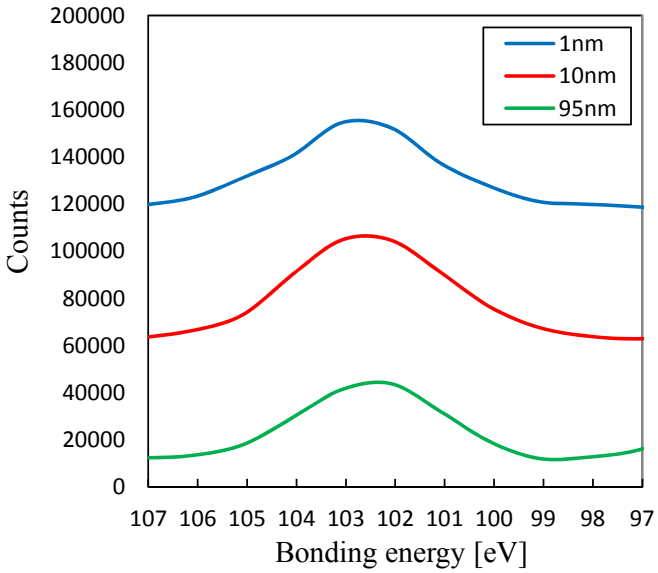

Fig. 3-17. The XPS peak spectra of Si 2p of silicone contaminants Expt.-No.1.

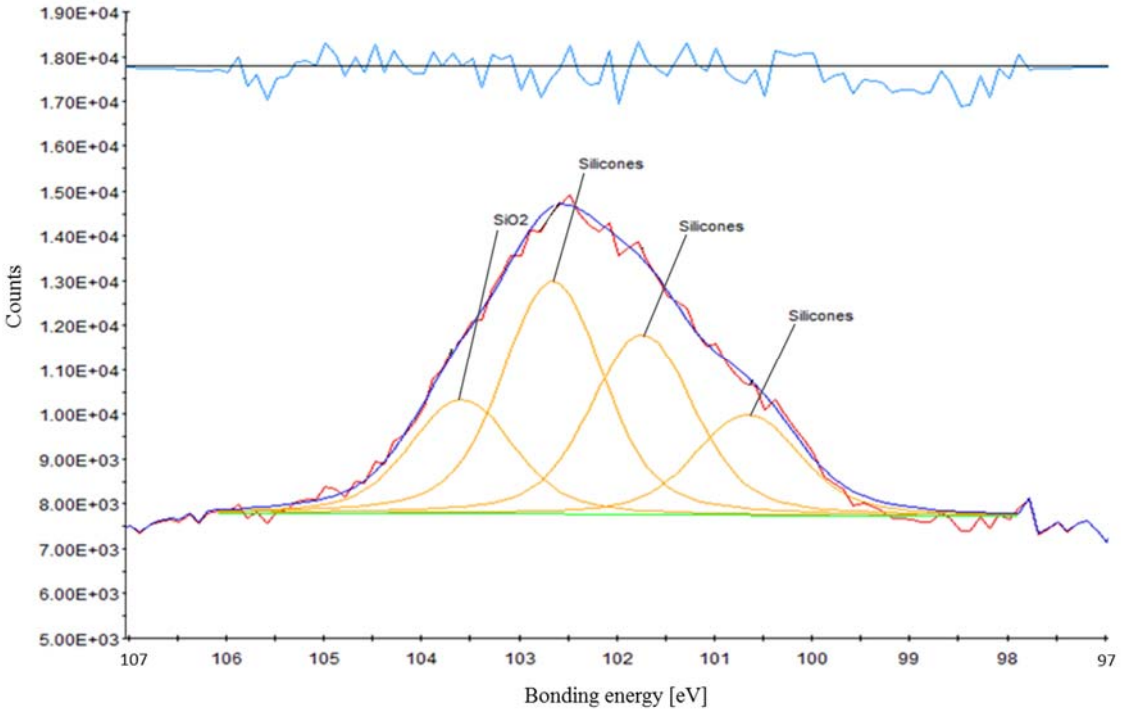

Fig. 3-18. The XPS peak identification of Si of silicone contaminants Expt.-No.1 at 10 nm from the surface.

Table 3-5. Atomic concentration of Si, O and C of Expt.-No.1 sample by XPS.

Depth from the surface	Atomic concentration (%)		
	Si	O	C
1 nm	34.09	32.51	33.27
10 nm	28.10	28.72	42.96
95 nm	13.09	13.00	29.65

3.6.3 Silicone Contaminants Irradiated with AO

The survey scan at the third point which is 124 nm from the surface of the sample is shown in Fig. 3-19. The expected peaks of silicon, oxygen and carbon were detected with fluorine and magnesium which are contained in the substrate material of the sample. However, the peak of carbon was weak. Fig. 3-20 shows the average depth profiles of silicone contaminants after AO irradiation. It can be seen from the figure that oxygen and silicon are the main components of contaminants layer irradiated by AO. Contents of carbon is very low. The peak spectra of Si 2p between 109 and 99 eV of bonding energy are shown in Fig. 3-21, and the measurement was conducted at the three points. The first point is 1 nm from the surface of the samples, the second point is 10 nm from the surface of the samples, and the third point is 124 nm from the surface of the samples. All spectra have the peak at ca. 155 eV to 103 eV. Fig. 3-22 shows the peak identification of Si at the second point (10 nm from the surface of the sample). It is confirmed that AO irradiation to silicone contaminants from RTV-S691 formed SiO_2. Table 3-6 indicates atomic concentrations. The table also suggests the formation of SiO_2 whose content ratio of Si : O is 1 : 2.

It is clarified that AO reacted with silicone contaminants from RTV-S691 and formed SiO_2, and atomic concentration of C was significantly reduced.

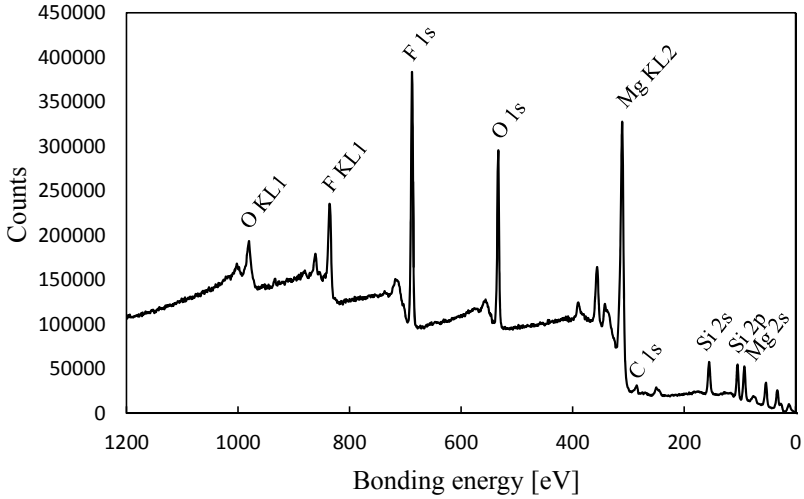

Fig. 3-19. The XPS survey scan of silicone contaminants irradiated with AO at 124 nm from the surface.

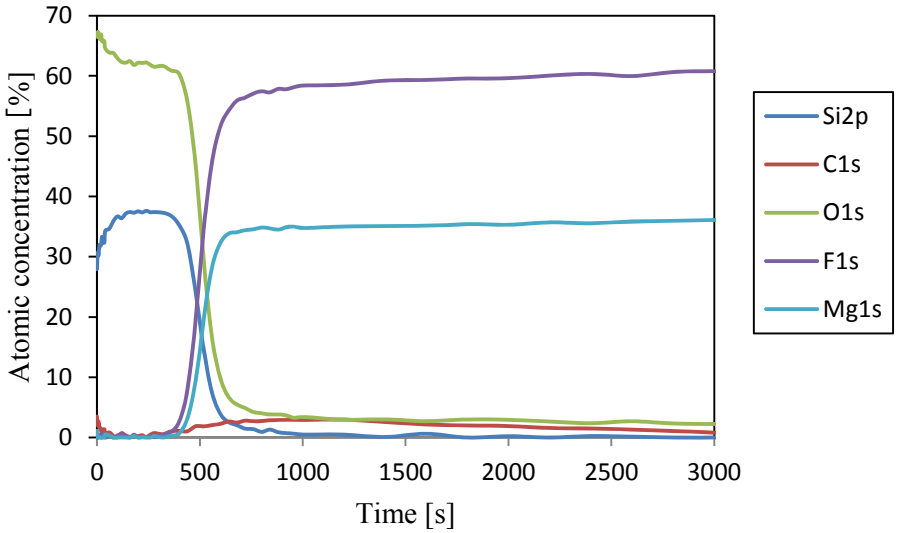

Fig. 3-20. The XPS depth profiles of silicone contaminants Expt.-No.2.

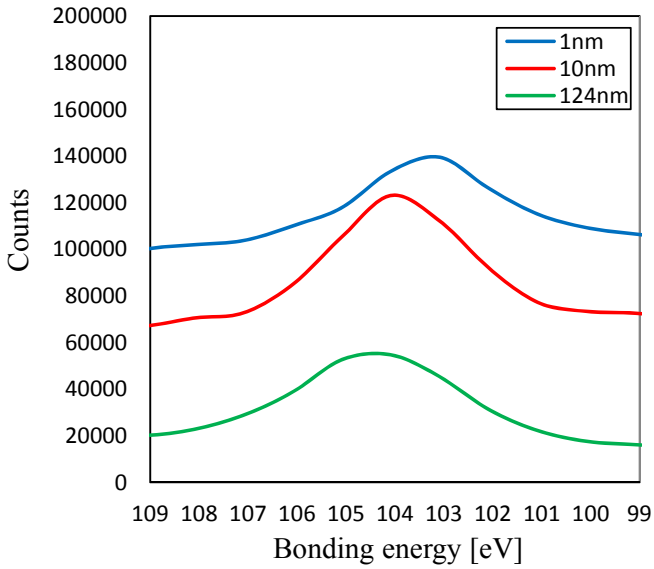

Fig. 3-21. The XPS peak spectra of Si 2p of silicone contaminants Expt.-No.2.

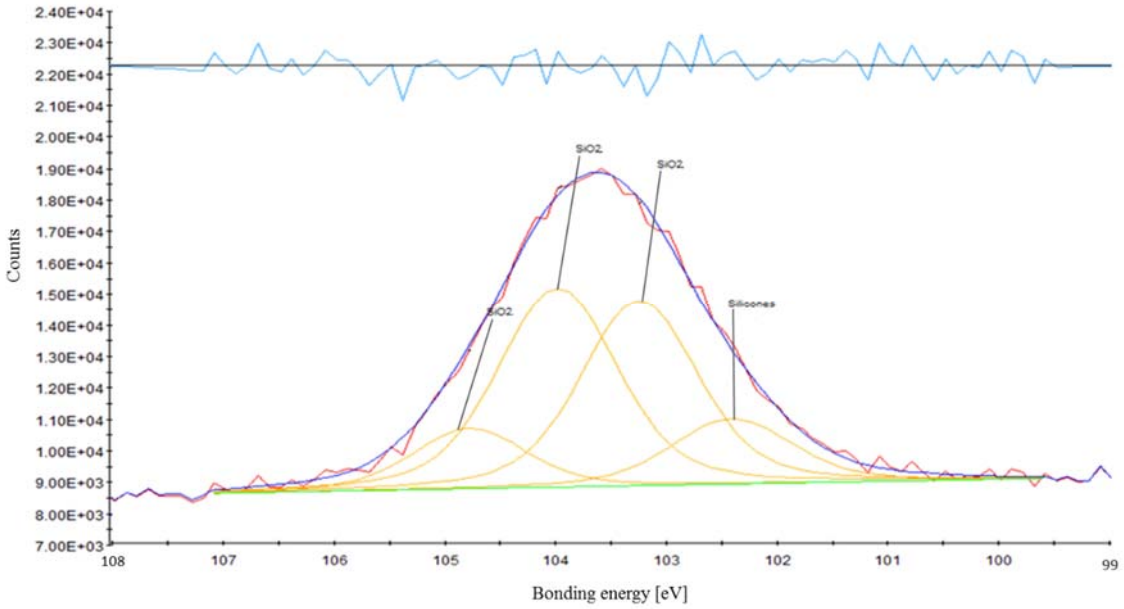

Fig. 3-22. The XPS peak identification of Si of silicone contaminants Expt.-No.2 at 124 nm from the surface.

Table 3-6. Atomic concentration of Si, O and C of Expt.-No.2 sample by XPS.

Depth from the surface	Atomic concentration (%)		
	Si	O	C
1 nm	30.69	67.30	2.01
10 nm	34.27	64.59	0.63
124 nm	14.34	28.84	1.86

3.6.4 Silicone Contaminants Irradiated with UV and AO

The survey scan at the third point which is 170 nm from the surface of the sample is shown in Fig. 3-23. The expected peaks of silicon, oxygen and carbon were detected with fluorine and magnesium which are contained in the substrate material of the sample. Fig. 3-24 shows the average depth profiles of silicone contaminants with UV and AO irradiation. It can be seen that main components are oxygen and silicon. The contents of carbon near the surface is very low.

The peak spectra of Si 2p between 108 and 98 eV of bonding energy are shown in Fig. 3-25 for the three points. The first point is 1 nm from the surface of the samples, the second point is 10 nm from the surface of the samples, and the third point is 124 nm from the surface of the samples. All spectra have the peak at ca. 103.5 eV to 102.5 eV. Fig. 3-26 shows the peak identification of Si at the second point (10 nm from the surface of the sample). The existence of SiO_2 and silicones is clarified. Table 3-7 indicates atomic concentrations. The table suggests that more silicones are contained in the sample of Expt.-No.3 than in the sample of Expt.-No.2.

It is clarified that combined action of UV and AO caused oxidation of silicone contaminants from RTV-S691 and formation of SiO_2, and atomic concentration of C near the surface was significantly reduced as same as in the case of silicone contaminants irradiated with AO. However, the reduction of C blocked at the depth etched in vicinity for 500 seconds by Ar-ion etching shown in Fig. 3-24.

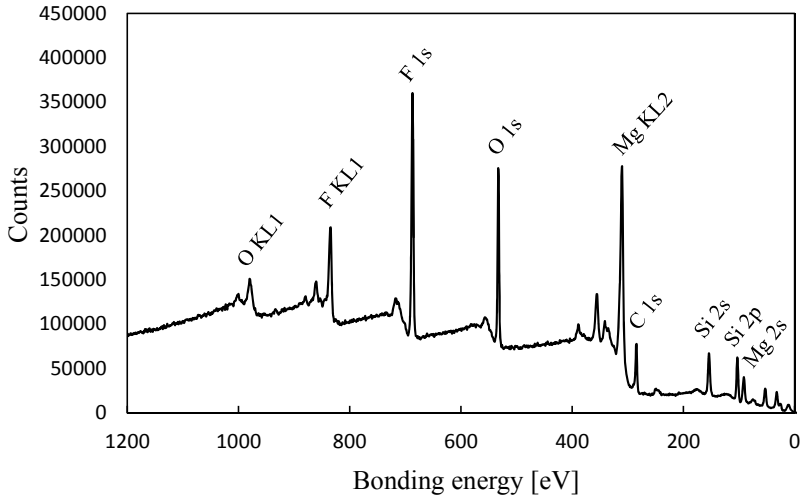

Fig. 3-23. The XPS survey scan of silicone contaminants irradiated with UV and AO at 170 nm from the surface.

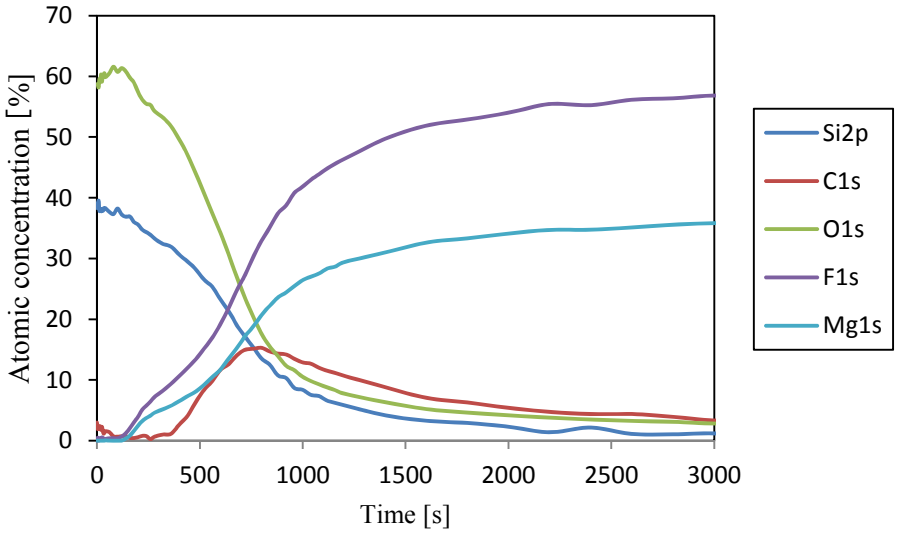

Fig. 3-24. The XPS depth profiles of silicone contaminants Expt.-No.3.

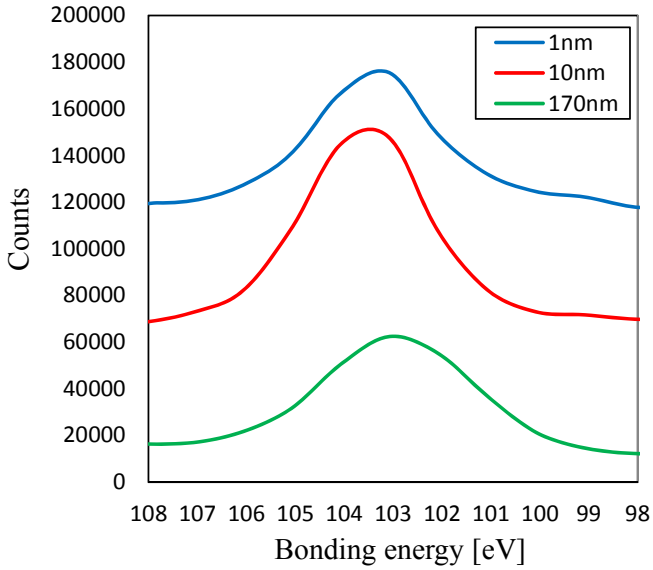

Fig. 3-25. The XPS peak spectra of Si 2p of silicone contaminants Expt.-No.3.

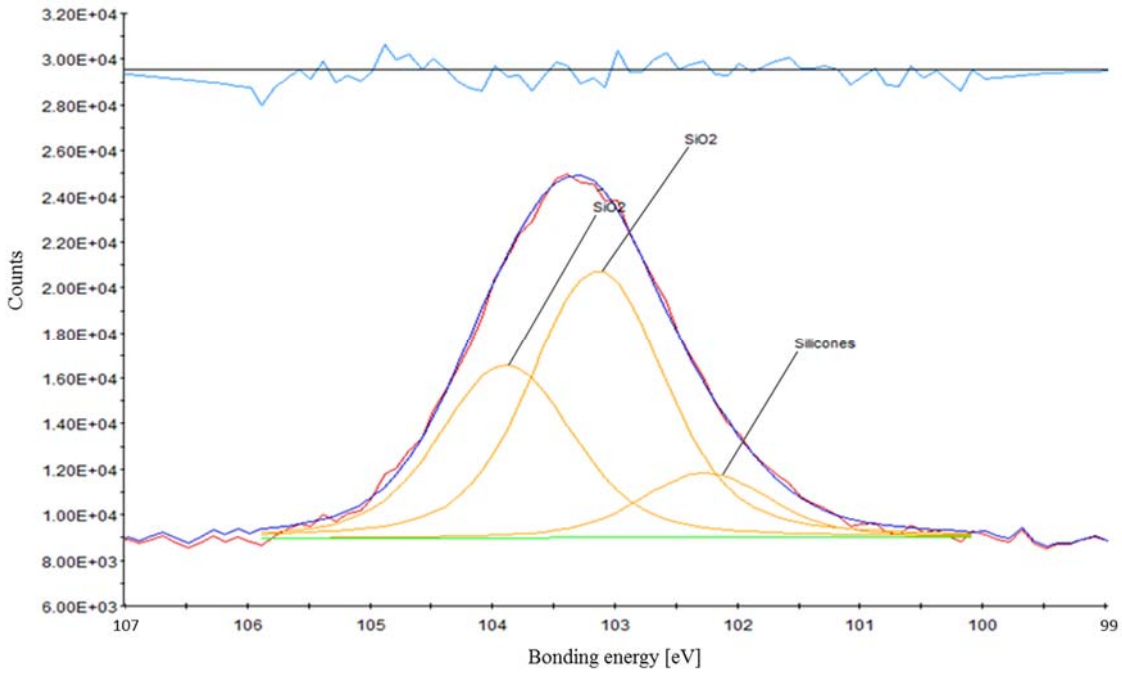

Fig. 3-26. The XPS peak identification of Si of silicone contaminants Expt.-No.3 at 170 nm from the surface.

Table 3-7. Atomic concentration of Si, O and C of Expt.-No.3 sample by XPS.

Depth from the surface	Atomic concentration (%)		
	Si	O	C
1 nm	38.99	58.63	1.89
10 nm	38.31	59,87	1.54
170 nm	17.11	23.37	14.96

3.7 Chemical Effects on Silicone Contaminants with UV and/or AO Irradiation

It was reported that AO generates silicon oxide (SiOx) including SiO_2 by reacting with silicone contaminants[3-23) - (3-25)]. Actually, the results of peak identification of Si clarified that SiO_2 was formed especially in Expt.-No.2 sample and Expt.-No.3 sample. But, silicones were also detected with SiO_2.

UV light can break the bond such as $-CH_2-CH_2-$ and C-H as shown in Chapter 1 Table 1-4, and AO can form such as SiOx, CO, and CO_2 by oxidizing silicones and hydrocarbons[3-23) - (3-26)]. It would be considered that the bonds of Alkanes, Alkenes, Si-CH_3, and Si-Ph were changed by the effects of UV and/or AO. The spectral peaks of Si-O-Si, and Si-CH_3 can be identified from the peaks in vicinity at wavenumbers, respectively. The intensity ratios of peaks measured at 800 cm^{-1} (Si-CH_3 group in polydimethylsiloxane), 1050 cm^{-1} (Si-O-Si vibration), and 1260 cm^{-1} (Si-CH_3 group in polydimethylsiloxane) of silicone contaminants calculated from transmittance are shown in Table 3-8. The intensity ratios of Si-CH_3 group in polydimethylsiloxane were reduced on Z-Expt. No.2 and Z-Expt. No.3 as shown in Table 3-8. The results conclude that especially AO react with Si-CH_3, and result of the reaction would lead the generation of SiO_2.

Signal of the broad spectral peak in vicinity of wavenumber 3400 cm^{-1} derived from hydroxyl group of silicone contaminants under UV and AO irradiation was stronger than that of silicone contaminants under AO irradiation. It suggest that the synergy effect of UV and AO was also occurred on the silicone contaminants under UV and AO irradiation.

The elemental depth profiles conduced that the thicknesses of silicone contaminants are different from the calculated values by using the masses of deposited silicone contaminants on the samples shown in Table 3-2. The reason is conceivable as follows. None irradiated silicone contaminants are liquid, therefore the etching rate of none irradiated silicone contaminants was higher than ca. 0.25 nm/s. As a result, the depth profile of none irradiated silicone contaminants is shown as Fig. 3-12. The reaction between AO and silicone contaminants led the reduction of C, the increase of oxygen

containing the components of silicone contaminants, and the formation of SiO_2 as shown in Table 3-6 and Table 3-7. As a result, the thickness of the silicone contaminants tested Expt.-No.2 became thinner than the calculated values shown in Table 3-2. On the other hand, it is thought that the same reaction occurred to the silicone contaminants tested Expt.-No.3, but the reduction of C was blocked at the depth etched in vicinity for 500 seconds by Ar-ion etching shown in Fig. 3-18. The block is conceivable that attribute to the reaction between UV and silicone contaminants. Polymerization reaction and cross-linking reaction are known to be caused by UV[(3-23), (3-24)]. The changes of chemical bonds are conceivable to be occurred by UV, and the reaction between UV and silicone has the possibility that attribute the thickness of silicone contaminants tested Expt.-No.1 shown in Fig. 3-14. However, the reaction could not be identified.

As shown in section 3.5.1, polydimethylsiloxane is considered to be one of the main silicone contaminants from RTV-S691. Reactions (1) to (9) show conceivable chemical change processes from polydimethylsiloxane to SiO_2-baseed components from the results of FT-IR spectroscopy and XPS.

The conceivable reactions of polydimethylsiloxane and UV are shown in reactions (1) to (3). Reaction (1) is the bond dissociation reaction under action of UV irradiation; a bond between Si atom and methyl group in polydimethylsiloxane is broken with formation of two radicals (Si-centered radical and methyl radical). Reaction (2) is the abstraction of hydrogen atom from methyl group in polydimethylsiloxane by methyl radical formed in reaction (1). As products methylene radical and gaseous methane are produced. Reaction (3) is the recombination between Si-centered radical produced in reaction (1) and methylene radical produced in reaction (2). As a result, two molecules of polydimethylsiloxane are cross-linked through methylene bridge.

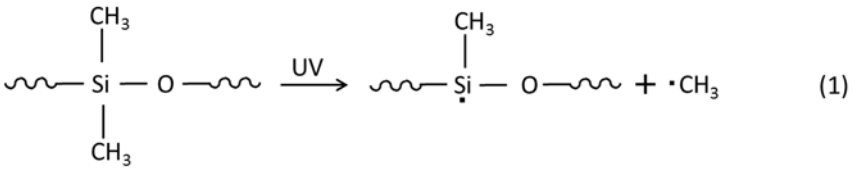

(1)

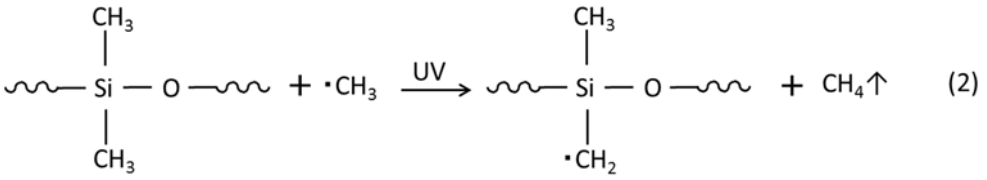

(2)

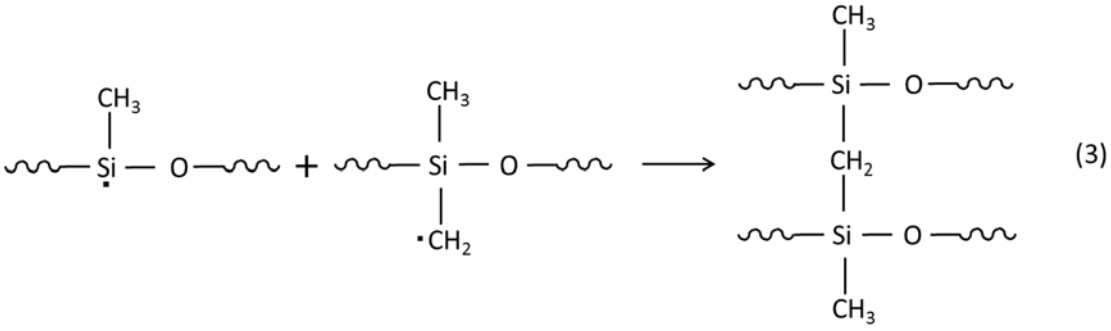

(3)

Next, reactions (4) to (7) show the conceivable reactions of polydimethylsiloxane and AO. Reaction (4) is the abstraction of hydrogen atom by AO from methyl group of polydimethylsiloxane. As a result, methylene radical and hydroxyl radical are formed. Reaction (5) is a reaction between methylene radical produced in reaction (4) and AO. AO oxidizes methylene radical with formation of Si-centered radical, carbon monoxide and water. Reaction (6) is the recombination reaction between Si-centered radical produced in reaction (5) and hydroxyl radical produced in reaction (4). As a result, silanol (Si-OH) group is formed. Reaction (7) is the condensation reaction between two molecules of polydimethylsiloxane with silanol groups. As a result, oxygen bridge (Si-O-Si) and water are produced.

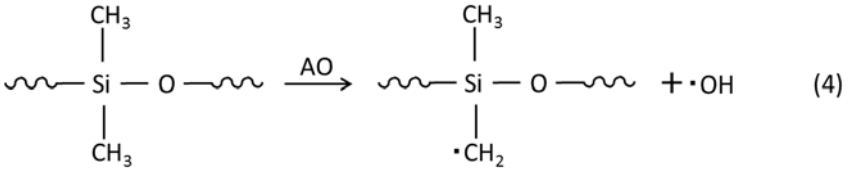

(4)

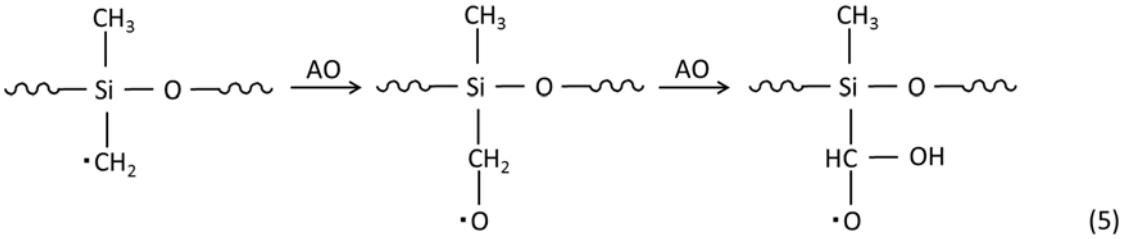

(5)

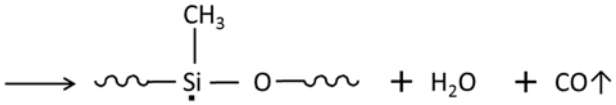

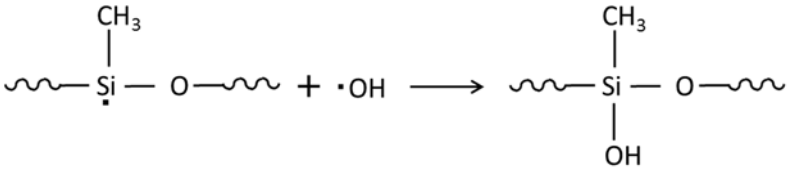

(6)

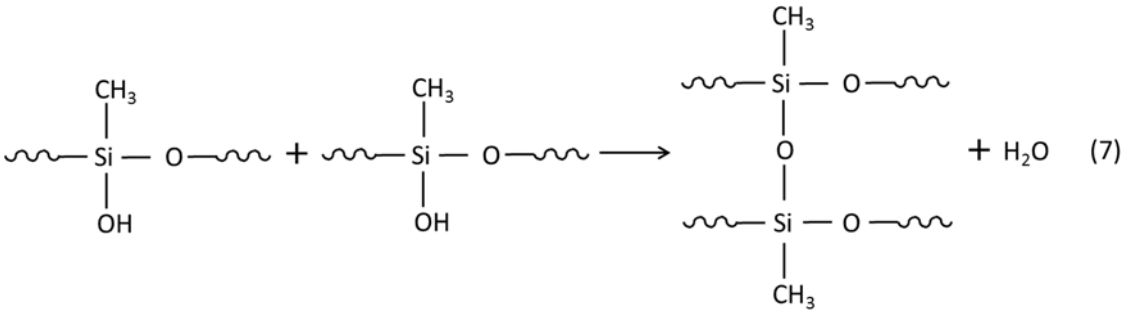

(7)

Therefore, reactions of polydimethylsiloxane and UV and AO are conceivable as shown in reactions (8) and (9). Reaction (8) is the cross-linking reaction between two molecules of polydimethylsiloxane under action of UV irradiation. As a result, methylene bridge and methane are formed. Reaction (9) is a reaction between cross-linked polydimethylsiloxane and AO. As a result, oxygen bridge between two cross-linked polydimethylsiloxane molecules is produced with evolution of water and carbon monoxide.

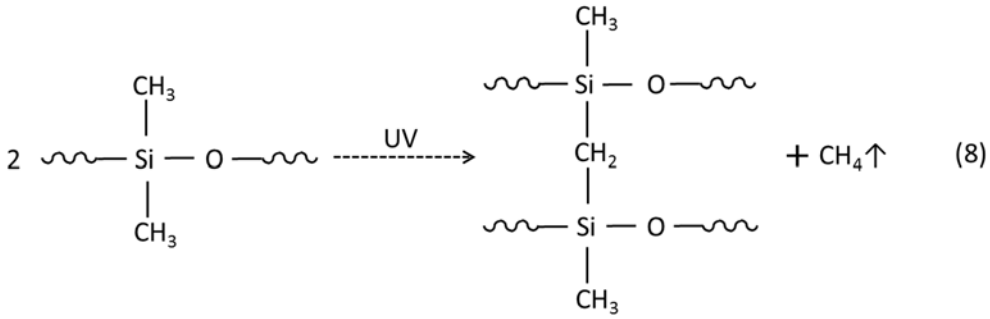

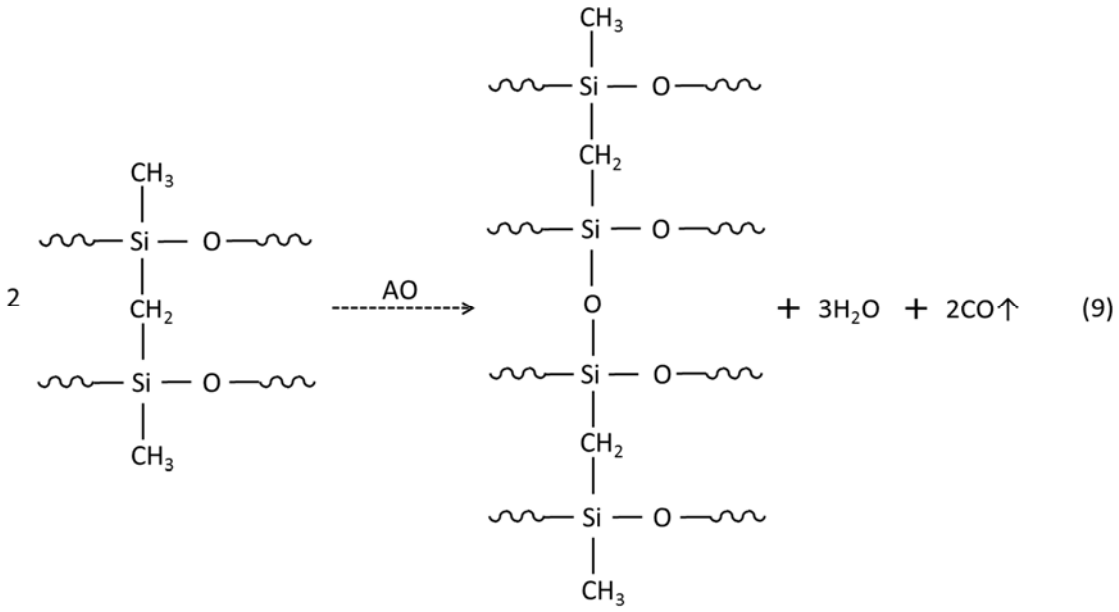

It is necessary to verify the volatile compositions for confirming that the reactions are correct or not. However, verification of the volatile compositions was not conducted here because the purpose of the present work is not to clarify the chemical reaction processes but to confirm the formation process of SiO_2-based microparticles derived from silicone contaminants in space. Sufficient clues about chemical changes of silicone contaminants could be obtained because it is confirmed that SiO_2 and SiO_2-based components were formed from silicone contaminants derived from RTV-S691 with only AO or UV and AO.

Table 3-8. The intensity ratios of silicone contaminants.

	Intensity (100-Transmittance, %)			Intensity ratio		
	$Si\text{-}CH_3$ (800 cm^{-1})	Si-O-Si (1050 cm^{-1})	$Si\text{-}CH_3$ (1260 cm^{-1})	$Si\text{-}CH_3$ (800 cm^{-1})	Si-O-Si (1050 cm^{-1})	$Si\text{-}CH_3$ (1260 cm^{-1})
None irradiated Silicone contaminants	3.9	4.41	2.87	0.88	1	0.65
Z-Expt. No.1	20.09	24.64	16.72	0.82	1	0.67
Z-Expt. No.2	6.80	11.12	5.71	0.61	1	0.51
Z-Expt. No.3	22.36	36.21	17.89	0.62	1	0.49

3.8 Conclusion

This chapter described the details of experimental conditions and the investigations of chemical changes of silicone contaminants affected with UV and/or AO for clarifying the formation process of microparticle space debris. For the sake of comparison the effects of UV and/or AO to silicone contaminants, the irradiation of UV and/or AO to silicone contaminants and detailed investigation by using FT-IR spectroscopy and XPS were performed. As a result, it is confirmed experimentally as follows;

1) Si-Ph bond was reduced especially by UV irradiation,
2) the content of C was reduced and the content of oxygen was increased in silicone contaminants by AO irradiation,
3) hydroxyl group was generated by oxidation reaction caused of AO irradiation,
4) SiO_2 was formed from silicone contaminants by AO irradiation, and
5) UV irradiation influences the reaction between AO and silicone contaminants.

Several results discussed in this chapter are published on Refs. (3-27) and (3-28) entitled as “Impact Assessment about UV- and AO-Irradiated Silicone Contaminants through Optical Property Measurement” and “The Effect of Ultraviolet Irradiation on Adhesion Behavior of Silicone Contaminants (in Japanese)," respectively.

The morphological changes of silicone contaminants affected with UV and AO are evaluated for obtaining the clues to clarify the formation process of microparticle space debris in Chapter 4.

References

(3-1) H. Onuma, M. Okada, and Y. Miyata, "Temperature Dependence of Density and Surface Tension for Silicone Oils," *Int. J. Microgravity Sci. Appl.*, **7** (3) (1990) pp. 109-115.

(3-2) R. Yamanaka, S. Baba, J. Matsuyama, E. Miyazaki, and T. Tamura, "Report on the Research and the Development of In-situ Contamination Spectroscopic Analysis Chamber," JAXA-RM-11-018, (2012). (in Japanese)

(3-3) Y. Kimoto, K. Yano, J. Ishizawa, and E.Miyazaki, "Post Retrieval Analysis of Space Environment Monitoring Samples: Radiation Effects, UV, and Atomic Oxygen Fluence," *Proc. International Symposium on "SM/MPAC & SEED Experiment"*, JAXASP-08-015E, (2008).

(3-4) Y. Kimoto, S. Ichikawa, E. Miyazaki, K. Matsumoto, J. Ishizawa, H. Shimamura, R. Yamanaka, and M. Suzuki, "Passive Space Environment Effect Measurement on JEM/MPAC&SEED," *Proc. of ICPMSE-9*, (2009) pp.207–211.

(3-5) K. Mori, and E. Miyazaki, "Evaluations of Polymeric Materials in Space Environment for Space Use," *Nippon Gomu Kyokaishi*., **86** (12) (2013) pp.367-372. (in Japanese)

(3-6) Y. Tanaka, M.Iwaki, S. Obara, and H. Nagata, "New High Vacuum Test Facilities for Mechanical Components (part 1) –UHV Surface Properties Test Facility and Combined Space Effects Test Facility," *Proceedings of 21st International Symposium on Space Technology and Science*, **21** (1998) pp.1078-1082.

(3-7) E. Miyazaki, H. Shimamura, and Y. Kimoto, "Ground Simulation Tests of Simultaneous Irradiation from Three Beam Sources on Materials at the Combined Space Effects Test Facility," *Proc. 11th International Symposium on Materials in a Space Environment*, (2009) pp.15-18.

(3-8) H. Shimamura, and E. Miyazaki, "Handbook of the combined Space Effects Test Facility," JAXA-RM-10-013, (2011).

(3-9) H. Shimamura, and E. Miyazaki, "Investigations into Synergistic Effects of Atomic Oxygen and Vacuum Ultraviolet," *J. Spacecraft and Rockets*, **46** (2) (2009) pp.241-247.

(3-10) ASTM Standard, “Standard Practices for Ground Laboratory Atomic Oxygen Interaction Evaluation of Materials for Space Application,” E-2089-00, (2014).

(3-11) K.K. de. Groh, and B.A. Banks, “Techniques for Measuring Low Earth Orbital Atomic Oxygen Erosion of Polymers,” NASA/TM-2002-211479, (2002).

(3-12) M. Okahara, T. Nishiyama, T. Shiroiwa, M. Nomura, A. Baba, S. Hamanaka, T. Fukuo, M. Fujiwara, I. Masuda, H. Matsuda, M. Miura, and H. Wakita, “Kikibunsekinotebiki (second edition),” Y. Izumi, M. Ogawa, S.Kato, J. Shiokawa, and T. Shiba , Kagakudojin, (2005). (in Japanese)

(3-13) M. Hesse, H. Meier, and B. Zeeh, “Spectroscopic Methods in Organic Chemistry,” Kagakudojin, (2005). (in Japanese)

(3-14) K. Yoshihara, “Nyumon Hyoumenbunseki,” A. Doyama, K. Ogawa, and M. Kitada, Uchida Rokakuho Publishing Co., LTD., (2003). (in Japanese)

(3-15) K. Tanaka, S. Tanuma, K. Domae, M. Nagoshi, and K. Nisawa, “Xsenkodennshibunnkouhou,” Nihonhyoumenkagakukai, Maruzen Co., LTD., (2005). (in Japanese)

(3-16) European Cooperation for Space Standardization (ECSS), “Space product assurance-Detection of organic contamination of surfaces by infrared spectroscopy,” Q-ST-70-05C, (2009).

(3-17) P.J. Launer, “Infrared analysis of organosilicon compounds: spectra-structure correlations,” *Silicone compounds register and review*, **100** (1987).

(3-18) J. Garrett, “Outgassing Measurements on RTV S691 Silicone Adhesive,” Outgassing Services International (OSI), (2006).

(3-19) D. Cai, A. Neyer, R. Kuckuk, and H.M. Heise, “Raman, mid-infrared, near-infrared and ultraviolet-visible spectroscopy of PDMS silicone rubber for characterization of polymer optical waveguide materials,” *J. Molecular Structure*, **976** (2010) pp.274-281.

(3-20) E.R. Lippincott, A.V. Valkenburg, C.E. Weir, and E.N. Bunting, “Infrared Studies on Polymorphos of Silicone Dioxide and Germanium Dioxide,” *J. Research of the National Bureau of Standards*, **61** (1) (1958) pp.61-70.

(3-21) A.L. Smith, “Infrared spectra-structure correlations for organosilicon compounds,”

Spectrochimica Acta, **16** (1-2) (1960) pp.87-105.

(3-22) G.A. Harvey, "Silazane to Silica," *Proc. the LDEF-69 months in Space SecondPost-Retrieval Symposium*, NASA CP-3194 Part 3, (1992) pp.797-810.

(3-23) Joyce A. Dever, "Low Earth Orbital Atomic Oxygen and Ultraviolet Radiation Effects on Polymers," NASA Technical Memorandum 103711, (1991).

(3-24) P.T. Chen, "Contamination Effects due to Space Environmental Interactions," *39th Aerospace Science Meeting & Exhibit, AIAA*, (2001) pp.1-11.

(3-25) J. Dever, B. Banks, and K.de Groh, "Degradatation of Spacecraft materials. Handbook of Environmental Degradation of Materials," *William Andrew Publishing*, (2005) pp.466-475, 477, 479-480.

(3-26) E. Grossman, and I. Gouzman, "Space environment effects on polymers in low earth orbit," *Nucl. Instr. and Meth. in Phys. Res,* B 2008, (2003) pp. 48-57.

(3-27) Riyo Yamanaka, Kazuyuki Mori, Eiji Miyazaki, Takao Yamaguchi, and Osamu Odawara "Impact Assessment about UV- and AO-Irradiated Silicone Contaminants through Optical Property Measurement." *International Journal of Microgravity Science*, Vol. 33, No. 4 (2016) pp.330408-1-330408-6.

(3-28) Riyo Yamanaka, Eiji Miyazaki, Takao Yamaguchi, and Osamu Odawara "The Effect of Ultraviolet Irradiation on Adhesion Behavior of Silicone Contaminants." *Proc. The 37th Japan Symposium on Thermophysical Properties*, (2016) pp.114-116. (in Japanese)

Chapter 4:

Morphological Changes of Silicone Contaminants

4.1 Introduction

The investigations of the effects of UV and/or AO to silicone contaminants from the viewpoint of chemical changes and morphological changes are important in order to obtain clues for clarifying the formation process of microparticle space debris. The chemical effects of UV and/or AO to silicone contaminants are studied in Chapter 3. And, it was confirmed that SiO_2 was formed by AO irradiation experimentally. The objective of this chapter is to study the morphological effects of UV and/or AO to silicone contaminants.

In this chapter, the followings are used as procedure to investigate the morphological effects of UV and/or AO to silicone contaminants. The conceptual diagrams of the experimental procedures are shown in Chapter 3 Fig. 3-1.

1) Preparation of materials.

2) Deposition of contaminants on substrate materials.

3) UV and/or AO irradiation to contaminants.

4) Morphological analysis of samples.

This chapter deals with the details of experimental conditions and describes about the investigations of morphological changes of silicone contaminants affected with UV and/or AO for clarifying the formation process of microparticle space debris. For the sake of comparison about morphological changes caused by UV and/or AO to silicone contaminants, the irradiation of UV and/or AO to silicone contaminants deposited on polyimide film, which is widely used for spacecraft, and detailed morphological investigation were performed. **S**canning **E**lectron **M**icroscopy (SEM) and EDX spectroscopy were used for evaluation of morphological changes of silicone contaminants with UV and/or AO irradiation. As a result, clues for clarifying the

formation process of microparticle space debris could be obtained from the viewpoint of morphological changes.

4.2 Experimental Conditions

Room-temperature-vulcanizing silicone adhesive No. 691 (RTV-S691) from Wacker Asahikasei Silicone Co., Ltd. was selected as a silicone outgassing source, the same material was used for the experiments described in Chapter 3. And, 125-μm-thick polyimide film from UPILEX-S®; UBE Industries, Ltd. was chosen as a substrate material to be deposited by silicone contaminants outgassed from silicone adhesive RTV-S691. The polyimide film is widely used as thermal control material for spacecraft, and the polyimide film was actually applied as a base film for the flexible solar array of the SFU.

4.3 Experimental Procedures

4.3.1 Preparation of Materials

Silicone adhesive RTV-S691, whose size was 40 mm X 40 mm X 6 mm, was cured at room temperature the same as described in Chapter 3. The samples of polyimide films, whose size was ϕ 25 mm and t 125 μm, were cleaned with ultrasonic cleaning using ethyl alcohol and acetone. The masses of polyimide film samples were measured before and after the deposition of silicone contaminants by using the microbalance, and the deposition thickness was calculated using data on the weight of deposited silicone contaminants divided by the deposition area. The detail of the microbalance and the way to calculate the deposition thickness of silicone contaminants are described in Chapter 3 Section 3.3.1. One point should be mentioned that the masses of silicone contaminants deposited on polyimide film samples are only rough indication, because the mass of

polyimide film is changed drastically by moisture absorption. Therefore the masses of silicone contaminants deposit to polyimide film samples were controlled to be thicker than 400 nm by TQCM (MK-20; QCM Research) which is equipped in *In-situ* Contamination Spectroscopic Analysis Chamber (hereafter "contamination chamber") and its details are described in Chapter 3 Section 3.3.2.

4.3.2 Depositing Contaminants on Substrate Materials

The deposition of silicone contaminants derived from RTV-S691 on polyimide film samples was conducted by using the contamination chamber[4-1], described in details in the Chapter 3 Section 3.3.2.

RTV-S691 as a silicone outgassing source was heated to 125°C in the contamination chamber under pressure of 10^{-3} Pa, while the surfaces of the polyimide film samples were kept at 25°C. The thermal conditions were decided in reference to ASTM E595[4-2]. Silicone contaminants were deposited on one side of all the polyimide film samples equally in terms of area (314 mm^2).

4.3.3 UV and/or AO Irradiation to Contaminants

After the deposition of silicone contaminants derived from RTV-S691 on the polyimide film samples, the deposited side of the polyimide film samples was irradiated with UV and/or AO in series for investigating the effects of UV and/or AO to the polyimide films with silicone contaminants. The conditions of UV and AO irradiation were decided with the results of passive environment measurement[4-3), (4-4]. Irradiation conditions are shown in Chapter 3 Table 3-1. Irradiation of UV-1st, AO-1st, UV-2nd, and AO-2nd was conducted in series. Table 3-1 is placed below again for promoting a better understanding of UV and AO irradiation conditions in the present work.

Table 3-1. UV and AO irradiation conditions.

Experiment No.	Irradiation in series				Irradiation angle
	UV-1st irradiation (J/cm^2)	UV-2nd irradiation (J/cm^2)	AO-1st irradiation ($atoms/cm^2$)	AO-2nd irradiation ($atoms/cm^2$)	
Expt.-No.1	0.9×10^5	0.6×10^5	none	none	90°
Expt.-No.2	none	none	1.5×10^{21}	1.0×10^{21}	90°
Expt.-No.3	0.9×10^5	0.6×10^5	1.5×10^{21}	1.0×10^{21}	Both UV and AO: 90°
Expt.-No.4	0.9×10^5	0.6×10^5	1.5×10^{21}	1.0×10^{21}	UV: 90°, AO: 90° for the 1st irradiation,45° and 135° for 2nd irradiation

ⅰ) Irradiation of Ultraviolet Light

UV was irradiated to silicone contaminants deposited on the polyimide film samples by using a high-vacuum chamber equipped with a Xe lamp (Type UXL-2501YA2.5kW Xe short-arc lamp) in vacuum less than 10^{-4} Pa at Tsukuba Space Center[4-5]. The Xe lamp has a wide range of wavelength. However, the flux of light having wavelength less than 250 nm was reduced by a lamp coating for avoiding the creation of ozone, and the IR region, which significantly increases the temperature, was reflected by using a dichroic mirror[4-5]. As a result, the main range of irradiation wavelength was 250-500 nm[4-5]. Irradiation intensity was 10 UV-sun in the present work. 1 UV-sun is equivalent to 11.8 mW/cm^2 which is integration of spectral intensity of 200-400 nm in orbit. UV irradiation fluence in the present work is shown in Table 3-1. The specifications of this facility are described in Chapter 3 Section 3.3.3.

ⅱ) Irradiation of Atomic Oxygen

AO was irradiated to silicone contaminants deposited on the polyimide film samples by using the Combined Space Effects Test Facility under a high vacuum (10^{-3}-10^{-2} Pa) [4-6]. The AO average flux was 5.5 X 10^{15} atoms/cm^2･s and the AO beam average speed was 8.1 km/s. Their values ware controlled referring from the values of space environment measurement[4-7]. AO irradiation fluence in the present work is shown in Table 3-1. The details of this facility are shown in Chapter 3 Section 3.3.3.

4.3.4 Sample Analysis

After the irradiation of UV and/or AO to silicone contaminants deposited on the polyimide film samples, morphological changes of the polyimide films with silicone contaminants were evaluated by using SEM[4-8] and EDX spectroscopy[4-9]. The samples for the observation represented the cross sections of polyimide films with deposited silicone contaminants irradiated by UV and/or AO. The cross sections of the polyimide films with silicone contaminants were prepared by using a microtome (Leica, RM2265). The cross section samples can be made by cutting with a microtome cooled under an extremely low temperature of approximately -150 °C. The platinum (Pt) coating was deposited on the surface of polyimide film samples with silicone contaminants for preventing the charge build-up.

Morphology of silicone contaminants was observed by SEM. SEM observation was performed by using JEOL JSM-6360 and Hitachi High-Technologies Corporation S-5500 microscopes.

The elemental distribution of silicone contaminants was evaluated by EDX spectroscopy. The elemental distribution was also investigated by using Hitachi High-Technologies Corporation S-5500 equipped with EDX spectroscopy. The acceleration energy of the X-ray was 5 kV.

4.4 Mass Measurement

Table 4-1 shows the masses of the polyimide film samples before and after the deposition of silicone contaminants. The deposition thicknesses described in Table 4-1 were calculated from the weight of deposited silicone contaminants measured by using the microbalance (MX6; Mettler Toledo International, Inc.).

As noted in Section 4.3.1, the masses of silicone contaminants deposited on polyimide film samples are only rough indication, because the mass of polyimide film is changed drastically by moisture absorption. Consequently, the masses of silicone contaminants deposited on the polyimide film samples were controlled to be thicker than 400 nm by TQCM (MK-20; QCM Research) equipped in the contamination chamber.

Table 4-1. The masses of polyimide film samples before and after the deposition of silicone contaminants and the deposition thicknesses.

Material	Sample No.	Deposited contaminants, mg			Deposition thickness, nm
		Before	After	Δ (After-Before)	
Polyimide film	PI-Expt. No.1	89.393	89.463	0.070	222.9
	PI-Expt. No.2	88.789	88.840	0.051	162.4
	PI-Expt. No.3	86.805	86.889	0.084	267.5
	PI-Expt. No.4	86.805	86.889	0.084	267.5

4.5 Characteristic Morphological Changes with UV and/or AO

The cross sections of the polyimide film samples with silicone contaminants irradiated with UV and/or AO were used for observing the effect of UV and/or AO irradiation on the shape of the polyimide films deposited with silicone contaminants and the elemental distribution.

4.5.1 Shape Observation

Fig. 4-1 shows SEM images of the cross sections of the polyimide film samples deposited with silicone contaminants. Darker lower part in the images is polyimide film, and lighter upper part is silicone contaminants' layer taken in perspective due to observation under a small inclination angle. As can be seen from Fig. 4-1 (A) the as deposited sample represents a thin layer of silicone contaminants with randomly distributed droplets having size about 20-30 μm.

Fig. 4-1 (B) shows polyimide film deposited by silicone contaminants after UV irradiation. As can be seen from the Figure, the general shape of the polyimide film and contaminants layer was not changed so much by UV irradiation, however the size of the droplets decreased to 20 μm in average. Much more serious morphological changes were observed for the samples irradiated by AO, as shown in Fig. 4-1 (C, irradiation by AO only) and Fig. 4-1 (D, irradiation by AO after UV). It can be seen from the Figures, that the surfaces of the polyimide films with silicone contaminants were considerably eroded by AO irradiation with and without UV irradiation (Fig. 4-1 (C) and (D)). The depth of etching reaches 40 μm in case of sample irradiated by AO only, and 30 μm in case of sample irradiated by AO and UV. However, in both cases, there are parts, which were not eroded. It is confirmed that the non-eroded parts represent areas of polyimide film covered by droplets of silicone contaminants by comparing Figs 4-1 (A), (B) with (C) and (D), as a result, column-like structure is produced. In addition, it is confirmed that the size of non-eroded parts is larger in case of the sample irradiated by both AO and UV, and it can be estimated to be about 30-40 μm by compering Fig. 4-1 (C) with Fig. 4-1 (D).

It is known that AO reacts with surface materials used on spacecraft in two ways. First, AO erodes hydrocarbon materials[(4-10) - (4-12)]. Secondly, silicone materials widely used for spacecraft are permanently fixed by oxidation with AO, because reaction between the silicone and AO generates silicon oxide (SiOx) [(4-10) - (4-12)]. Taking into account these information can be supposed that in the present work, areas of polyimide film deposited by silicone contaminants lacking a sufficient thickness to generate silicon oxide layers

were eroded by AO. However, parts of polyimide film covered with droplets of silicone contaminants were not eroded as shown in Fig. 4-1 (C) and (D).

AO actually irradiates surface materials of spacecraft from not only one angle but from various angles on orbit, therefore the morphological impacts were also verified under different angles of AO irradiation (Fig. 4-1 (E)). It can be seen from the Figure, that irradiation by AO from various angles led to eroding of polyimide film under droplets of silicone contaminants, while droplets remained at the same place. As a result, a reversed pyramidal structure is observed (Fig. 4-1 (E)). It means that if irradiation continues longer, like under space conditions, the droplets of silicone contaminants can be cut from polyimide film by AO irradiation. This fact can serve as a verification of the morphological process of forming microparticles mainly consisting of silicone contaminants deposited on polyimide film as droplets (ca. 20 μm) shown in Fig. 4-1 (A). Under the effects of AO irradiation, the droplets could transform into microparticles as can be imagined from Fig. 4-1 (E).

Fig. 4-2 shows high-resolution SEM images of the cross section of the sample irradiated by AO and UV (PI-Expt. No.4). Under high magnification many microparticles much smaller than the microparticles mentioned above were found by detailed observation of the parts eroded by AO as shown in Fig. 4-2. It can be seen from the Figure, that in the areas of polyimide film eroded by AO, numerous round-shaped particles with size 100-150 nm exist. As will be shown later, these particles also have origin in silicone contaminants. The existence of these smaller microparticles suggests that there are two processes of forming large microparticles (20 μm) and small microparticles (100 nm). Smaller microparticles different from that of forming microparticles.

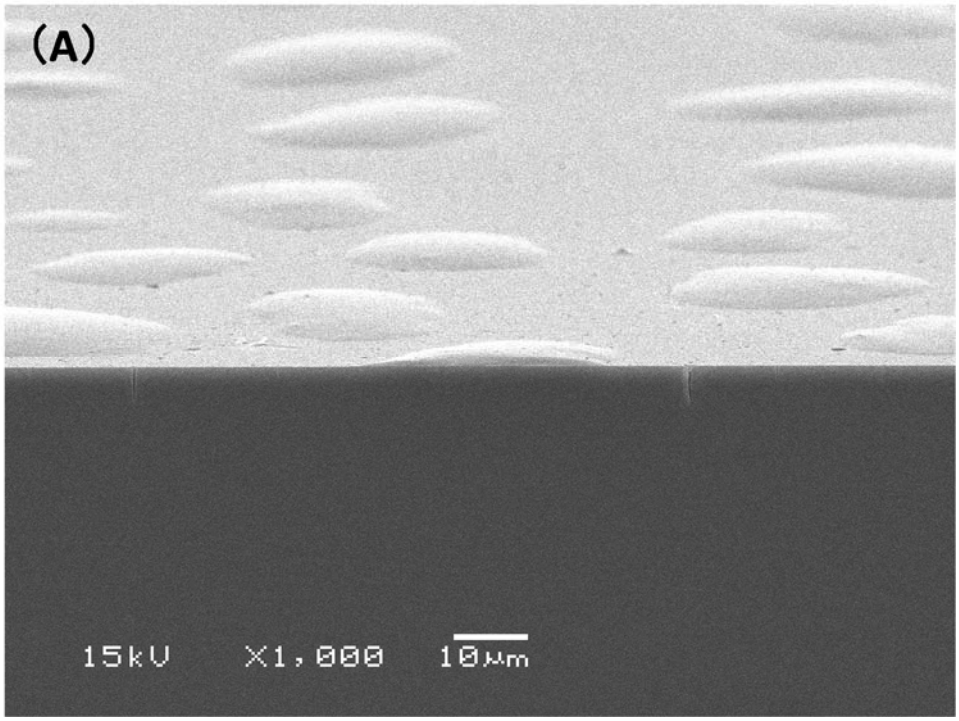

Fig. 4-1 (A). SEM image of the cross section of polyimide film as deposited with silicone contaminants.

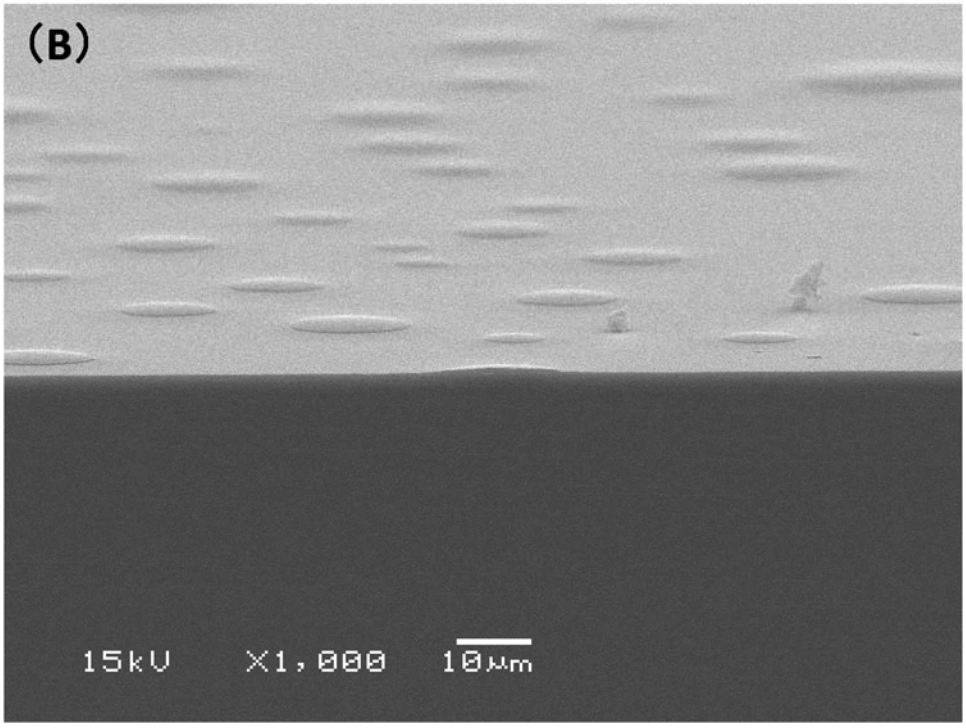

Fig. 4-1 (B). SEM image of the cross section of PI- Expt. No.1.

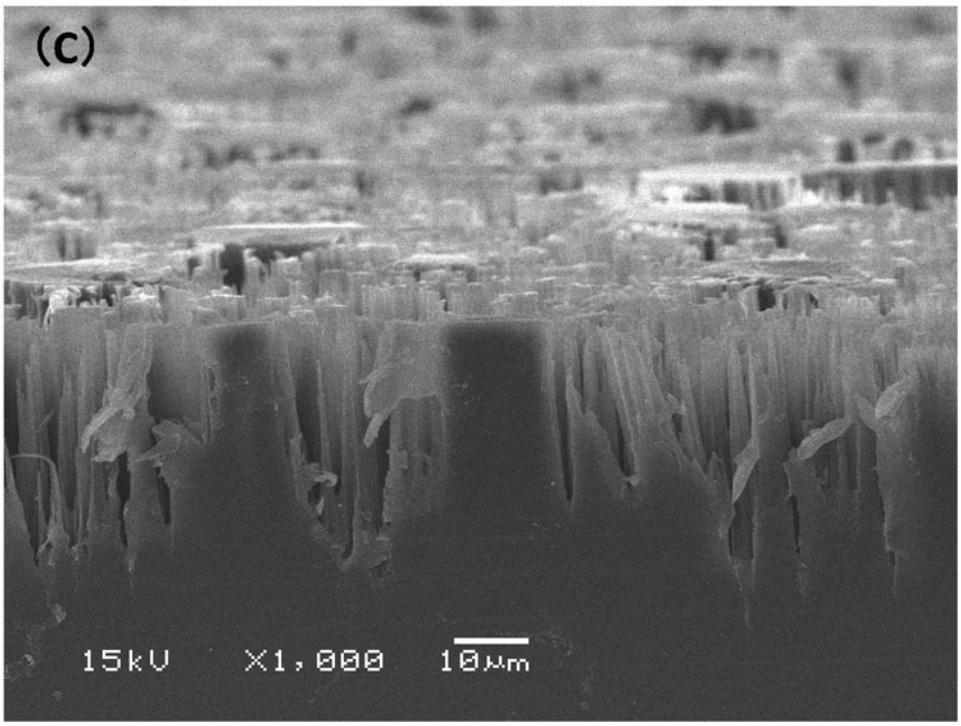

Fig. 4-1 (C). SEM image of the cross section of PI- Expt. No.2.

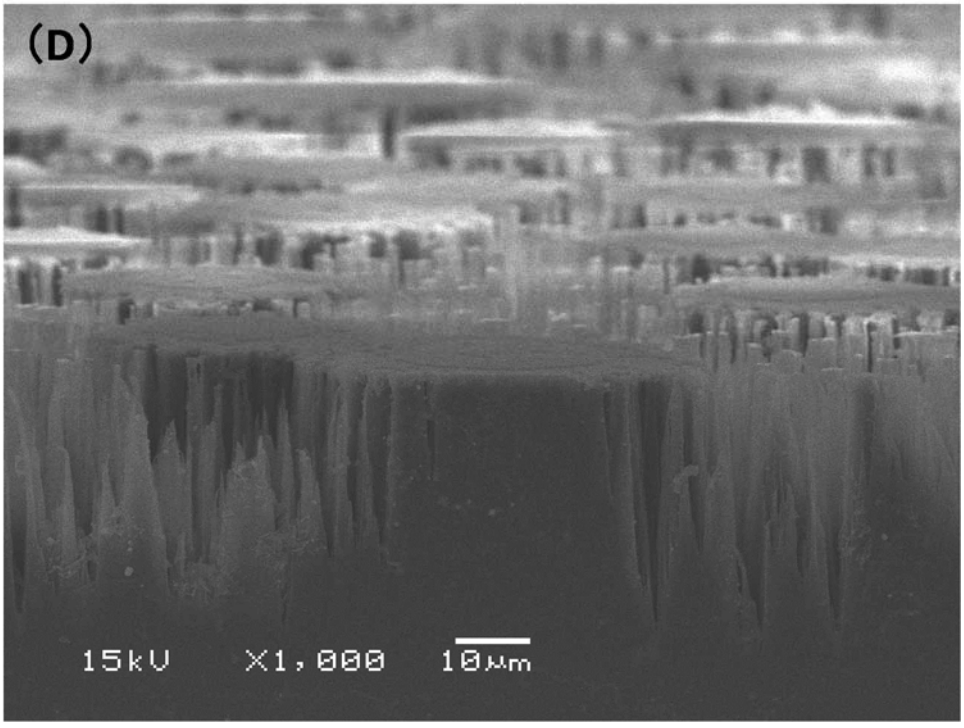

Fig. 4-1 (D). SEM image of the cross section of PI- Expt. No.3.

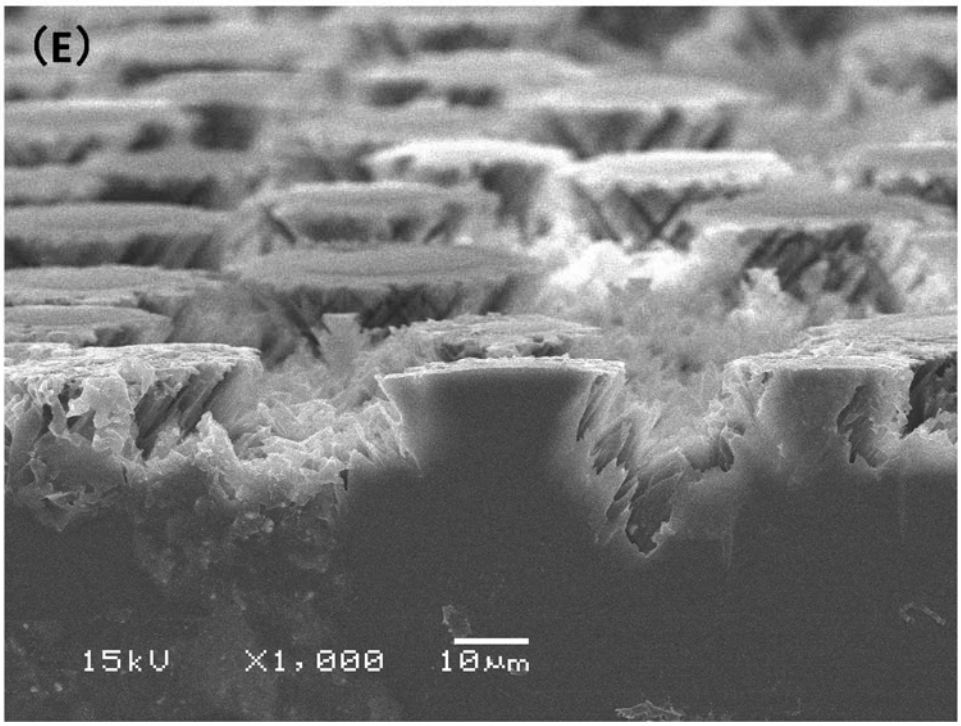

Fig. 4-1 (E). SEM image of the cross section of PI- Expt. No.4.

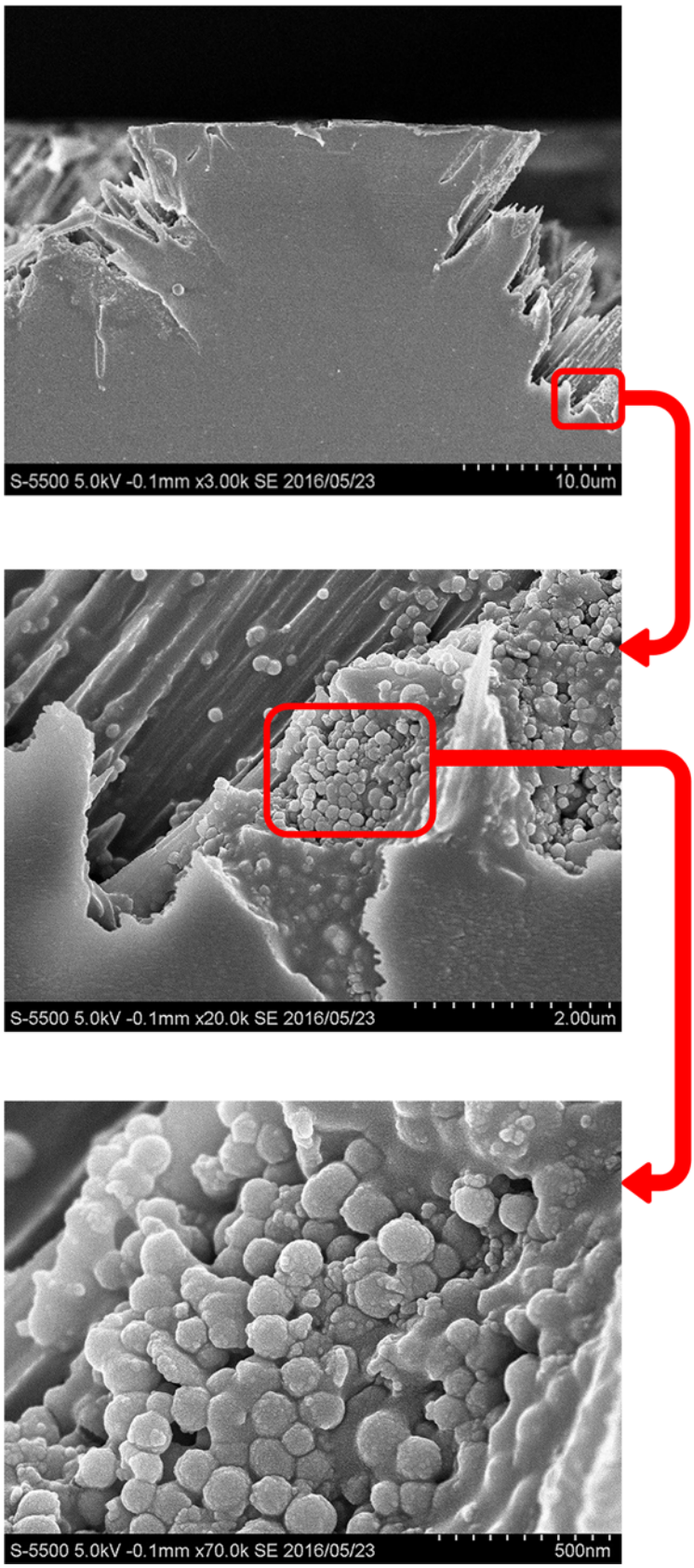

Fig. 4-2. High-resolution SEM images of the cross section of PI-Expt. No.4.

4.5.2 Elemental Distribution

Elemental distributions of Si, C, O, and Pt were investigated by EDX spectroscopy to confirm the connection between deposited silicone contaminants and formed microparticles observed by SEM. The cross section of the sample PI-Expt. No.4, coated by Pt, was used for analysis.

Fig. 4-3 (A) shows SEM image of the sample with the points used for EDX analysis. The point 1 is located on the surface of the droplet of silicone contaminants effected with UV and AO irradiation, and the point 2 is located on the surface of polyimide film; the point 3 represents the part of polyimide film eroded by AO and effected with UV and AO irradiation as shown in Fig. 4-3 (A). C, O, and Pt were detected at every analyzed points (Fig. 4-3 (B), (C) and (D)). However, Si was detected at the analyzed points 1 and 3 (Fig. 4-3 (B) and (D)). It can be explained that C and O were derived from the polyimide films, because the structure of the polyimide film (UPIREX-S®: DuPont registered material) shown in Fig. 4-4 is containing C and O. Additionally, C and O detected at the analyzed points 1 and 3 are thought to be derived from the silicone contaminants on PI-Expt. No.4, because the XPS analysis results of the elemental depth profile of silicone contaminants deposited on the M-Expt. No.3 clarified the existence of C and O in the silicone contaminants with UV and AO irradiation. On the other hand, Si is not contained in the structure of the polyimide film. Thus, the Si detected at the analyzed points 1 and 3 was conceivable that only derived from the silicone contaminants on the PI-Expt. No.4. In other words, Si was distributed particularly in the silicone contaminants deposited on the surface of the polyimide film and the part of the polyimide film eroded by AO. In addition, the analysis spectra are corresponding between the analyzed points 1 and 3 as shown in Fig. 4-3 (B) and Fig. 4-3 (D). The fact suggests that the components of the analyzed points 1 and 3 are the same, which means that the two kinds of microparticles confirmed in Section 4.5.1 consist of the same components. These facts indicate three things. First is that the part of the polyimide film covered with droplets of silicone contaminants was not eroded by AO, second is that the eroded silicone contaminants, which are thought to form smaller microparticles,

remained at the part of the sample eroded by AO, and the elemental composition of large microparticles and small microparticles is the same.

Elements of Si, O and C were also contained within the microparticles captured by aerogel mounted on the MPAC units[4-13] as well as the analyzed points 1 and 3.

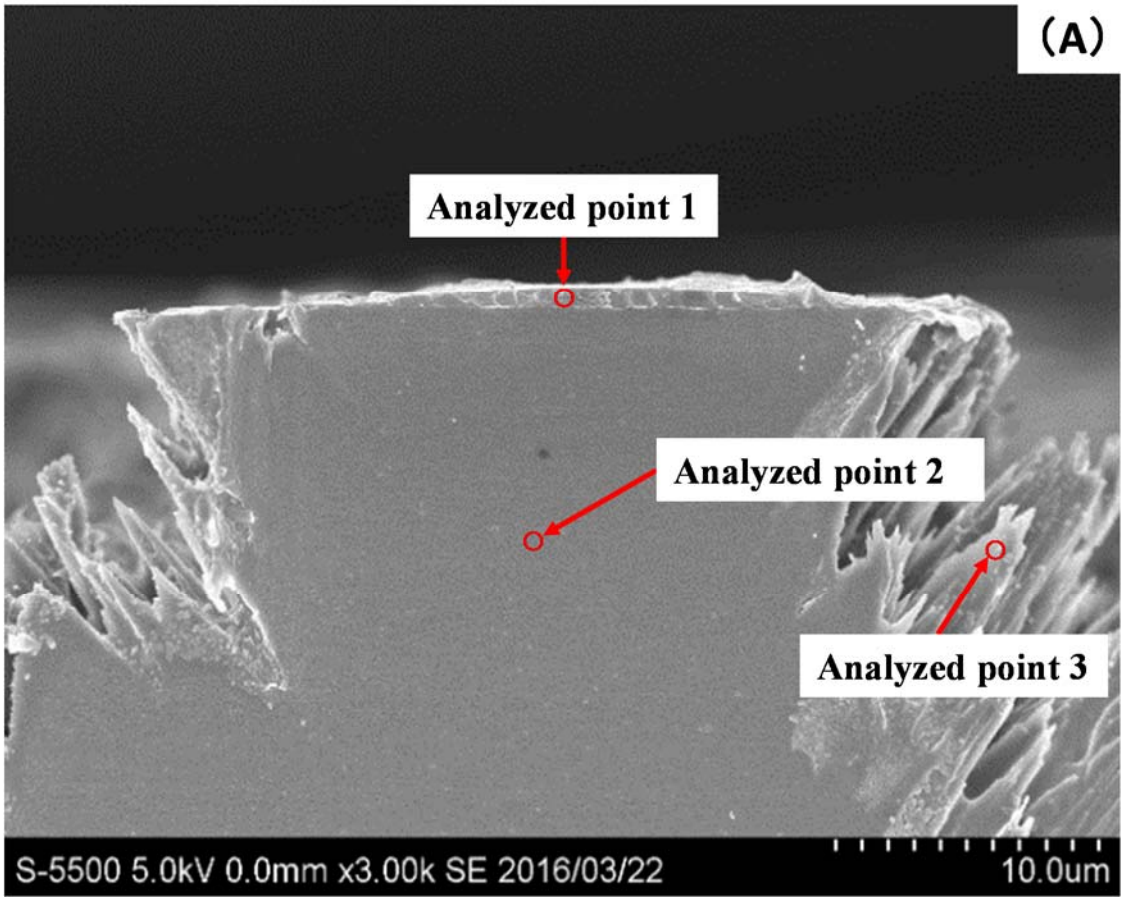

Fig. 4-3 (A). The analyzed points by SEM image.

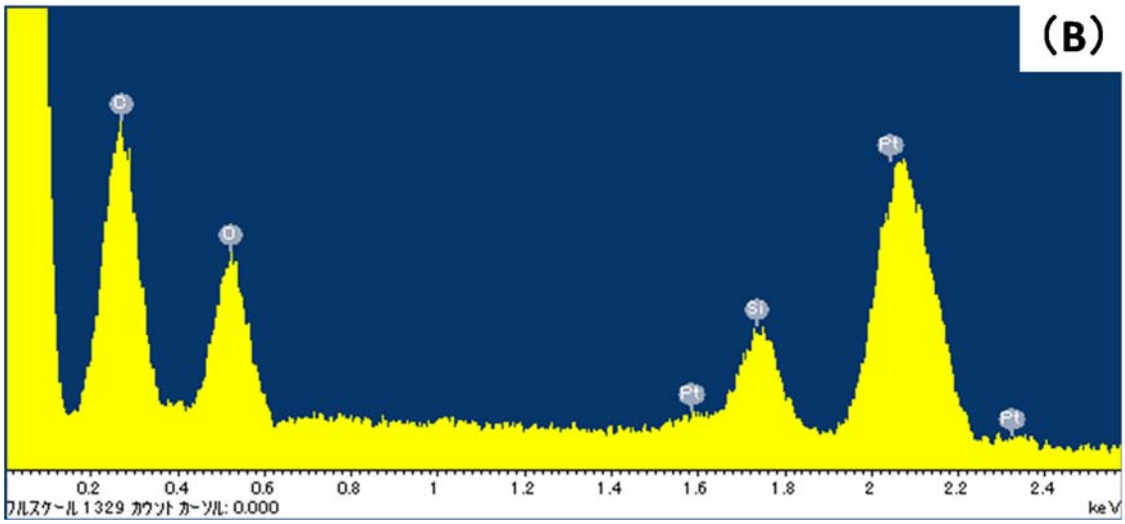

Fig. 4-3 (B). EDX spectrum of analyzed point 1.

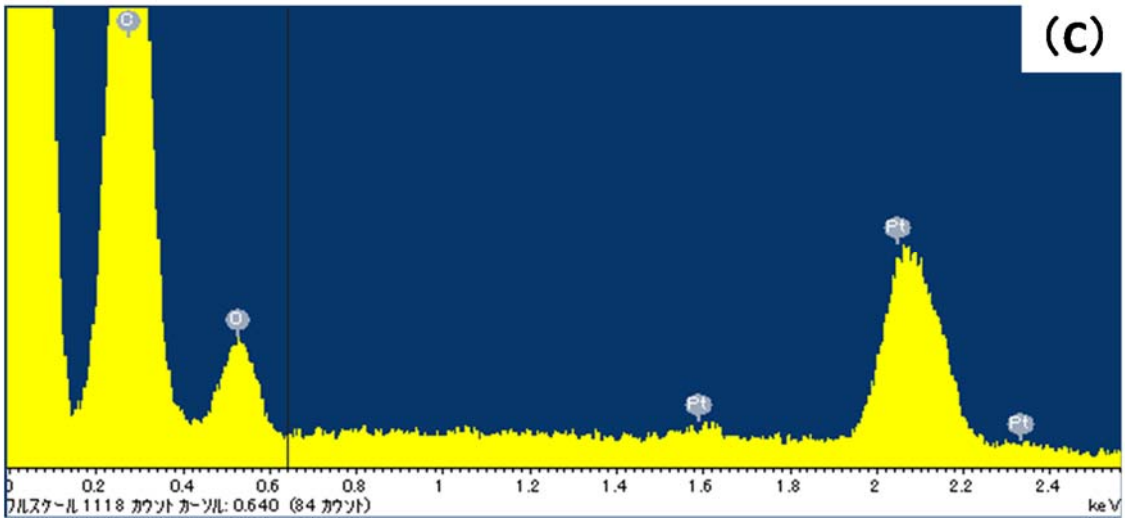

Fig. 4-3 (C). EDX spectrum of analyzed point 2.

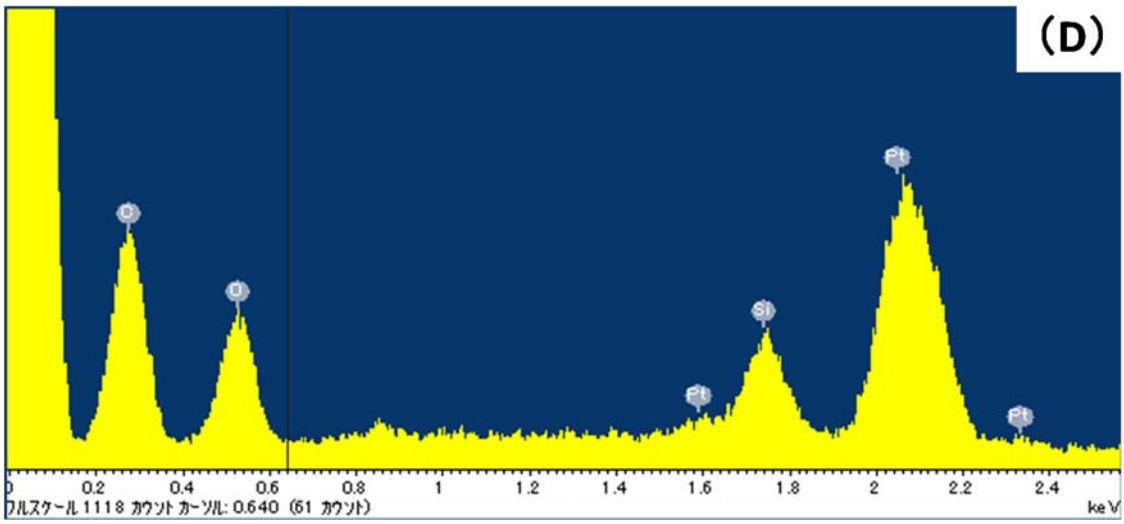

Fig. 4-3 (D). EDX spectrum of analyzed point 3.

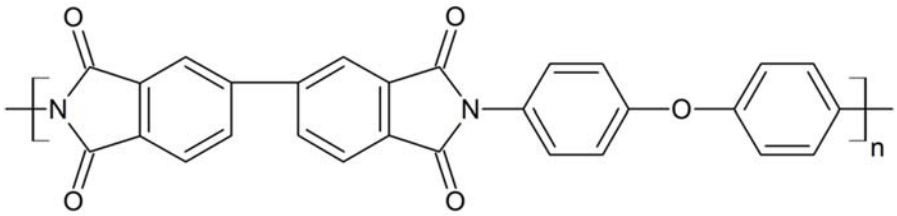

Fig. 4-4. Structure of UPILEX-S®.

4.6 Conclusion

This chapter shows the results of the experimental investigation on the effects of UV and/or AO to silicone contaminants deposited on polyimide films from the viewpoint of morphological changes. The clues were obtained for clarifying the formation process of microparticle space debris by the results of the investigations.

Evaluation of morphological changes of silicone contaminants deposited on polyimide films with UV and/or AO irradiation clarified that the shape of silicone contaminants deposited on polyimide film was not changed by UV irradiation, and large microparticles (ca. 20 μm) and small microparticles (ca. 100 nm) are formed from silicone contaminants deposited on polyimide film with AO irradiation by similar but different processes. And, both of large microparticles and small microparticles are consisted of the same elemental components.

The formation processes of microparticle space debris which were confirmed by the experiments in this chapter will be discussed in Chapter 5 on the basis of the investigations of Chapter 3 and Chapter 4.

References

(4-1) R. Yamanaka, S. Baba, J. Matsuyama, E. Miyazaki, and T. Tamura, “Report on the Research and the Development of In-situ Contamination Spectroscopic Analysis Chamber,” JAXA-RM-11-018, (2012). (in Japanese)

(4-2) American Society for Testing and Materials (ASTM) Standard E-595, “Standard Test Method for Total Mass Loss and Collected Volatile Condensable Materials from Outgassing in a Vacuum Environment,” (1996).

(4-3) Y. Kimoto, K. Yano, J. Ishizawa, and E.Miyazaki, “Post Retrieval Analysis of Space Environment Monitoring Samples: Radiation Effects, UV, and Atomic Oxygen Fluence,” *Proc. International Symposium on “SM/MPAC & SEED Experiment”*, JAXASP-08-015E, (2008) pp.11-17.

(4-4) Y. Kimoto, S. Ichikawa, E. Miyazaki, K. Matsumoto, J. Ishizawa, H. Shimamura, R. Yamanaka, and M. Suzuki, “Passive Space Environment Effect Measurement on JEM/MPAC&SEED,” *Proc. of ICPMSE-9*, (2009) pp.207–211.

(4-5) K. Mori, and E. Miyazaki, “Evaluations of Polymeric Materials in Space Environment for Space Use,” *Nippon Gomu Kyokaishi*. **86** (12) (2013) pp. 367-372. (in Japanese)

(4-6) E. Miyazaki, H. Shimamura, and Y. Kimoto, “Ground Simulation Tests of Simultaneous Irradiation from Three Beam Sources on Materials at the Combined Space Effects Test Facility,” *Proc. 11th International Symposium on Materials in a Space Environment*, (2009) pp.15-18.

(4-7) H. Shimamura, and E. Miyazaki, “Handbook of the Combined Space Effects Test Facility,” JAXA-RM-10-013, (2011).

(4-8) M. Okahara, T. Nishiyama, T. Shiroiwa, M. Nomura, A. Baba, S. Hamanaka, T. Fukuo, M. Fujiwara, I. Masuda, H. Matsuda, M. Miura, and H. Wakita, “Kikibunsekinotebiki (second edition),” Y. Izumi, M. Ogawa, S.Kato, J. Shiokawa, and T. Shiba , Kagakudojin, (2005). (in Japanese)

(4-9) K. Yoshihara, “Nyumon Hyoumenbunseki,” A. Doyama, K. Ogawa, and M. Kitada, Uchida Rokakuho Publishing Co., LTD., (2003). (in Japanese)

(4-10) Joyce A. Dever, “Low Earth Orbital Atomic Oxygen and Ultraviolet Radiation Effects on Polymers,” NASA Technical Memorandum 103711, (1991).

(4-11) P.T. Chen, “Contamination Effects due to Space Environmental Interactions,” *39th Aerospace Science Meeting & Exhibit, AIAA*, (2001) pp.1-11.

(4-12) J. Dever, B. Banks, and K.de Groh, “Degradatation of Spacecraft materials. Handbook of Environmental Degradation of Materials,” *William Andrew Publishing*, (2005) pp. 466-475, 477, 479-480.

(4-13) R. Yamanaka, T. Noguchi, and Y. Kimoto, “Analysis Results of Microparticles Capture Experiment Samples on Service Module,” *J. Spacecraft and Rockets*, **48** (5) (2011) pp.867-873.

Chapter 5:

Modeling of the Formation Process of Microparticle Space Debris from Silicone Contaminants

5.1 Introduction

The experimental results shown in Chapters 3 and 4 provide the clues for clarifying the formation process of microparticle space debris from silicone contaminants. The main findings concerning chemical and morphological changes of silicone contaminants under UV and/or AO irradiation can be summarized as follows;

1) Morphological changes:

1-1) The surface shape of the polyimide film deposited by silicone contaminants is not significantly changed by UV.

1-2) The surface of the polyimide film deposited by silicone contaminants is etched by AO except the parts covered with droplets of silicone contaminants.

1-3) When the AO irradiation angles were varied during the irradiation process, the formation process of microparticles (ca. 20 μm) mainly originated from droplets of silicone contaminants deposited on the polyimide film was observed.

1-4) Smaller microparticles (ca. 100 nm) having the same elemental composition as droplets were observed at the parts of the polyimide film eroded by AO.

2) Chemical changes:

2-1) Bond of Si-Ph is reduced under action of UV.

2-2) AO reduces carbon content and increases oxygen content in silicone contaminants.

2-3) Silicone contaminants are oxidized by AO and as a result hydroxyl group appears.

2-4) Bond of Si-CH_3 decreases under action of AO and as a result SiO_2 is generated.

2-5) UV irradiation influences the reaction between AO and silicone contaminants.

Given this experimental background, the Chapter 5 presents the modeling of the

formation process of the microparticles from silicone contaminants.

5.2 Modeling of the Formation Process of Microparticles Derived from Silicone Contaminants

From the experimental data on morphological changes of silicone contaminants under UV and/or AO irradiation described in Chapter 4, it became evident that microparticles can be formed from silicone contaminants. It has been found that microparticles with size around 20 μm (large microparticles) and much smaller particles with size around 100 nm (small microparticles) were formed.

The formation process of the large microparticles is presented in the form of a conceptual diagram shown in Fig. 5-1.

As it can be seen from the figure, the formation process consists of the next steps;

1) Silicone contaminants deposit on the surface of polymer film as shown in Fig. 5-1 (1) which is comparable to the SEM image shown in Fig. 4-1 (A).
2) Chemical bonds of silicone contaminants are changed by space environment (e.g. UV and AO) as shown in Fig. 5-1 (2) in a way which leads to increase of oxygen content and decrease of carbon content.
3) Polymer film is eroded by AO except the parts of the film covered with droplets of silicone contaminants as shown in Fig. 5-1 (3) which is comparable to the SEM image shown in Fig. 4-1 (D).
4) Polymer film under droplets of silicone contaminants is eroded by AO coming not from right angle.

As a result, microparticles, which can be considered to be identical to the microparticle space debris, are formed as shown in Fig. 5-1 (4) which is comparable to the SEM image shown in Fig. 4-1 (E).

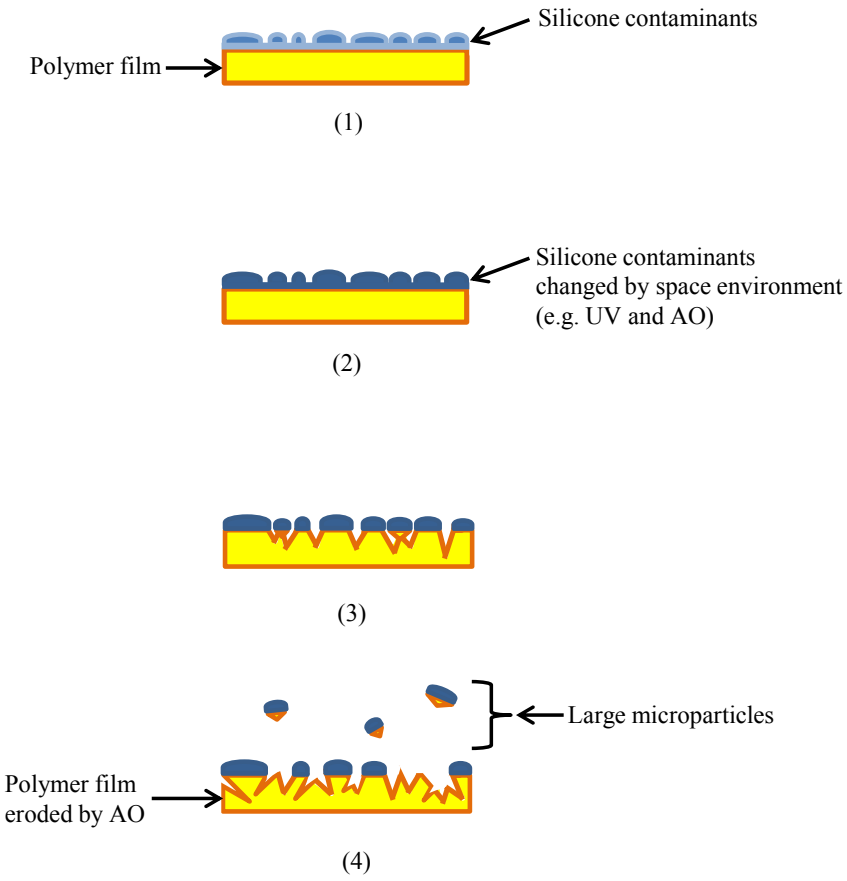

Fig. 5-1. Conceptual diagrams of the formation process of large microparticles on the surface of polymer film.

In the experiments described in Chapter 4, formation of small microparticles was also observed. Here the formation process of such particles is explained. The conceptual diagrams of the formation process in the case of polymer film which is eroded by AO are shown in Fig. 5-2. The next detailed steps of the formation process are shown;

1) Silicone contaminants deposit on the surface of polymer film as shown in Fig. 5-2 (1) which is comparable to the SEM image shown in Fig. 4-1 (A)).
2) Chemical bonds of silicone contaminants are changed by space environment (e.g. UV and AO) as shown in Fig. 5-2 (2), which leads to increase of oxygen content and decrease of carbon content. And, oxidized species are formed.

3) Silicone contaminants deposited on the surface are affected by AO. A part of silicone contaminants may leave from the surface and the other remains on the surface. The remaining silicone contaminants aggregate under the effect of energy of AO irradiation like a snowball, and accordingly small microparticles are formed on the surface as shown in Fig. 5-2 (3) which is comparable to the SEM image shown in Fig. 4-2.

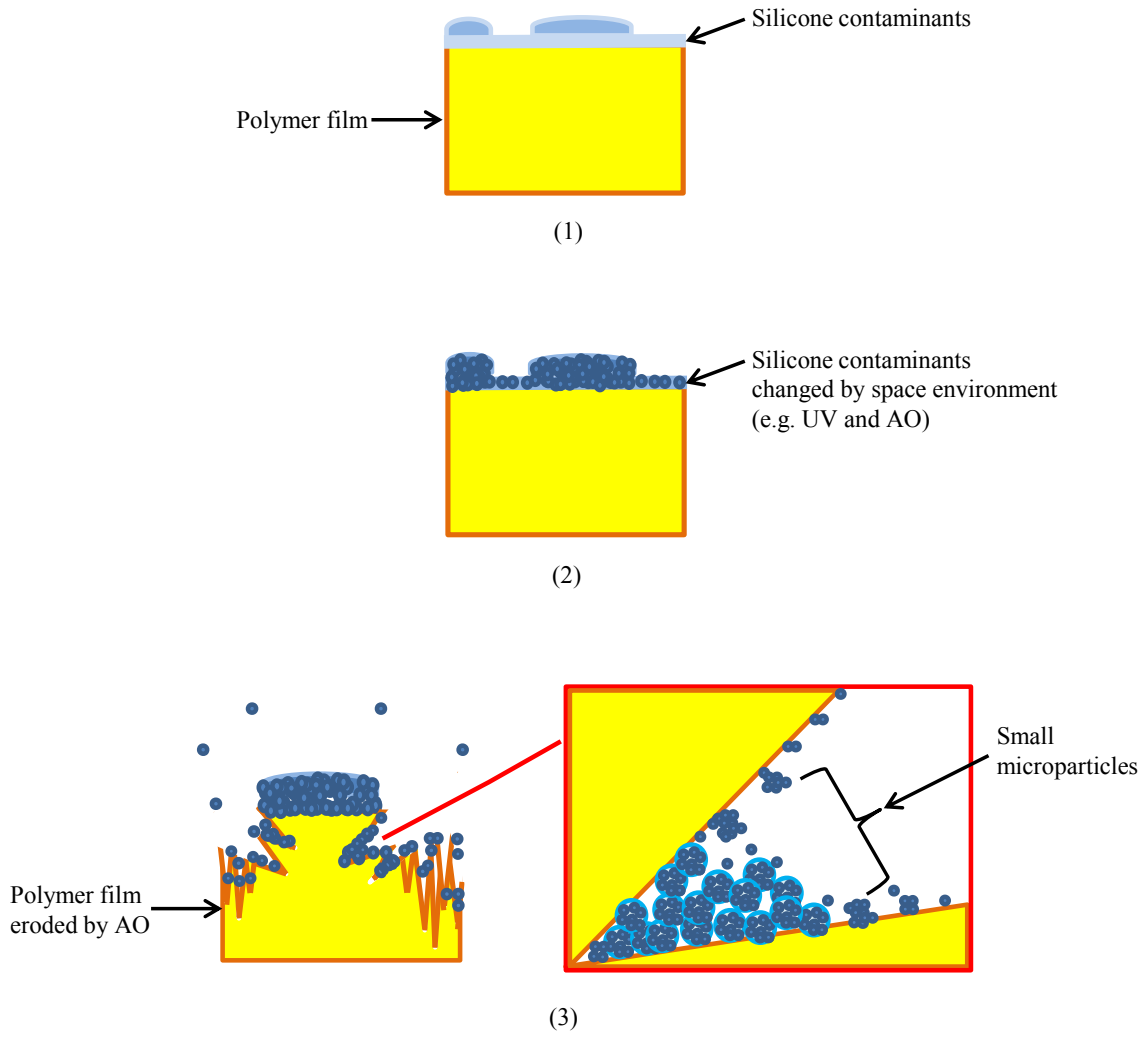

Fig. 5-2. Conceptual diagrams of the formation process of small microparticles on the surface of polymer film.

5.3 Conceptual Approach to the Present Model

The model of the formation of microparticles from silicone contaminants deposited on polymer films, which are eroded by AO, under effects of UV and AO irradiation has been presented in this chapter. It can be considered, that this model works not only in the conditions of the experiment designed in the present work, but also in a wider range of conditions existing in space. As is well known, silicone materials are widely applied for bonding, sealing, and protection of spacecraft. And, polymer films, such as polyimide, which are eroded by AO, are widely used as structural materials and thermal control materials of spacecraft. It is well known that not only polyimide but many polymer films are eroded by AO[5-1]. Therefore the phenomenon of the formation process of large microparticles derived from silicone contaminants may occur on the surface of various polymer materials. In addition, it is confirmed that there is also exist the formation process of small microparticles derived from silicone contaminants which may occur on the surface of many types of space materials of spacecraft that are operated on orbit where AO and silicone contaminants exist. It is confirmed that the both microparticles, large and small, which can be formed on the surface of many polymer films and on the surface of many types of space materials, are consisting of the same components which contain SiO_2, hydroxyl group, Alkanes and so on as was shown by the investigation results of chemical analyses in Chapter 3.

It was reported that not only Ram side of spacecraft but also Wake side of spacecraft is irradiated with UV because of the Earth albedo[5-2], and Wake side of spacecraft is also irradiated with AO because a part of the unreacted AO is scattered from the surface of materials[5-3]. So, both Ram side and Wake side of spacecraft are irradiated by UV and AO. Moreover, it is also reported that the unreacted AO scatters below the protective coating and react with the substrate material, which lead to the cause of undercutting[5-4], [5-5], [5-6]. Additionally, dominant component of upper air near orbit around planets Mars and Venus is also AO as well as of the Earth[5-2]. Silicone materials are widely designed for bonding, sealing, and protection of spacecraft, and polymer films are widely used as

structural materials and thermal control materials of spacecraft. These facts mean that there are sufficient conditions exist at the all sides of spacecraft operated not only near the Earth but also near Mars and Venus to produce microparticles derived from silicone contaminants with UV and AO. Before using polymer films as thermal control materials to spacecraft, the effects of UV and AO to thermal characteristics of polymer films without being deposited with contaminants are evaluated. However, it is conceivable that microparticles are formed after deposition of contaminants on the surface of polymer films on orbit by the results of present work. It is reported that formal difference of materials mean the difference of optical absorption features[5-7]. If many microparticles attach on thermal control materials, the properties of thermal control materials should be changed. Thus, evaluation of effects including microparticles is necessary to obtain the correct thermal characteristics of thermal control materials on orbit.

The development of interplanetary exploration is forwarded in recent years. Therefore, the present work will also contribute to the development of interplanetary exploration in the future.

5.4 Conclusion

This chapter presents modeling of the formation processes of large and small microparticles derived from silicone contaminants, which is based on the clues obtained experimentally by SEM, EDX spectroscopy, FT-IR spectroscopy, and XPS as shown in Chapters 3 and 4. The formation process of large microparticles can occur basically on the surface of various polymer materials, which are eroded by AO, but the process of formation of small microparticles can occur on the surface of many types of space materials. It can be said, that if there are existing silicone contaminants, UV and AO, there is possibility to form SiO_2-based microparticles from silicone contaminants affected with UV and AO.

Those two formation processes are possible at the all sides of spacecraft operated not only near the Earth but also near Mars and Venus, where silicone contaminants, UV and AO exist[5-2].

Comparison between the microparticles captured on orbit and the microparticles produced experimentally in the present work will be demonstrated in Chapter 6 in order to study the microparticles experimentally formed from silicone contaminants are actually produced on orbit or not.

A paper with main findings cleared in this chapter and Chapter 4 have been submitted to the International Journal of Microgravity Science entitled as “Formation of Microparticles from Silicone Contaminants under Simulated Space Environment,” which is in review.

References

(5-1) J.A. Dever, “Low Earth Orbital Atomic Oxygen and Ultraviolet Radiation Effects on Polymers,” NASA/TM 103711, (1991).

(5-2) M. Onishi, J. Abe, J. Ishizawa, M. Iwata, A. Okamoto, S. Okamoto, H. Kawasaki, A. Kobayashi, Y. Shinozaki, H. Sugita, M. Tagawa, S. Tachikawa, Y. Tanaka, K. Toyota, H. Nagano, T. Harada, I. Mase, S. Miyazaki, K. Mori, T. Yamada, and R. Yamanaka, “Thermal Design of Spacecraft,” The University of Nagoya Press, (2014). (in Japanese)

(5-3) B.A. Banks, K.K. de Groh, and S.K. Miller, “MISSE Scattered Atomic Oxygen Characterization Experiment,” NASA/TM-2006-214355, (2006).

(5-4) R.C. Tennyson, “Atomic oxygen effects on polymer-based materials,” *Canadian Journal of Physics*, **69** (8-9) (1991) pp.1190-1208.

(5-5) K.K. de Groh, and B.A. Banks, “Atomic-Oxygen Undercutting of Long Duration Exposure Facility Aluminized-Kapton Multilayer Insulation,” *J. Spacecraft and Rockets*, **31** (4) (1994) pp. 656-664.

(5-6) B.A. Banks, S.K. Rutledge, B.M. Auer, and F. DiFilippo, “Atomic oxygen undercutting of defects on SiO_2 protected polyimide solar array blankets,” NASA CP-19910065180, (1990) pp.15-33.

(5-7) K. Nakasa, T. Kubo, A. Yamamoto, and T. Sumomogi, “Visible Light and Infrared Ray Absorbance of Fine Protrusions Formed by Sputter Etching of Steels and Copper Alloys,” *J. Japan Inst. Met. Mater.*, **78** (9) (2014) pp.350-358.

Chapter 6:

Comparison of the Microparticles Obtained in the Present Work with the Ones Captured on Orbit

6.1 Introduction

As the results of the chemical and morphological approaches to the formation of microparticles from silicone contaminants, it has been confirmed that main components of the microparticles are Si and O, and the forming process of the microparticles derived from silicone contaminants could be estimated as follows;

1) deposition of silicone contaminants on the surface of polymer film,
2) chemical change of silicone contaminants such with irradiations of UV and/or AO,
3) erosion of the polymer by AO irradiation except the parts covered with droplets of silicone contaminants, and
4) small-sized segmentation of the SiO_2-based parts with further AO irradiation, resulting in "microparticles."

The sizes of the microparticles obtained in the present work could be classified in ten-micrometer and hundred-nanometer levels. The former can be briefly explained with the above estimation, and the latter would be explained with an successive process after the microparticles stripped from the polymer film; silicone contaminants on polymer film would be also influenced directly with AO, and much smaller particle derived from the contaminant itself would leave and deposit again as snowball-like shape on the part of the film.

Since silicone adhesives and sealants have been designed for a wide range of bonding for sealing and protection of spacecraft in space activities, problems occurred from such microparticles formations as discussed in the present work should be important to be solved by analyzing various types of space materials of spacecraft that are operated on

orbit where AO and silicone contaminants exists.

In this chapter, comparison between the SiO_2-based microparticles captured on orbit and the ones produced experimentally in the present work is conducted in order to study that the microparticles, which formed from silicone contaminants affected with UV and AO, are actually produced on orbit or not.

6.2 Microparticles Captured with the MPAC Experiment Units

The MPAC experiment units had been developed in order to clarify the abundance and composition of micrometeoroid and space debris, and exposed to space environment on the ISS. Silica aerogel (hereafter "aerogel") was mounted on the MPAC experiment units, and it was clarified that retrieved aerogel captured space debris (Chapter 1 Fig. 1-4 (A)), secondary debris (Chapter 1 Fig. 1-4 (B)), micrometeoroid (Chapter 1 Fig. 1-4 (C)), and a large number of microparticles. The microparticles were analyzed by using XMA and a microscope FT-IR spectroscopy. Consequently, it was clarified that their main container is SiO_2, but their origin was not clarified[6-1].

This section compared the characteristics of the SiO_2-based microparticles captured by the aerogel mounted on the MPAC experiment units with the characteristics of the microparticles experimentally formed from silicone contaminants affected with UV and AO in the present work. Table 6-1 shows the characteristic comparison between the microparticles captured on orbit and the microparticles experimentally formed from silicone contaminants.

First, the elemental composition of microparticles was compared.

The XMA analysis results of the SiO_2-based microparticles captured by the aerogel mounted on the MPAC experiment units revealed that silicon (Si), carbon (C), and oxygen (O) are main components of the microparticles. Meanwhile, the sample of the cross section of PI-Expt. No.4, which is the polyimide film deposited by silicone contaminants affected with UV and AO, was analyzed by using EDX spectroscopy. The

analysis results of the two analyzed points (one is silicone contaminants affected with UV and AO, and the silicone contaminants will form large microparticles. The other is the point on where small microparticles exist) clarified that the inclusion elements of large and small microparticles formed from silicone contaminants affected with UV and AO are Si, C, and O. Consequently, it could be confirmed that the elemental composition of the SiO_2-based microparticles captured by the aerogel mounted on the MPAC experiment units and the elemental composition of the microparticles experimentally formed from silicone contaminants affected with UV and AO in the present work are the same.

Next, the FT-IR spectrum of the SiO_2-based microparticles captured by the aerogel mounted on the MPAC experiment units and silicone contaminants affected with UV and AO were compared.

The SiO_2-based microparticles captured by the aerogel mounted on the MPAC experiment units were analyzed by using FT-IR spectroscopy. And, the sample of Z-Expt. No.3, which is zinc selenide (ZnSe) deposited by silicone contaminants affected with UV and AO, was analyzed by using FT-IR spectroscopy. Significant difference of spectral peaks between the spectrum of the SiO_2-based microparticles captured by the aerogel mounted on the MPAC experiment units and the silicone contaminants affected with UV and AO is intensity ratio of $Si\text{-}CH_3$ (800 cm^{-1}), $Si\text{-}CH_3$ (1260 cm^{-1}) and Alkanes (2960 cm^{-1}) peaks. And, both of spectral peaks of the SiO_2-based microparticles captured by the aerogel mounted on the MPAC experiment units and the silicone contaminants affected with UV and AO showed that they contain vitreous SiO_2, $Si\text{-}CH_3$, Si-O-Si, Alkane, and Hydroxyl group. And, the difference bonds are Alkenes and Si-Ph. However, it is found that Alkanes, Alkenes, $Si\text{-}CH_3$, and Si-Ph are changed chemically by irradiation conditions of UV and/or AO. Therefore, it would be considered that the difference of bonds are caused by a little difference of UV and/or AO irradiation fluence.

In addition, the depth profiles obtained by XPS clarified that the reduction of C content and the increase of O content in silicone contaminants were occurred by AO irradiation,

and the effects of AO irradiation to silicone contaminants were rejected by the effects of UV irradiation to silicone contaminants. It would be presumed that UV fluence was too strong, thus the effects of AO irradiation to silicone contaminants were rejected and C was remained in silicone contaminants. As a result, C was detected in silicone contaminants affected with UV and AO irradiation.

Actually, the new layer was formed on the surface of retrieved F-OSRs which is one of materials mounted on the SEED experiment units. And, the main components of the new layer were also Si, C and O, which were clarified by STEM-EDX analysis. In addition, the thickness of the new layer was become thicker belonging to exposure periods. Therefore, the new layer is conceivable to be formed from the deposition of silicone contaminants on the ISS[(6-2)].

It is found that there are sufficient conditions (silicone contaminants, UV and AO) exist at the exterior of the ISS from the facts shown in the above. In other words, there are sufficient conditions exist at the exterior of the ISS to occur the formation processes of large and small microparticles presented in Chapter 5.

Consequently, it would be considered that both of the SiO_2-based microparticles captured by the aerogel mounted on the MPAC experiment units and formed from the silicone contaminants affected with UV and AO have the same origin.

Table 6-1. Characteristic comparison between the microparticles captured on orbit and the microparticles experimentally formed from silicone contaminants.

Property	Microparticles captured on orbit	Microparticles experimentally formed from silicone contaminants	Notes
Size, μm	10	20 (0.1)	See Chapter 2 Section 2.3.2, and Chapter 4 Section 4.5.1.
Elemental composition	Si, O, C	Si, O, C	See Fig. 2-11, and Fig. 4-3
Chemical bonds	Alkanes, CO, Si-CH_3, Si-O-Si, Hydroxyl group	Alkanes, Alkenes, Si-CH_3, Si-O-Si, Si-Ph, Hydroxyl group	See Fig. 2-12, and Fig. 3-10.
Base material	SiO_2	SiO_2	See Fig. 2-12, Fig. 3-10, and Fig. 3-10.

6.3 Microparticles Captured with World Wide Space Exposure Experiments

Many kinds of materials were mounted on various space exposure experiments and were exposed to space environment, and retrieved materials were investigated for detailed studies about a variety space environmental effects including impacts of micrometeoroid and space debris, deposition of contaminants, UV light exposure, AO exposure and so on. However, micrometeoroid and space debris smaller than 1 mm in diameter could not be collected for analyzing and evaluating their components because their shapes were destroyed upon collision with spacecraft[(6-3)]. Thus, the impact residues of them are analyzed for obtaining the information of those space debris. The residue may be remnants of glass and residues enriched in Si and C were detected on solar cells of HST[(6-3), (6-4)], and the residues which contain Si were reported on materials mounted

on LDEF[6-5), (6-6)]. However, most of their origins are unknown.

Most of space exposure experiments such as the MPAC&SEED experiment[6-7], LDEF[6-8], EURECA[6-9], and MEEP[6-10] reported that silica, silicate, and silicones were detected as contaminants on the surfaces of their retrieved samples. In addition, the surface observation of the retrieved mirror which was mounted on HST clarified that contaminants do not generally deposit as a uniform film, but rather form small droplets as same as ground tests through simulating the conditions in space. In the case of the mirror of HST, contaminants were deposited as numerous circular droplet-like features 1 to 2 μm in diameter[6-11].

HST, LDEF, MPAC&SEED experiment, EURECA and MEEP were operated in space environment with UV and AO.

The facts described above mean that there are sufficient conditions (silicone contaminants, UV and AO) exist at the all sides of those spacecraft operated on orbit include the ISS to produce both of large and small microparticles derived from silicone contaminants with UV and AO by the formation processes presented in Chapter 5. And, it would be conceivable that the Si contained impact residues, which found on the surfaces of retrieved materials mounted on HST and LDEF, are residues of the microparticles derived from silicone contaminants such as large and small microparticles.

6.4 Conclusion

This chapter compared the microparticles captured on orbit and the microparticles produced experimentally in the present work. The results confirmed in this chapter are as follows;

1) The both of the SiO_2-based microparticles captured by the aerogel mounted on the MPAC experiment units and the SiO_2-based microparticles originated by silicone

contaminants affected with UV and AO in the present work have the same origin. And, the impact residues found on the surfaces of retrieved materials mounted on HST and LDEF are conceivable the residues of microparticles derived from silicone contaminants.

3) There are sufficient conditions (silicone contaminants, UV and AO) at the all sides of spacecraft operated in the LEO include the ISS to produce microparticles derived from silicone contaminants with UV and AO by the formation processes shown in Chapter 5.

In other words, the microparticles produced experimentally in the present work are actually produced on orbit.

References

(6-1) R. Yamanaka, T. Noguchi, and Y. Kimoto, "Analysis Results of SM/MPAC Experiment Samples," *J. Spacecraft and Rockets*, **48** (5) (2011) pp.867-873.

(6-2) E. Miyazaki, and I. Yamagata, "Results of Space-Environment Exposure of the Flexible Optical Solar Reflector," *J. Spacecraft and Rockets*, **46** (1) (2009) pp.28-32.

(6-3) G.A. Graham, N. Mcbride, A.T. Kearsley, G. Drolshagen, S.F. Green, J.A.M. Mcdonnell, M.M. Grady, and I.P. Wright, "The Chemistry of Micrometeoroid and Space Debris Remnants Captured on HUBBLE Space Telescope Solar Cells," *Int. J. Impact Engng*, **26** (2001) pp.263-274.

(6-4) G.A. Graham, A.T. Kearsley, R.M. Hough, I.P. Wright, G. Drolshagen, and M.M. Grady, "Interstellar Silicon Carbide Captured in Low Earth Orbit," *Meteoritics and Planetary Science Supplement*, **34** (1999) pp.47.

(6-5) C.G. Simon, J.L. Hunter, J.J. Wortman, and D.P. Griffis, "Ion Microprobe Elemental Analyses of Impact Features on Interplanetary Dust Experiment Sensor Surfaces," *Proc. the LDEF-69 Months in Space First Post-Retrieval Symposium*, NASA CP-3134 Part1, (1991) pp.529-548.

(6-6) T.E. Bunch, F.R. diBrozolo, R.H. Fleming, D.W. Harris, D. Brownlee, and T.W. Reilly, "LDEF Impact Creators Formed by Carbon Rich Impactors: a Preliminary Report," *Proc. the LDEF-69 Months in Space First Post-Retrieval Symposium*, NASA CP-3134 Part1, (1991) pp.549-564.

(6-7) N. Baba, and Y. Kimoto, "Contamination Growth Observed on the Micro-Particles Capturer and Space Environment Exposure Device," *J. Spacecraft and Rockets*, **46** (1) (2009) pp.33-38.

(6-8) G.A. Harvey, "Silazane to Silica," *Proc. the LDEF-69 months in Space Second Post-Retrieval Symposium*, NASA CP-3194 Part 3, (1992) pp.797-810.

(6-9) M.V. Eesbeek, M.Froggatt, and G. Gourmelon, U. Rieck, H. Kersting, B. Schwarz, and H.J. Rosik, "Post Flight Material Investigation of EURECA Preliminary Findings and Recommendations," *EURECA Technical Report*, ESA WPP-069,

(1994) pp.513-527.

(6-10) J.M. Zwiener, R.R. Kamenetzky, J.A. Vaughn, and M.M. Finckenor, “Contamination Observed on the Passive Optical Sample Assembly-I (POSA-I) Experiment,” *Proc. SPIE's International Symposium on Optical Science, Engineering, and Instrumentation, International Society for Optics and Photonics.*, (1998) pp.186-195.

(6-11) J.L. Tveekrem, D.B. Leviton, C.M. Fleetwood, and L.D. Feinberg, “Contaminantion-induced degradation of optics exposed to the Hubble Space Telescope Interior,” *Proc. SPIE, Optical System Contamination V, and Stray Light and System Optimization*., 2864 (1996) pp.246-257.

Chapter 7:

General Conclusion

Many space debris are existing on orbit, and they will remain in orbit for hundreds of years or more, and pose a long-term hazard to future space exploration. It causes a great concern that not only large space debris but also space debris smaller than 1 mm in diameter can damage spacecraft. Nevertheless, the origin of small space debris remains mainly unknown because their shapes are destroyed upon collision with spacecraft. The fact that a lot of the SiO_2-based microparticles were captured by the aerogel mounted on the MPAC experiment units reveals the concern about the problem of small space debris to our future space exploration. If the origin of small space debris were clarified, the new methods which can play effective roles in reducing spacecraft problems damaged from space debris on orbit would become possible to develop. From the other side, it was reported that silicone contaminants were detected on the surfaces of materials mounted on worldwide previous space exposure experiments. Indeed, silicone materials are widely applied to spacecraft such as bonding solar cells and potting components. Therefore, it would be considered that silicone contaminants are possible to be the origin of the SiO_2-based microparticles.

In the present work, main focus is possible connection between the SiO_2-based microparticles captured on orbit and silicone contaminants derived from silicone materials which are widely used in spacecraft. And, the purpose of the present work is the followings;

1. to find out the formation process of the SiO_2-based microparticles derived from silicone contaminants with comparison of the results of the MPAC experiment, and
2. to make a model of small space debris formation process with the results of the SiO_2-based microparticles formation from silicone contaminants.

First, silicone contaminants which were derived from Room-temperature-vulcanizing silicon adhesive No. 691 (RTV-S691) were deposited on the surface of optical materials

(zinc selenide (ZnSe) and magnesium fluoride (MgF_2)) and polyimide film (125-μm-thick UPILEX-S®). The reason to choose the silicone adhesive is that the adhesive is actually used on spacecraft, and contaminants on orbit can be imitated by using the silicone adhesive as an outgassing source. The optical materials were selected for investigating chemical changes of silicone contaminants affected with UV and/or AO and the polyimide film was chosen for evaluating morphological changes of silicone contaminants affected with UV and/or AO. RTV-S691 as a silicone outgassing source was heated to 125 ℃, while the optical materials and the polyimide film for collecting silicone contaminants were maintained at 25 ℃.

Second, UV and/or AO irradiation to silicone contaminants were demonstrated in series. The irradiation angle is not always 90°on the surface of spacecraft on orbit. Chemical changes would not be effected by irradiation angles, but morphological changes would be affected with irradiation angles. Thus, one of the polyimide film samples was irradiated with AO not only from the angle of 90° but also from the angles of 45° and 135° (AO-2nd irradiation).

The next step, detailed investigations of chemical and morphological changes were performed by using FT-IR spectroscopy and XPS, SEM, and EDX spectroscopy.

Experimental results provide the following chemical and morphological clues for clarifying the formation process of the SiO_2-based microparticles derived from silicone contaminants.

1) Oxidation of silicone contaminants was confirmed (content of carbon was reduced, content of oxygen was increased, Si-CH_3 bond was decreased, and formation of hydroxyl group and SiO_2 was observed by AO irradiation).
2) Si-Ph bond was decreased by UV irradiation. And, UV irradiation influences the reaction between AO and silicone contaminants.
3) The surface shape of the polyimide film deposited by silicone contaminants is not significantly changed by UV irradiation.
4) The surface of the polyimide film deposited by silicone contaminants was eroded by AO except the parts covered with droplets of silicone contaminants, and the

formation process of microparticles (ca. 20 μm, large microparticles) mainly originated from droplets of silicone contaminants deposited on the polyimide film was observed.

5) Smaller microparticles (ca. 100 nm, small microparticles) having the same elemental composition as the microparticles mainly originated from droplets of silicone contaminants were observed at the part of the polyimide film eroded by AO.

Consequently, two models of small space debris (large and small microparticles) formation processes were made from experimental backgrounds described above, and followings were clarified with comparing between the SiO_2-based microparticles captured by the aerogel mounted on the MPAC experiment units and the microparticles produced experimentally in the present work.

1) The formation processes of large and small microparticles derived from silicone contaminants affected with UV and AO were clarified.
2) The formation process of large microparticles can occur basically on the surface of various polymer materials, which can be eroded by AO, but the formation process of small microparticles can occur on the surface of many types of space materials. As a result of the formation of small microparticles on the surface of materials leads the change of optical absorption feature.
3) The microparticles formed from silicone contaminants affected with UV and AO are SiO_2-based microparticles.
4) The formation processes of the SiO_2-based microparticles can occur at the all sides of spacecraft operated not only near the Earth but also near Mars and Venus where silicone contaminants, UV and AO exist.
5) The both of the SiO_2-based microparticles captured by the aerogel mounted on the MPAC experiment units and the SiO_2-based microparticles derived from silicone contaminants affected with UV and AO have the same origin.

Finally, the facts that the two models of small space debris (large and small microparticles) formation processes which were made from the experimental results of the present work actually occur on orbit and produce the SiO_2-based microparticles

derived from silicone contaminants were clarified in this study. In other words, the formation processes of microparticle space debris derived from silicone contaminants affected with UV and AO are confirmed by this study.

Identifying the origin of the SiO_2-based microparticles in this study will contribute to promote the development of new methods which can play effective roles in reducing spacecraft problems damaged from space debris on orbit.

List of Publications Concerning This Thesis

≪Chapter 1 and Chapter 2≫

1) **Riyo Yamanaka**, Takaaki Noguchi, and Yugo Kimoto "Analysis Results of SM/MPAC Experiment Samples." *J. Spacecraft and Rockets*, **48** (5) (2011) pp.867-873.

≪Chapter 3≫

2) **Riyo Yamanaka**, Kazuyuki Mori, Eiji Miyazaki, Takao Yamaguchi, and Osamu Odawara "Impact Assessment about UV- and AO-Irradiated Silicone Contaminants through Optical Property Measurement." *Int. J. Microgravity Sci. Appl.*, **33** (4) (2016) pp.330408-1-330408-6.

3) **Riyo Yamanaka**, Eiji Miyazaki, Takao Yamaguchi, and Osamu Odawara "The Effect of Ultraviolet Irradiation on Adhesion Behavior of Silicone Contaminants." *Proc. The 37th Japan Symposium on Thermophysical Properties*, (2016) pp.114-116. (in Japanese)

4) **Riyo Yamanaka**, Susumu Baba, Junko Matsuyama, Eiji Miyazaki, and Takashi Tamura, "Report on the Research and the Development of In-situ Contamination Spectroscopic Analysis Chamber," JAXA-RM-11-018, (2012).

≪Chapter 4≫

5) **Riyo Yamanaka**, Anna Gubarevich, Eiji Miyazaki, Takao Yamaguchi, and Osamu Odawara "Formation of Microparticles from Silicone Contaminants under Simulated Space Environment." *Int. J. Microgravity Sci. Appl.* (in review).

Acknowledgement

I appreciate all people who helped and supported me. This thesis would not have been completed without their help and support.

First of all, I would like to express my deepest appreciation to the supervisor Prof. Osamu Odawara. His help, support, suggestions, and encouragements always helped me in all time of my research and writing this thesis. And, I would like to give my deepest thankfulness to the superviser Prof. Takao Yamaguchi, who gave me the big chance to earn my degree and supported me.

In addition, I would like to express my gratitude to Prof. Toyohiko Yano, Prof. Mamoru Yoshimoto, Associate Prof. Kazutaka Nakamura, and Associate Prof. Hiroyuki Wada. They gave me constructive and valuable advices to complete this thesis.

I would like to show my greatest appreciation to Assistant Prof. Anna Valeyevna Gubarevich. Her help, support, suggestions, and encouragements always helped me to continue my research and write this thesis. I studied a lot of things from her.

I would like to express my deepest thankfulness to Dr. Eiji Miyazaki. He is the person responsible my on the job training in JAXA. He always taught, helped and encouraged me to continue my job in JAXA and writing this thesis.

I also would like to acknowledge Mr. Takashi Tamura (Safety and Mission Assurance Officer), Mr. Koichi Suzuki (Deputy Director of Research Unit I), and Mr. Koji Yamanaka (Director of Research Unit I). They gave me the chance to continue my research in JAXA.

I would like to acknowledge Mr. Shigeki Kamigaichi (Director of Flight Crew Operations and Technology Unit), Mr. Hiroshi Miyoshi (Deputy Director of Earth Observation Research Center), and Mr. Kazuyuki Tasaki (Director of JEM Utilization Center). They gave me the chance to earn my degree and supported my work in JAXA.

I would like to express my thankfulness to members of Research Unit I. They supported and encouraged me to continue my challenge.

Finally, I wish to give my special thanks to my family. My parents and my husband always keep understanding, supporting and encouraging all challenges in my life. Their patient support encouraged and enabled me to write this thesis and to keep working in JAXA.

Riyo YAMANAKA

March 2017